Energy, Mines and Resources Canada
Énergie, Mines et Ressources Canada

CANMET

Canada Centre for Mineral and Energy Technology

Centre canadien de la technologie des minéraux et de l'énergie

POTASH MINING PROJECT

PROJET D'EXPLOITATION DE LA POTASSE

PROGRAMME DE RECHERCHE SUR LES MINÉRAUX
LABORATOIRES DE RECHERCHE MINIÈRE

MINERALS RESEARCH PROGRAM
MINING RESEARCH LABORATORIES

PREDICTION AND MONITORING OF EXCAVATION BEHAVIOUR

FINAL REPORT

BY

COMINCO FERTILIZERS

POTASH OPERATIONS

Work on this project was conducted under the auspicies of the Canada Centre for Mineral and Energy Technology, Energy, Mine and Resources, Canada

DSS FILE NUMBER: 07SQ.23440-5-9082
DSS CONTRACT SERIAL NUMBER: OSQ85-00211
CANMET PROJECT NUMBER: 140901
CANMET SCIENTIFIC AUTHORITY: G. Herget

171 pp

MICROMEDIA

Submitted By:

A. Dave Mackintosh
Mine Engineer

Approved By:

D. S. Boyle
General Manager

TABLE OF CONTENTS

1. **EXECUTIVE SUMMARY**

2. **INTRODUCTION**

3. **FIELD MONITORING**

   3.1 Geology
   3.2 Site Discription
   3.3 Updated Curves of Field Data
   3.4 Discussion

4. **LABORATORY TESTING**

   4.1 Unconfined Tests
   4.2 Results and Conclusions
   4.3 Creep Tests

5. **NUMERICAL MODEL**

   5.1 Introduction
   5.2 Program Enhancements
   5.3 Material Laws
   5.4 Material Properties

6. **ANALYSIS**

   6.1 Yield Pillars
   6.2 Roof Beams
   6.3 Single Rooms
   6.4 Five-Entry System

TABLE OF CONTENTS - (continued)

APPENDIX A USER'S GUIDE TO PC VERSION OF GEOROC

APPENDIX B UNDERGROUND REFRACTION SEISMIC SURVEY

APPENDIX C GENERAL SPECIFICATIONS OF THE SRC TRIAXIAL TEST FACILITY

1.0 EXECUTIVE SUMMARY

The work described in this report was carried out under D.S.S. contract number OSQ85-00211, file number 07SQ-23440-5-9082. Cominco Fertilizers, Potash Operations, as the prime contractor managed the project through Mr. A. D. Mackintosh.

Major sub-contractors contributing to the successful completion of the project were the Saskatchewan Research Council and Beddoes and Day Materials Research.

The project integrates three components:

1. The development of a two dimensional finite element model.
2. Creep parameters determined through large sample triaxial testing.
3. Convergence measurement from Potash mine openings.

These components were originally separate projects initiated under the START program. (Short Term Aid to Industry for Research and Technology).

Field measurements were continued at the Cominco test site for approximately 1,500 days. An excellent record of room closures, pillar deformation and stresses has resulted. Level surveys intended to determine the proportions of room closure due to the roof and floor respectively have also continued.

Difficulties in obtaining suitable samples for laboratory testing delayed the creep testing program significantly and forced an extension to the contract. Replacing the carbides in the coring bit solved the problems and five acceptable potash samples were obtained.

Long term creep tests, directed by Mr. J. Jones of the Saskatchewan Research Council, were completed on four of the 200 mm dia. by 400 mm long samples (8" x 16"). Axial and confining pressures used were comparable to loading conditions observed in-situ.

Computer analysis was initiated by Re/Spec Ltd., developers of the Georoc model, however the major portion was completed by Mr. R. Beddoes of Beddoes and Day Materials Research.

The model has undergone significant improvements, first to remove or correct problems plaguing the original code, and secondly to enable it to be used on I.B.M. compatible personnal computers. Problem size is restricted by MS.DOS however Unix or Xenix systems allow somewhat larger problems to be modeled.

Pre and post processors have been added to help with data input, output file generation, and graphical display of original and deformed meshes. A revised users manual has also been produced.

1.0 SOMMAIRE DE LA DIRECTION

Le travail décrit dans ce rapport fut exécuté sous le contrat numéro OSQ85-00211, numéro de dossier 07SQ-23440-5-9082 du Département de l'approvisionnement et des services. C'est Cominco Fertilizers de Potash Operations qui a géré le projet en tant qu'entreprise principale par l'entremise de Monsieur A. D. Mackintosh.

Le "Saskatchewan Research Council" et "Beddoes and Day Materials Research" furent des sous-traitants importants qui ont contribué à la réussite du projet.

Le projet englobe trois composantes:

1. La réalisation d'un modèle d'éléments finis à deux dimensions.

2. Les paramètres de fluage déterminés au moyen d'essais triaxiaux à grande échelle.

3. La mesure de convergence dans les ouvrages des mines de potasse.

Au début ces composantes étaient des projets séparés qui avaient été entrepris sous le programme START. (Aide à court terme à l'industrie pour la recherche et la technologie).

On a continué les mesures de terrain au site d'analyse de Cominco pendant approximativement 1 500 jours. On a ainsi pu obtenir un excellent enregistrement de la convergence des chambres ainsi que de la déformation et des pressions dans les piliers. On a également poursuivi les études topographiques en vue de déterminer les parts de la convergence des chambres relative au toit et au mur.

Des difficultés dans l'obtention d'échantillons adéquats pour les essais en laboratoire ont grandement retardé le programme d'analyse de fluage et ont nécessité une prolongation de contrat. On a résolu le problème en remplaçant les carbures des têtes de carottage et ainsi obtenu cinq échantillons acceptables de potasse.

Des essais de longue durée de fluage, réalisés sous la direction de Monsieur J. Jones du "Saskatchewan Research Council", ont été menés à bien sur quatre des échantillons de 200 mm de diamètre sur 400 mm de long (8" x 16"). Les pressions axiales et de confinement qu'on a utilisées étaient comparables aux conditions de charge observée in-situ.

Re/Spec Ltd., créateur du modèle Gyroc, a entrepris l'étude informatique dont la majeure partie a cependant été exécutée par Monsieur R. Beddoes de "Beddoes and Day Materials Research".

On a fait subir au modèle plusieurs améliorations importantes, premièrement, afin d'éliminer ou de corriger des problèmes affectant le code d'origine et, deuxièmement, afin de permettre son utilisation sur des ordinateurs personnels compatibles avec I.B.M. MS.DOS limite la taille des projets qu'on peut étudier, alors que les systèmes Unix et Xenix devraient permettre de modaliser des projets plus importants.

On a ajouté un préprocesseur afin d'améliorer l'introduction des données ainsi qu'un programme d'adaptation pour la génération des dossiers de résultats et l'affichage graphique de grilles originales et déformées. On a également rédigé une révision du manuel d'utilisation.

2.0 INTRODUCTION

In 1984 eight contracts to study various potash related problems were funded under START (Short Term Aid to Industry for Research and Technology). Cominco Fertilizers, Potash Operations carried out one of these projects titled "Collection and Evaluation of Field Data around Excavations in Potash to Evaluate Excavation Performance or Concepts for New Mining Layouts". This project involved cutting a five entry system in virgin ground well away from any induced mining loads, instrumenting the rooms and collecting data on room convergence, pillar deformation, roof and floor displacements and stress conditions. This project was completed in March, 1985.

Similarily the Saskatchewan Research Council obtained a contract titled "Creep Cell Evaluation and Laboratory Testing of Large Evaporite Samples".

This project was to bring into operation one of the S.R.C. triaxial testing pressure vessels in order to adequately evaluate the test facility. This was completed in November, 1984 and included a successful long term potash creep test.

Also funded was a Re/Spec Ltd. contract to develop a numerical model capable of simulating visco-elastic behaviour of potash and halite rocks around openings in deep potash mines.

In order to keep the momentum going and ensure that the work carried out by the START program was not lost, Cominco proposed an additional research program which would integrate the three previous projects in hopes of developing a truly useful rock mechanics tool.

The objectives of the resulting study, funded by the Canada Centre for Mineral and Energy Technology, were to continue the deformation and stress data collection at the Cominco test site, determine in the laboratory rock property and creep parameters suitable for use in the analytical model, and finally compare the model predictions with the field data.

The Saskatchewan Research Council's large sample triaxial test facility (LSTTF) under the direction of Mr. J. Jones carried out the long term creep test.

The continued development of the analytical model, although initiated by Re/Spec Ltd., was carried out by Dr. R. Beddoes of Beddoes and Day Material Research.

Mr. A. D. Mackintosh of Cominco was the project manager responsible for administrating the project, associated invoicing and payment, reporting, and the continued collection of field data.

The project was started in November, 1985 and concluded March 31, 1988.

FIELD MONITORING

COMINCO TEST SITE

3.0 FIELD MONITORING

3.1 GEOLOGY

The Cominco mine site lies towards the North West margin of the Williston Basin. The Prairie Evaporite Formation occurs in the Elk Point Group in the lower part of a thick succession of the Middle and Upper Devonian rocks. Three potash rich zones occur in this formation and the upper or Patience Lake Member contains the Cominco ore zone at depths from 1,066 to 1,112 meters (3,500 to 3,650 ft.) below surface.

The Patience Lake Member, in the Cominco area, is overlain by a salt cover which varies between 12 and 18 meters, (40 to 60 ft.) with an average thickness of 14 meters (47 ft.). Immediately above this lies the Dawson Bay Formation, a dolomitic limestone which, in some areas, contains water.

The immediate back of the mining zone consists of an approximate 1 meter thick halite bed, followed by a 2 meter potash section containing dispersed shale laminae with a .15 meter thick red and grey shale bed at the base and a .5 Meter thick red shale bed at the top.

The remaining cover consists of thick halite beds with few shale or "clay seams" partings.

The overall Prairie Evaporite thickness varies from 120 meters (400 ft.) to 215 meters (700 ft.).

Because of the concern regarding the introduction of water to the mine, any drill holes into the back always stop well short of the estimated top of salt. This means an accurate value for salt cover at any given location is difficult to obtain. An underground refraction seismic survey was conducted by Mr. G. Phillips of the Earth Sciences Division of the Potash Corporation of Saskatchewan.

The data collected indicated a salt cover thickness, in the area of the test site, of 17.2 meters (57 ft.). This is consistent with surface exploration drill holes in the area which indicated cover thickness varying from 15 meters to 18.9 meters (53 to 62 ft.). A detailed stratigraphic section is shown in Figure 1.

3.2 SITE DESCRIPTION

A detailed description of the test site including opening dimensions and completion dates as well as a description of the field instrumentation is adequately provided in our previous report 26SQ.23440-3-9206-2 titled "Collection and Evaluation of Field Data around Excavations in Potash to Evaluate Excavation Performance or Concepts for New Mining Layouts".

Site location with respect to current mine operations as well as an "as cut" cross section is shown in Figure 3.

Instrumentation which had "failed" since first installed was rehabilitated. This included several pressure cells in the back and yield pillars as well as extensometers in the floor.

Additional pressure cells, oriented to monitor horizontal stresses, were installed in the yield pillars.

Figure 2 shows a general layout of the field site.

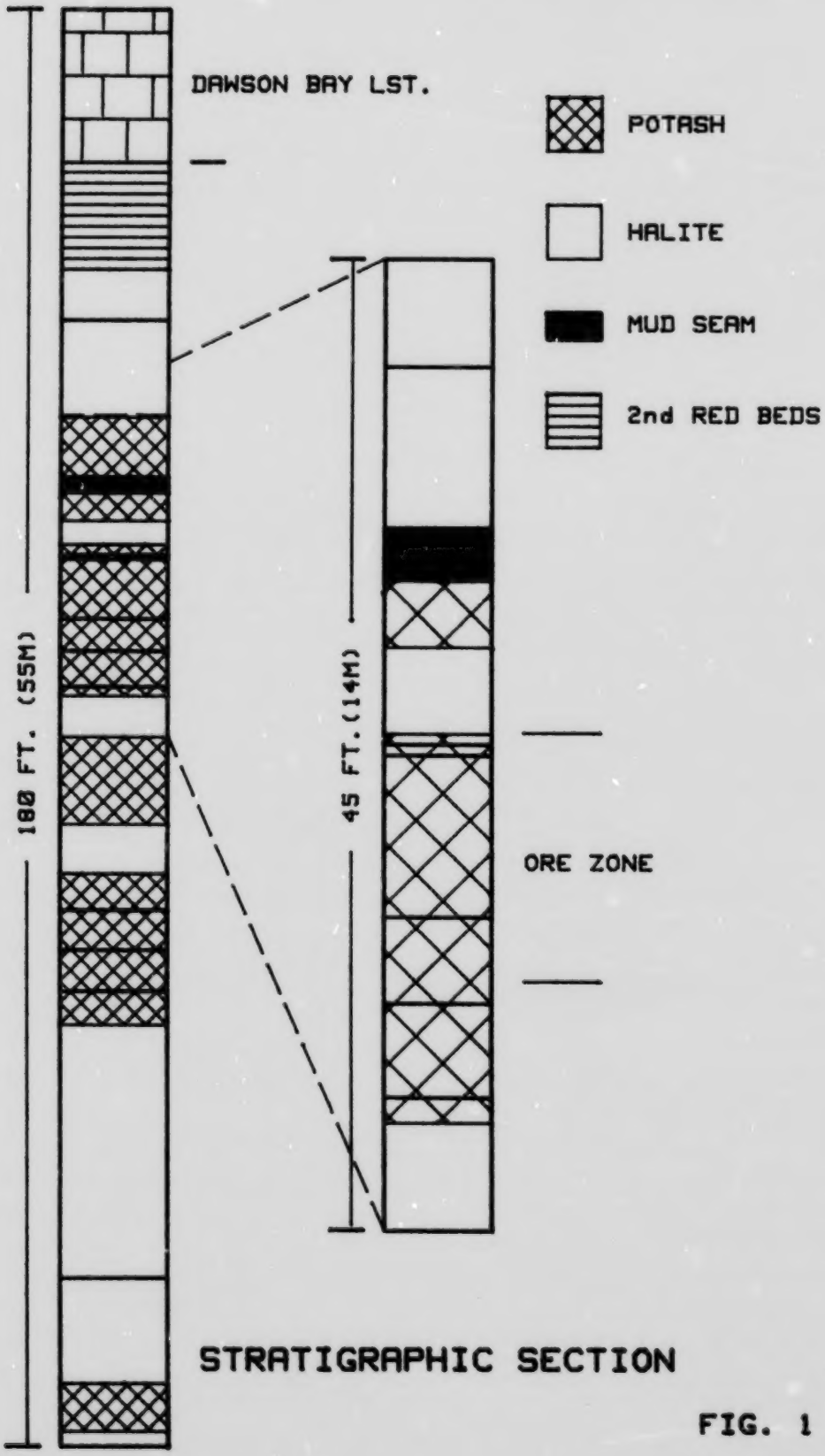

STRATIGRAPHIC SECTION

FIG. 1

SPECIFY TRACING OR DRAWING PAPER
MADE IN CANADA

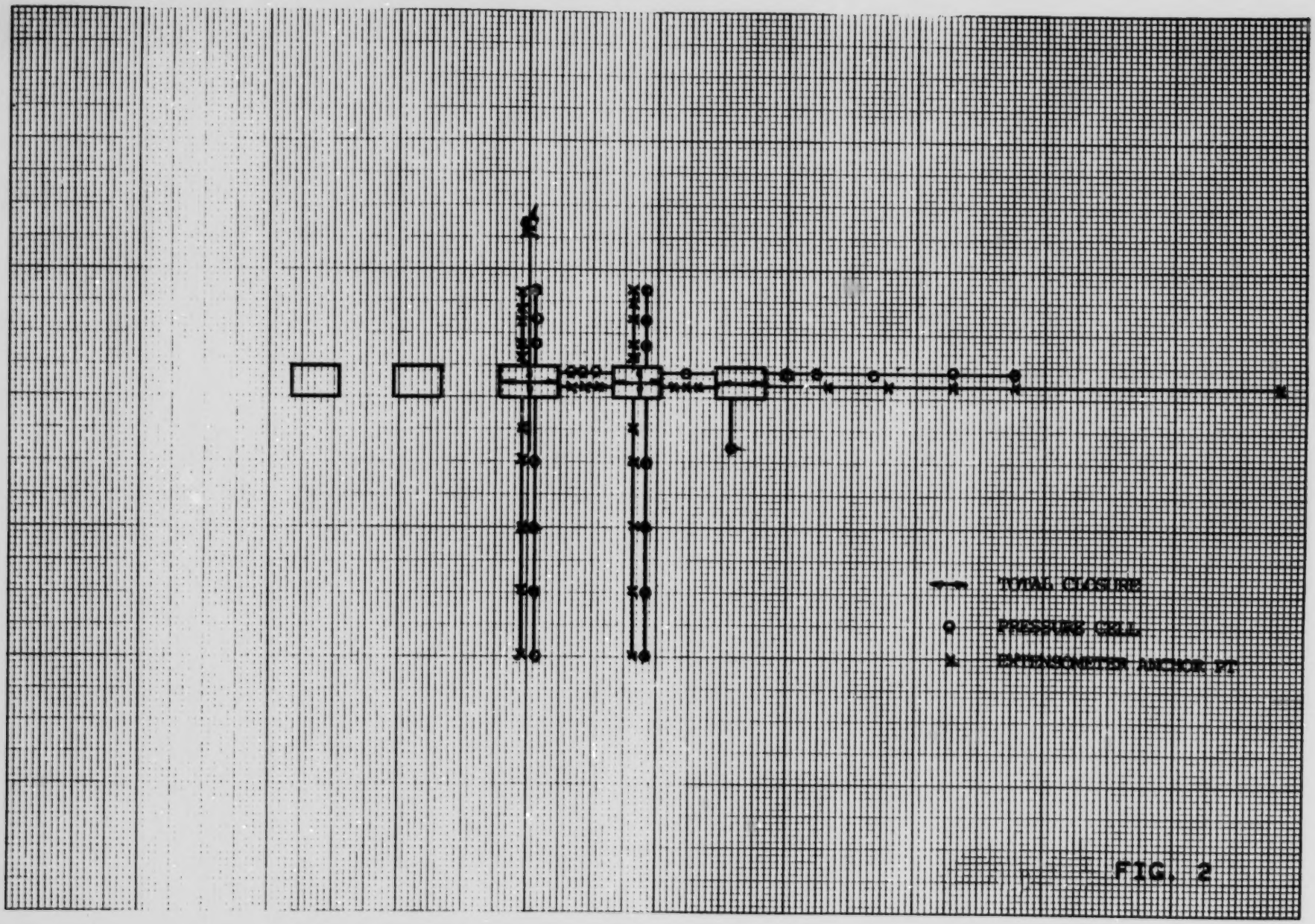

FIG. 2

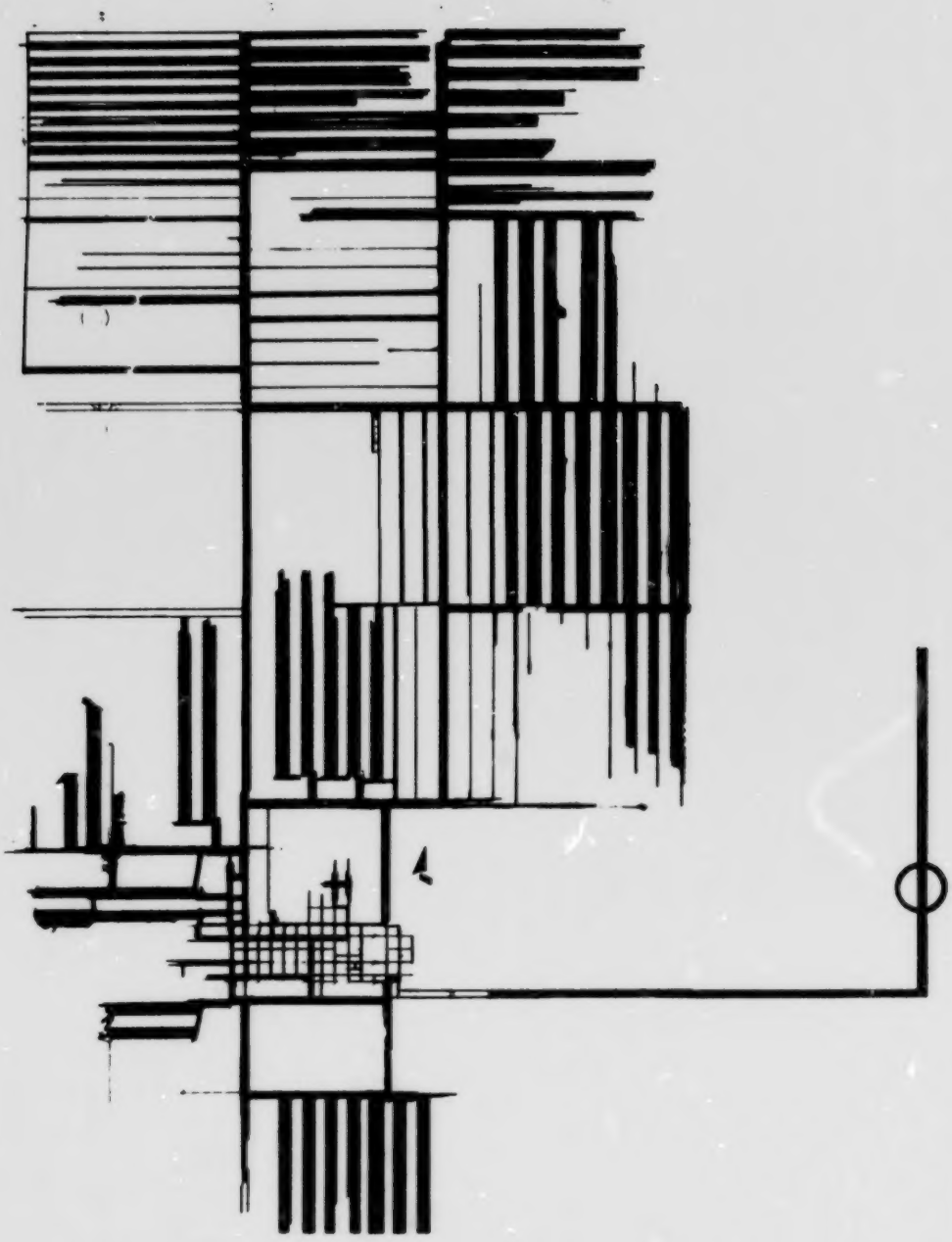

FIG. 3

3.3 FIELD MONITORING

Most field sites have been monitored continously since 1984; Selected sites are summarized as follows:

1. Room Closure
   2104

   Total Vertical Closure Rate (Figure 4-7)
   Two graphs are provided covering the periods 1 to 1,000 days and 10 to 10,000 days. Note the continuation after 1,000 days of the same decay rate established on the 1 to 1,000 day plot. This can be seen on the 1 - 10,000 day plot although the grid is not provided.

   Horizontal Closure Rate (Figure 8-10)
   Again two graphs are provided. Although the characteristic decay rate is the same slope after reloading as that observed prior to reloading, the closure rate appears incrementally higher.

   Pillar Deformation (Figure 11-13)
   The skewness described in the previous report persists. The centre of deformation of the outer pillar (2104-2105) is skewed towards the protected room. This is noted by the significantly greater deformation on the 5.5 to 11 ft. pins than on the 15 to 21.5 ft. pins at 2104 east wall site 1 and between the 5 to 10 ft. pins and 15 to 22 ft. pins at site 2.

   Back (Figure 14)
   There is some question as to whether or not this site is operating properly, particularly between 500 and 900 days. However results do show that 50 percent of the expansion noted on the 25 ft. pin is taking place in the immediate 10 ft. of back. Very little expansion is taking place from 20 to 30 ft. and the 30 ft. pin shows dilation.

2103 (Figure 15-19)

Closure rates are comparable to rates observed in 2104. Back sites again show the most movement is taking place in the immediate 10 ft. with very little taking place from 20 to 30 ft. Dilation is also indicated on the deeper pins.

Overall back expansion is greater than in 2104 and may be a function of room width.

2105 (Figure 20)

Horizontal closure is not significantly greater than in 2104 even though this room has undergone several cycles of reloading. (Cutting 2103 and 2104).

The major portion of the horizontal closure (65%) is contributed by expansion of the 2104-2105 yield pillar. The remainder can be accounted for on the east wall internal site.

2105 East Wall (Figure 21)

The east wall 200 ft. pin has always indicated less movement than the 100 ft. pin. This is not expected to be dilation at such a depth, however after 1,000 days the difference amounts to approximately .2 inches. A possible explanation is provided in the discussion.

2. Pressure Cells

For the most part, pressure cells have survived the monitoring period quite well.

Floor Cells (Figure 22-24)

Floor cells show considerable variation across the entry system but generally show lower stress levels close to the floor near the centre of the system and higher levels near the floor at the outer edge.

The high stress zone 20 ft. (6 meters) above and 50 ft. (15 meters) below the central room, noted in the previous project report, has persisted with time.

Back Cells (Figure 25-26)

Back cells are much more consistent across the two rooms monitored with the 10 ft. (3 meter) cells displaying identical results. The 20 ft. (6 meter) cells show slightly higher levels above the central room. 30 ft. (9 meter) cells continued to give problems and have been replaced several times. In all cases the stress levels dropped to zero or very low values.

Infinite Wall (Figure 27)

Cells in the infinite east wall stabilized at levels much lower than expected. The distribution pattern and lower values may be indicative of stresses around the 2105 entry itself but are inconsistent with abutment loading characteristics determined by historical closure data and mine experience. The deeper cell at 100 ft. (30 meters) may have shed some light on the problem but could not be replaced due to unsafe drilling conditions.

Creep of the matrix around the flat jack cell at low strain rates has since been identified as a potential problem.

Yield Pillars (Figure 28-30)

Yield pillars display much more realistic results.

The 2104-2105 yield pillars stabilized early at approximately 2,850 PSI (20 MPa) somewhat lower than levels observed in the central pillar. This may be due to the lack of confinement on one side of the pillar due to the caved relief drift (2105) however previous studies have determined that the central pillars are the main closure control and accept a higher proportion of the available load, actually protecting the outer pillars so that the load the outer pillars accept is somewhat less than capacity.

2103 - 2104 Yield Pillars

Cells installed in this pillar indicate a higher degree of loading. The 8 ft. (2.4 meter) and 11 ft. (3.4 meter) cells were damaged shortly after installation. The 8 ft. cell was rehabilitated however it was probably not in equilibrium with the ground until after 800 - 1,000 days. The 14 ft. (4.2 meter) cell came into equilibrium early and has displayed on ongoing load transfer process.

The 11 ft. cell was reinstalled later and has not yet reached equilibrium but does indicate a yielding pillar type stress distribution with the peak load at the centre.

Cells oriented to monitor horizontal stresses have also been installed and have not yet stabilized. These also show a yielding pillar distribution pattern.

Although somewhat premature a distribution pattern is shown (Figure 31). Of interest is the fact that horizontal and vertical stresses at the pillar centre are similar. Further work is required to determine if this is a true picture or a function of the instrumentation.

3.4 DISCUSSION

3.4.1 Field Results

A number of relationships arising out of the field data presented here should be noted and may help in any future reviews.

Room Closure

Yield pillar expansion rates (full pillar width) follow decay curves parrallel to the total vertical closure rates observed along each rib (Figure 32). This identifies a horizontal to vertical room closure relationship which is dependent upon the yield pillar rather than opening geomtry (Figure 33). In other words, entry system closure is controlled by the yield pillars and is independent of opening width to height ratio.

Stress-Strain Observations

Within yield pillars a stress-strain relationship can be identified at lower strain rates. Two distinct comparisons can be observed, (Figure 34)one from the confined inner pillar (2103-2104) and one from the outer pillar (2104-2105).

Cell Comparison

In 2105 the pressure cells 10 ft. (3 meter) into the infinite east wall and 12.5 ft. (3.8 meters) into the yield pillar approach similar values. (Figure 35). Initially it was suggested that a load transfer was taking place where any decrease in the loading on the yield pillar was being taken up by an apparent increase in the 10 ft. abutment cell.

This is not believed to be the case and the following explanation is offered:

The 12.5 ft. west wall cell was installed prior to completing 2103 and responded to the cutting by rising from approximately 2,500 PSI (17 MPa) to over 4,200 PSI (29 MPa). At this time the cell is considered to

be in equilibrium with the ground and responded to cutting the double pass in 2103, then monitors the decay in stress levels as loads are transferred to the abutments. The 10 ft. east wall cell was installed after cutting 2103. Indicated pressures increased until approximately day 175 at which time the cell reached equilibrium with the ground and immediately began to monitor a similar decay in stress levels as loads were transferred deeper into the abutment. Loads at the east wall site actually follow a curve similar to the west wall site but the cell could not display this until it came into equilibrium.

Back Cells

Cells monitoring stress levels in the back and floor are non-directional plastic cells which are not subject to any possible creep of the matrix surrounding flat jack calls. However, this also means the cells can only monitor the minimum stress or at least some proportion of the average stress. Any attempt to increase cell pressure very much beyond the minimum stress will result in creep of the borehole parrallel to the minimum stress direction.

Notwithstanding this constraint, monitored stresses do indicate a transfer of load away from the openings into the back taking place during the first 3 years. Stress levels monitored after 1,200 days show some indication of a static stress condition developing. (Figure 26, 36).

The very low values observed on the 30 ft. (9 meter) cells have been a concern. The 30 ft. depth is an area where extensometer results show dilation. This is also an area where vertical stress trajectories diverge to get around openings. The resultant forces can create tensions. (Figure 37). Similarily where trajectories again converage in the floor below openings on area of compression can result. This is offered only as a possible explanation for the anomalous cell response but could also contribute to the greater proportion of total room closure being due to uplift of the floor.

Wall Deformations

The apparent dilation observed deep into the infinite wall (2105 east wall) may be due to instrumentation malfunction. 200 feet (61 meters) of rod is quite heavy and may cause the anchor to slip. A second possible explanation is offered in Figures 38 and 39. Figure 38a which initiated this discussion is taken from "Rock Mechanics in Mining Practise," edited by Prof. S. Budavari, 1983.

Prior to mining a vertical stress σ_o, due to overburden load, exists across the ore horizon. As a result of mining, this stress is removed from both the back and floor within the mined area. The resulting relaxation causes the back and floor beds to expand into the opening by volumes Vh and Vf respectively. (Stress relief creep).

Both before and after mining the total stress across the horizon must balance the weight of overburden. Therefore, the stress in the abutments surrounding the openings must increase. The effect of this induced stress σ_i, is to depress the plane of the floor beds around the openings. (Figure 38a). The volume by which the plane is depressed Vr is equal to Vf. The roof beds also move down equal to the amount by which the floor is depressed plus the relaxaton Vh.

This would become a near static situation in competent elastic rocks. In potash however, because of the plastic behavior characteristics, a stress distribution similar to Figure 38b results. This is not a static situation but a continuous yield/load transfer process resulting in a transition from the case immediately after mining (Figure 38a) to a situation where confinement is sufficient to allow support of overburden loads. (Figure 38b).

The floor plane in the region of peak abutment load can similarily be depressed into the rock mass below causing not only the floor beds but also the pillar/floor bed contact for some distance into the surrounding ground to be pushed up, extruding the pillar material into the openings. This zone has been observed to penetrate in excess of 15

meters (50 feet) into the infinite wall rock around old entry systems.

Pillar instrumentation could show a variety of deformations including what may appear to be dilation depending upon where the anchors are placed with respect to the region subject to depression and when during the evolutionary process they are installed.

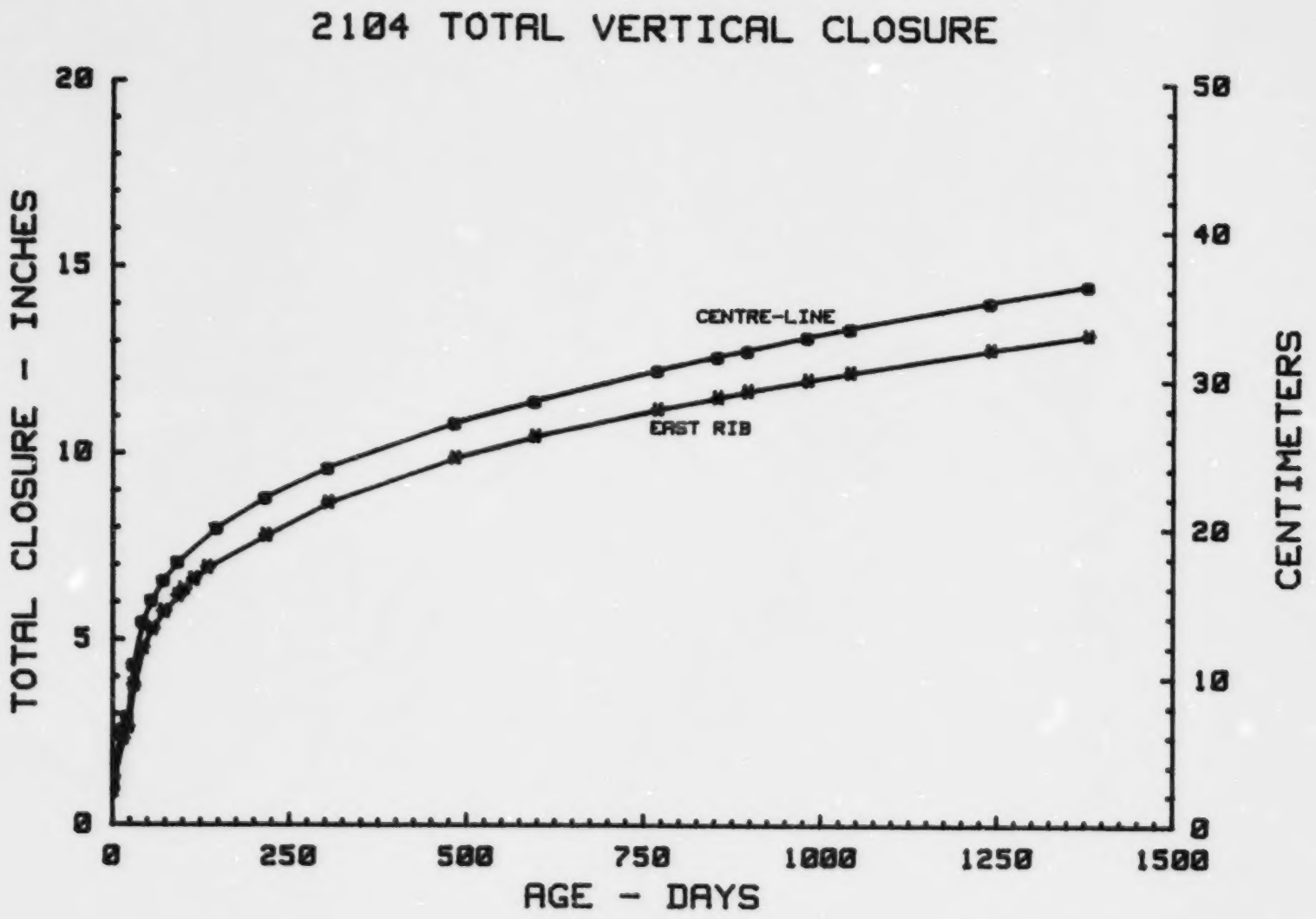
2104 TOTAL VERTICAL CLOSURE
TOTAL CLOSURE - INCHES
CENTIMETERS
AGE - DAYS
CENTRE-LINE
EAST RIB
0
5
10
15
20
0
10
20
30
40
50
0
250
500
750
1000
1250
1500

FIG. 4

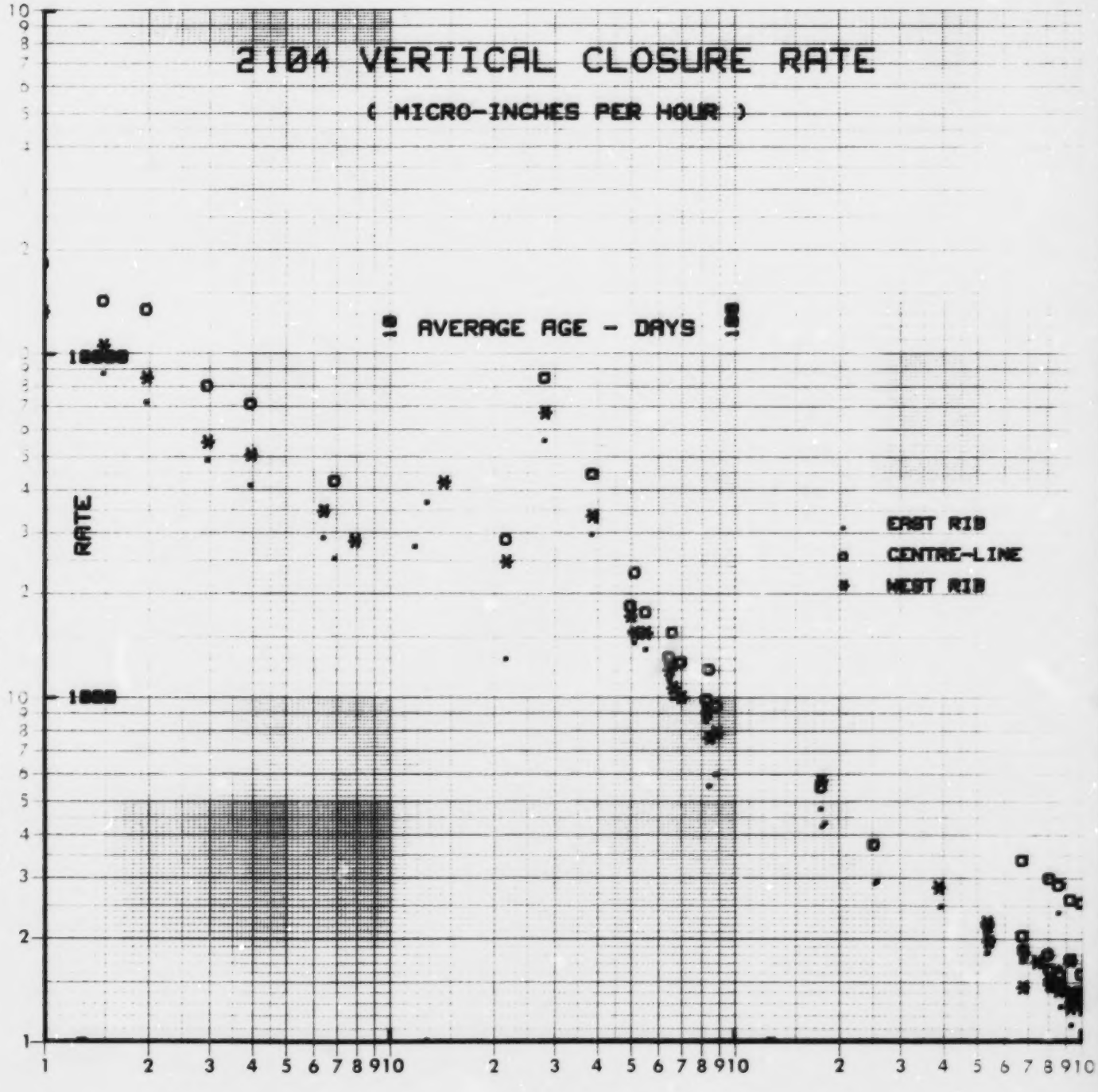
2104 VERTICAL CLOSURE RATE
(MICRO-INCHES PER HOUR)
AVERAGE AGE - DAYS
RATE
EAST RIB
CENTRE-LINE
WEST RIB
1000
1000
1
2
3
4
5
6
7
8
9
10
2
3
4
5
6
7
8
9
10
2
3
4
5
6
7
8
9
10

FIG. 5

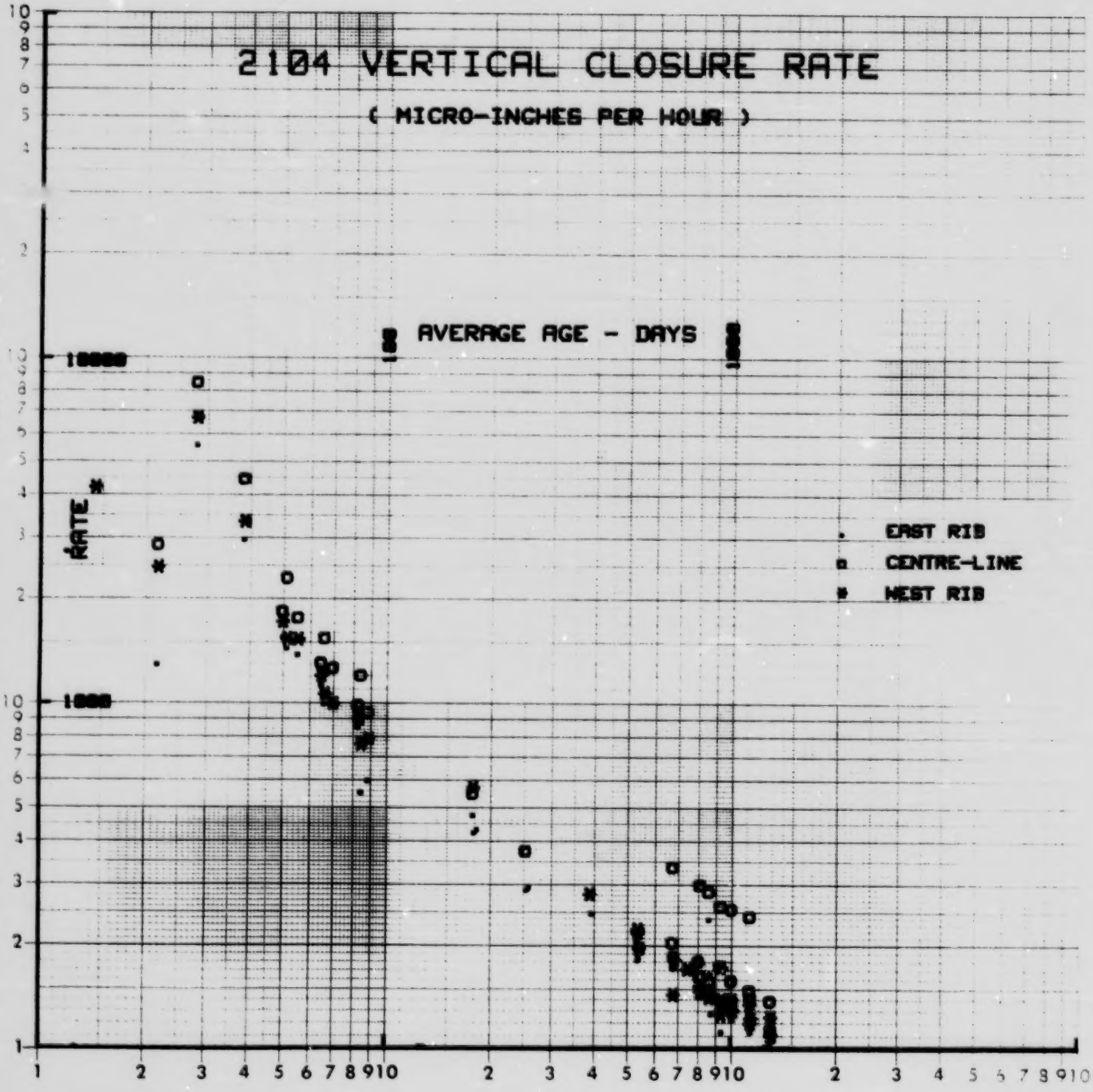
2104 VERTICAL CLOSURE RATE
(MICRO-INCHES PER HOUR)
AVERAGE AGE - DAYS
RATE
EAST RIB
CENTRE-LINE
WEST RIB
GRF G120 LOGARITHMIC
SPECIFY TRACING OR DRAWING PAPER

FIG. 6

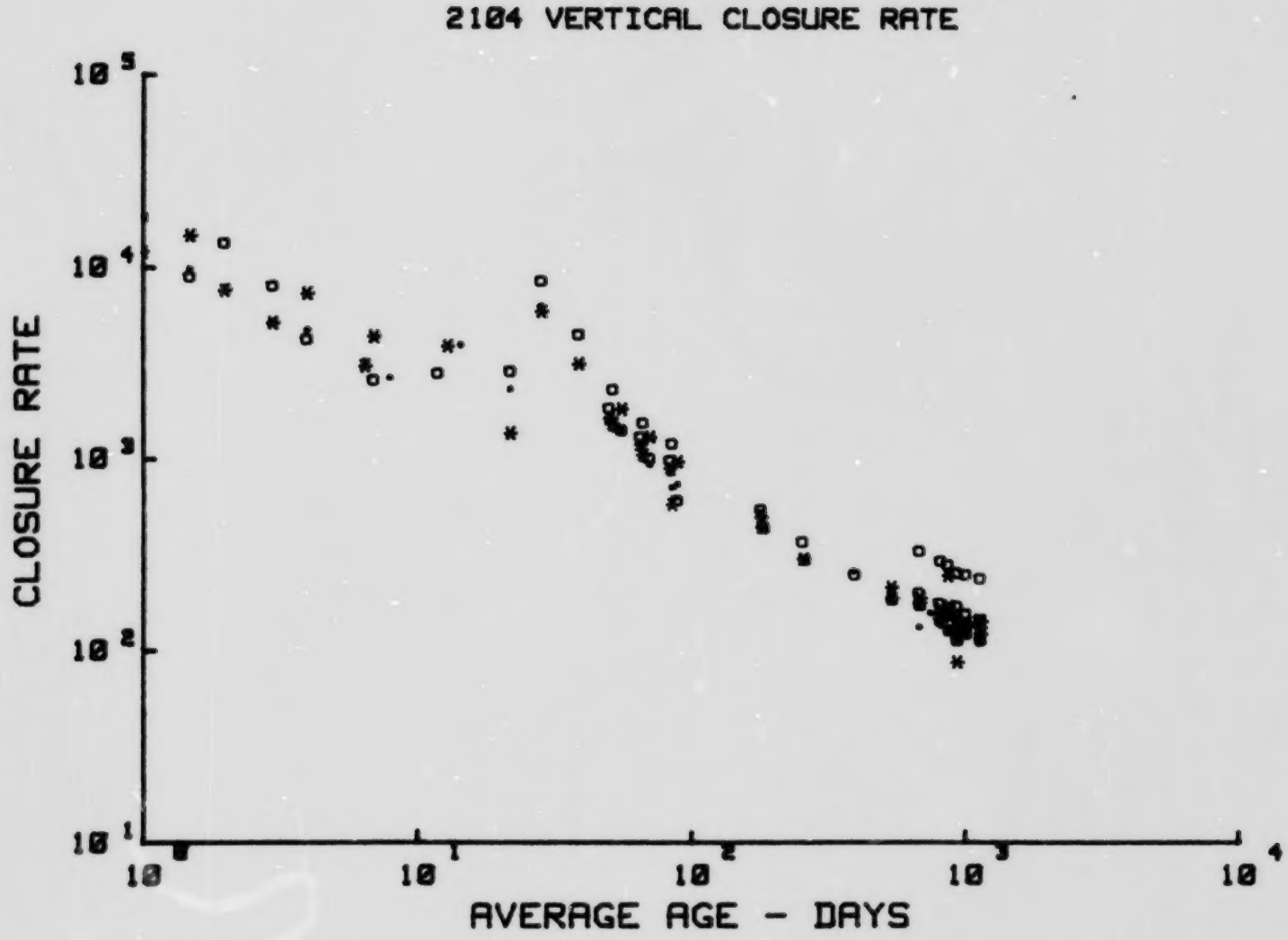

FIG. 7

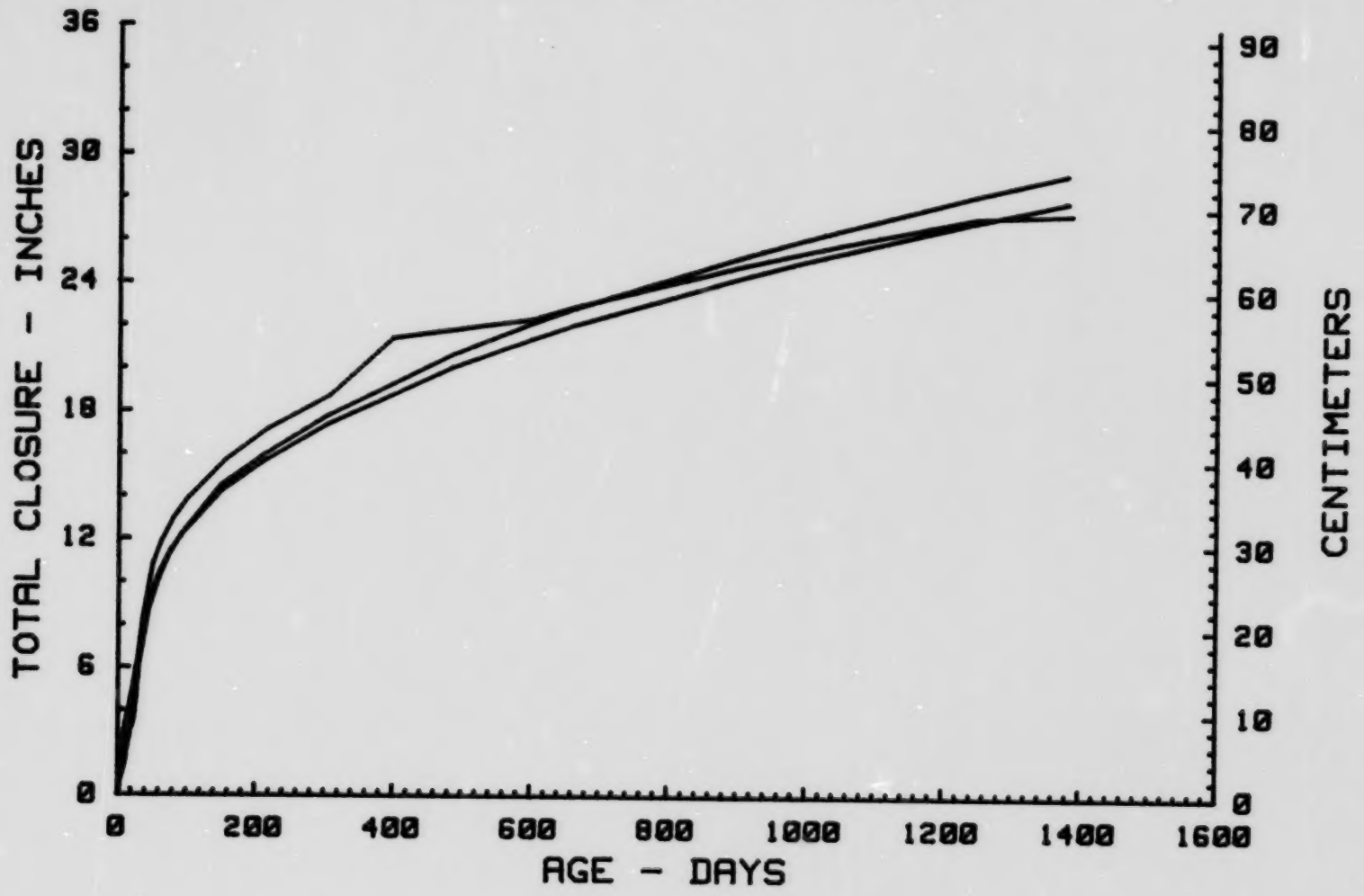
2104 HORIZONTAL CLOSURE
TOTAL CLOSURE - INCHES
36
30
24
18
12
6
0
CENTIMETERS
90
80
70
60
50
40
30
20
10
0
0
200
400
600
800
1000
1200
1400
1600
AGE - DAYS

FIG. 8

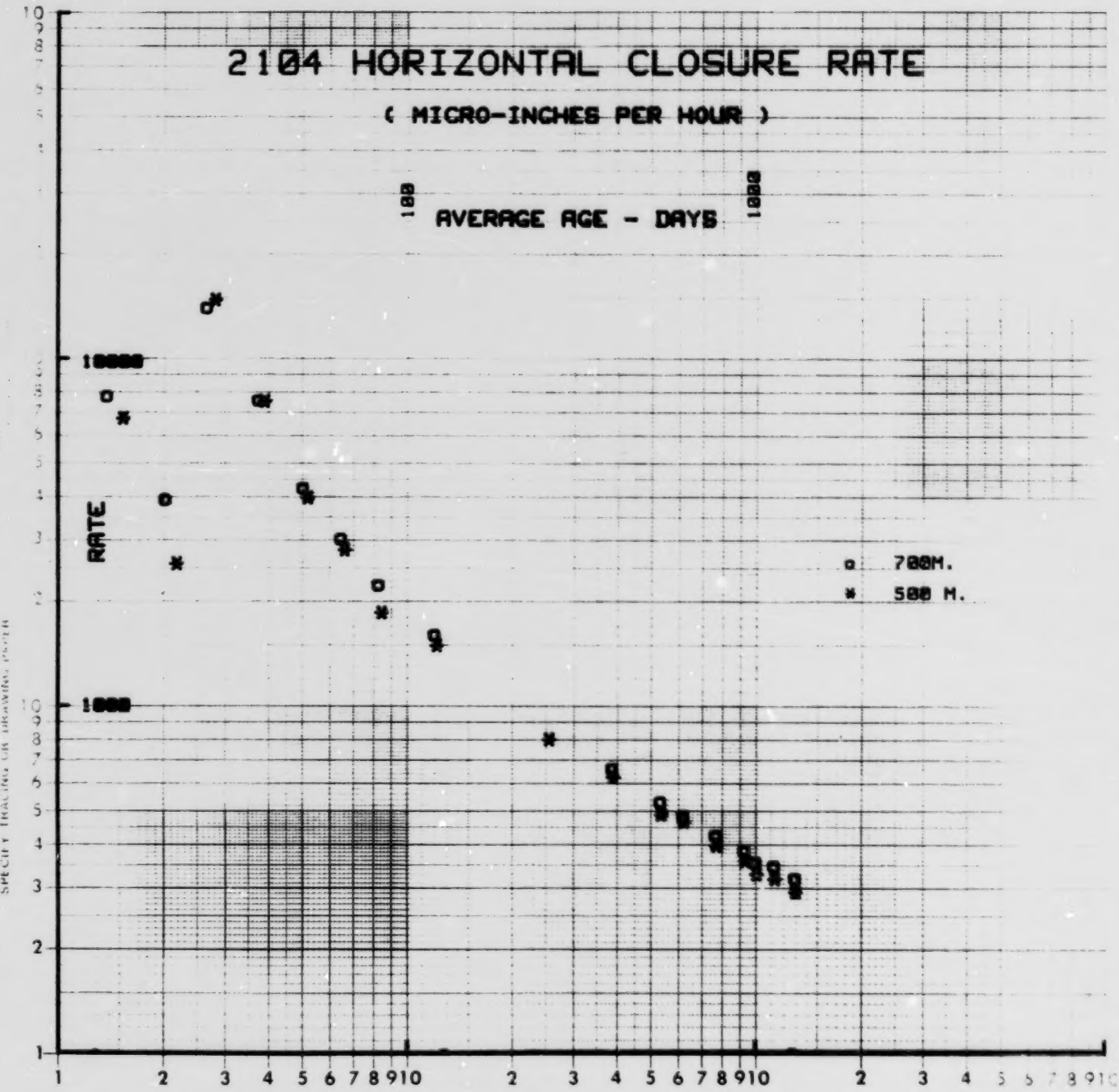
2104 HORIZONTAL CLOSURE RATE
(MICRO-INCHES PER HOUR)
AVERAGE AGE - DAYS
RATE
700M.
500 M.

FIG. 9

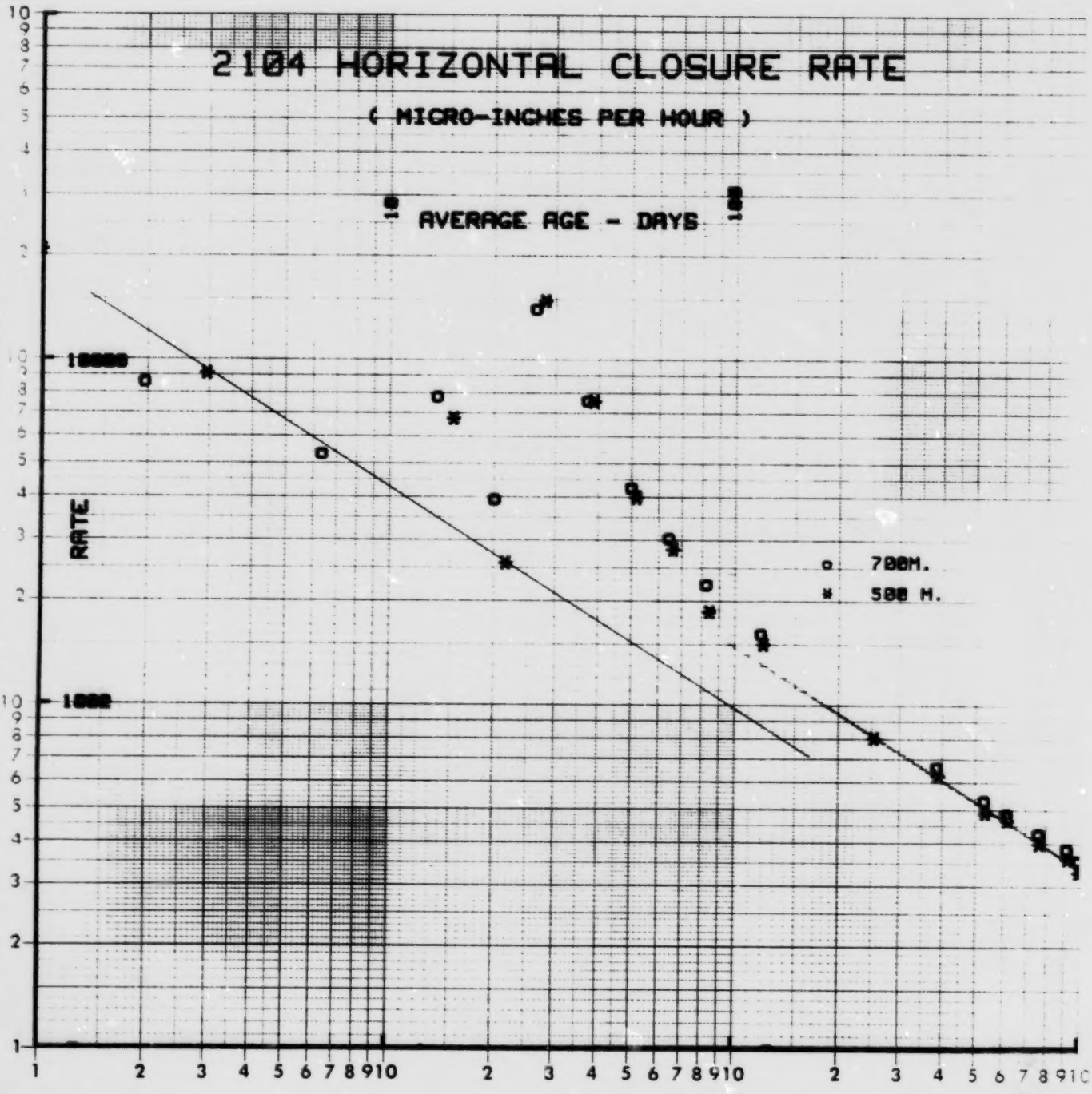
2104 HORIZONTAL CLOSURE RATE
(MICRO-INCHES PER HOUR)
AVERAGE AGE - DAYS
RATE
10000
1000
o 700M.
* 500 M.

FIG. 10

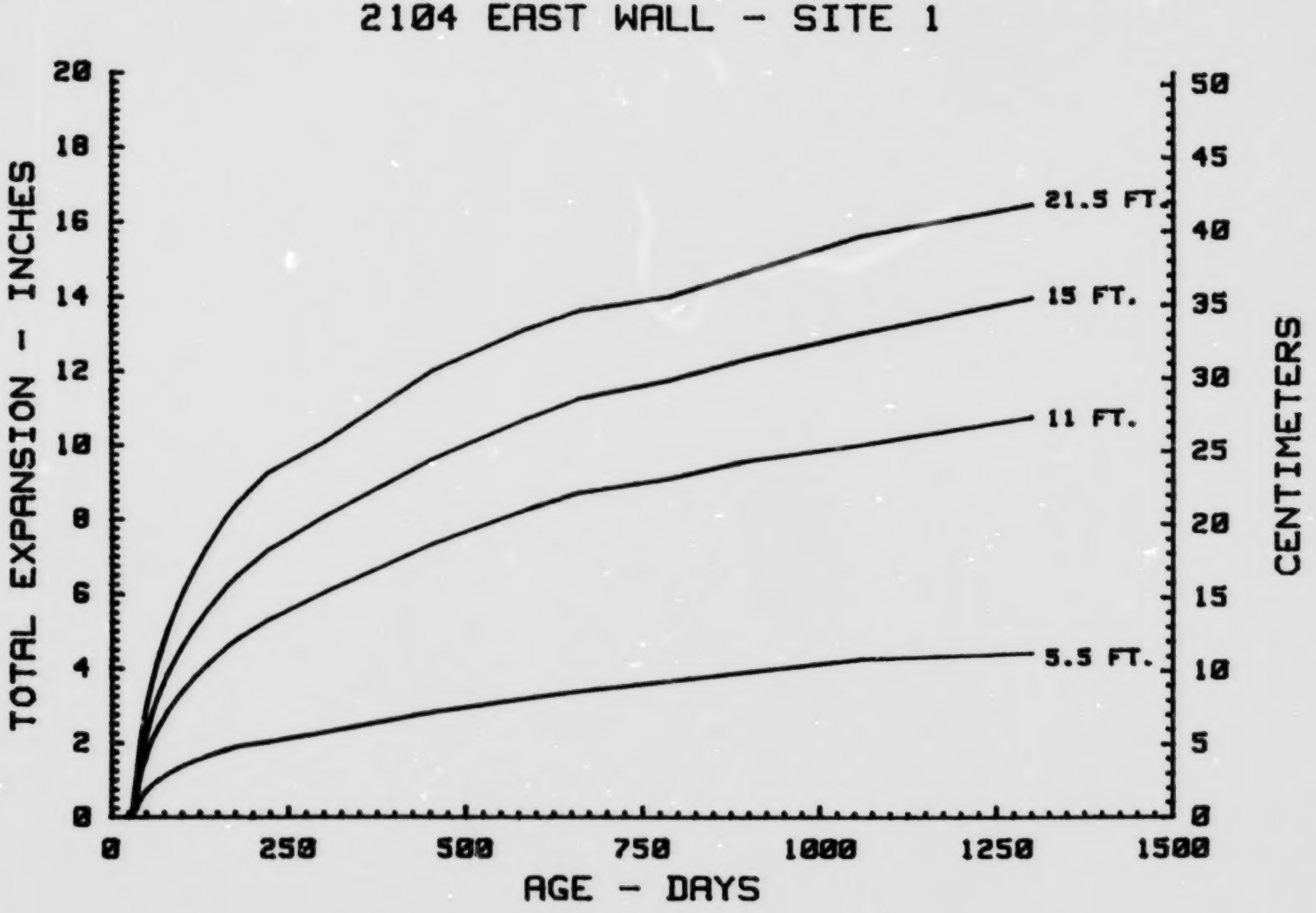
2104 EAST WALL - SITE 1
TOTAL EXPANSION - INCHES
CENTIMETERS
AGE - DAYS
21.5 FT.
15 FT.
11 FT.
5.5 FT.
0
2
4
6
8
10
12
14
16
18
20
0
5
10
15
20
25
30
35
40
45
50
0
250
500
750
1000
1250
1500

FIG. 11

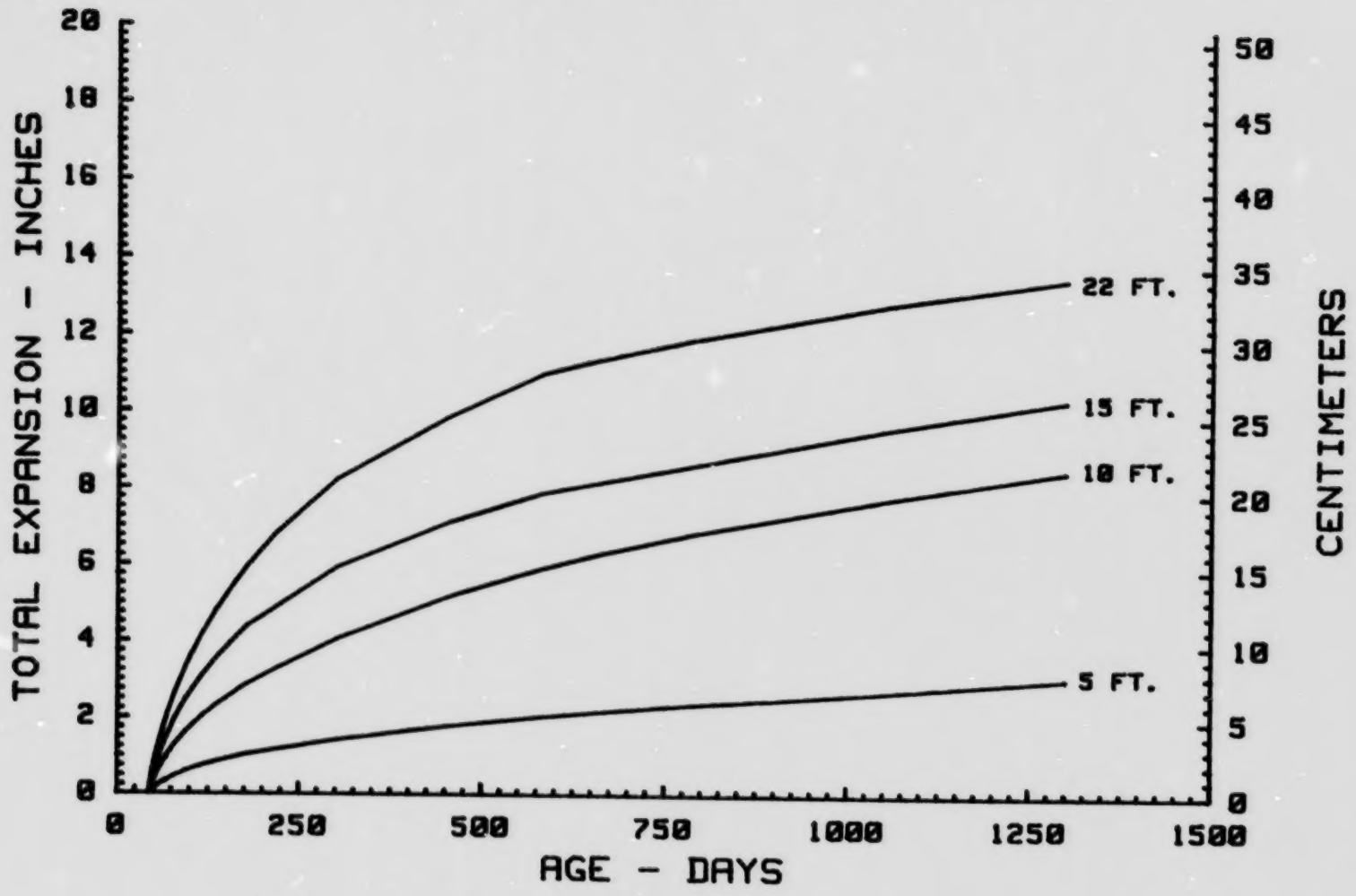
2104 EAST WALL - SITE 2
TOTAL EXPANSION - INCHES
0
2
4
6
8
10
12
14
16
18
20
CENTIMETERS
0
5
10
15
20
25
30
35
40
45
50
22 FT.
15 FT.
10 FT.
5 FT.
0
250
500
750
1000
1250
1500
AGE - DAYS

FIG. 12

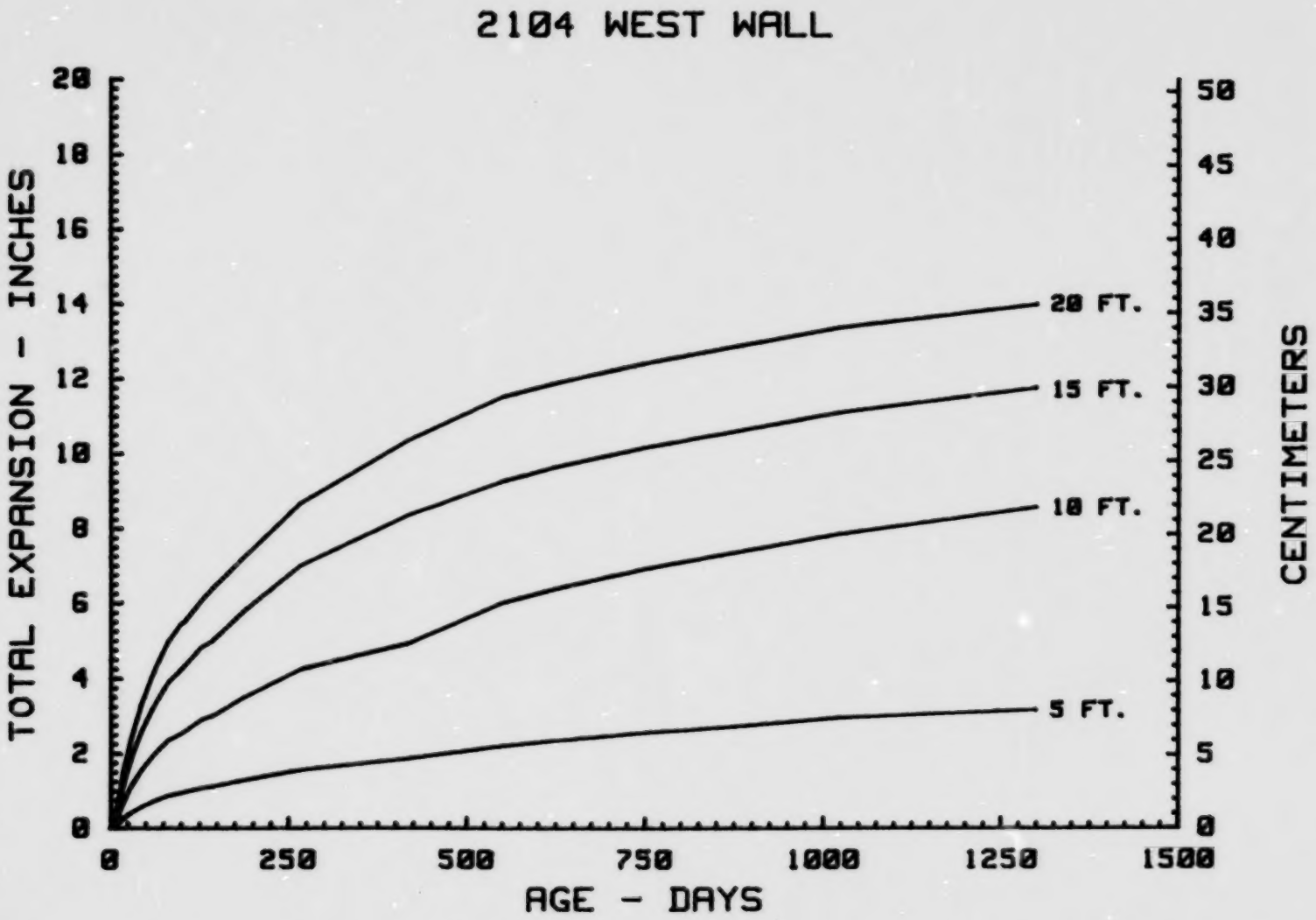
2104 WEST WALL
TOTAL EXPANSION - INCHES
CENTIMETERS
AGE - DAYS
20 FT.
15 FT.
10 FT.
5 FT.
0
2
4
6
8
10
12
14
16
18
20
0
5
10
15
20
25
30
35
40
45
50
0
250
500
750
1000
1250
1500

FIG. 13

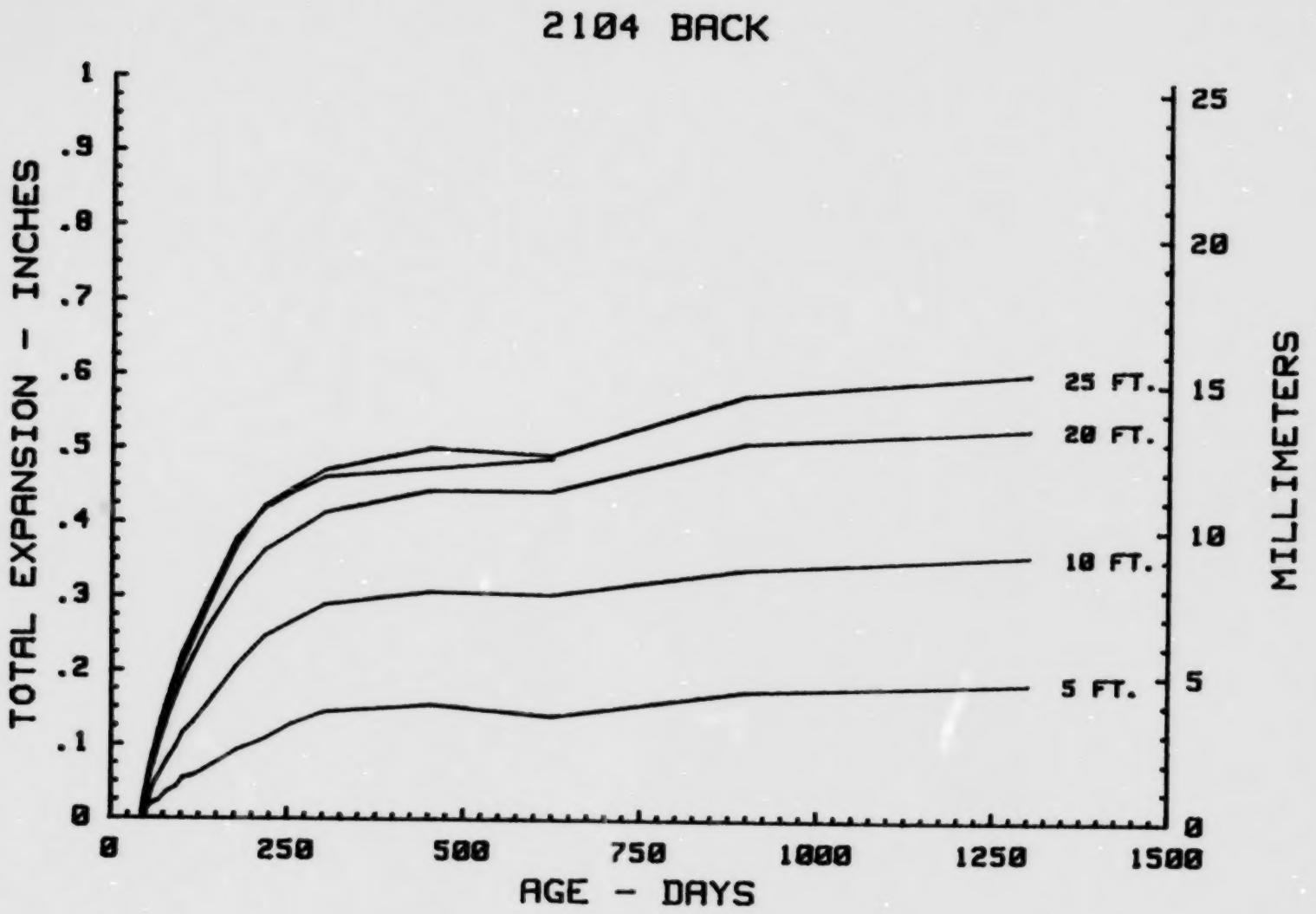
2104 BACK
TOTAL EXPANSION - INCHES
0
.1
.2
.3
.4
.5
.6
.7
.8
.9
1
MILLIMETERS
0
5
10
15
20
25
0
250
500
750
1000
1250
1500
AGE - DAYS
25 FT.
20 FT.
10 FT.
5 FT.

FIG. 14

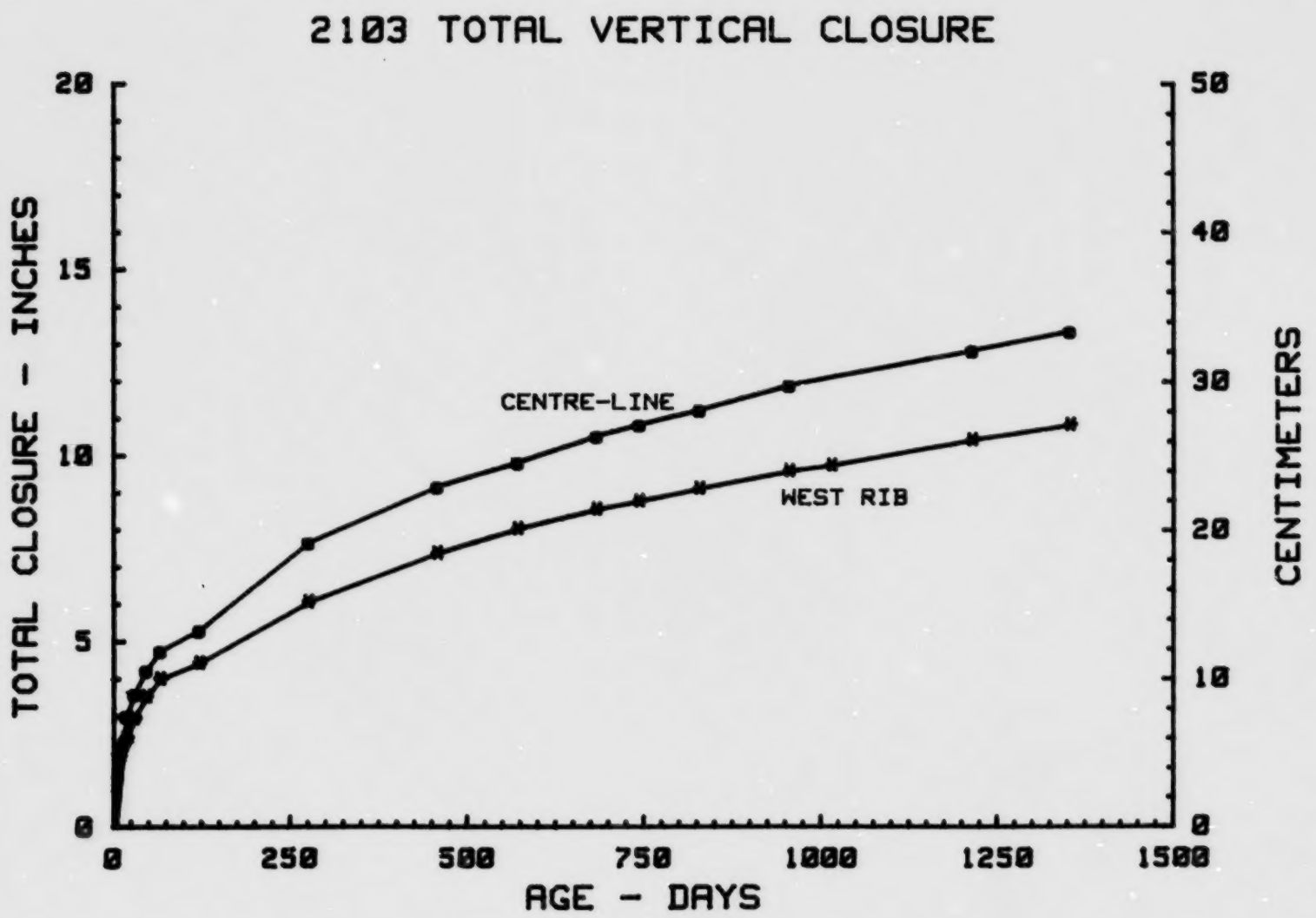
2103 TOTAL VERTICAL CLOSURE
TOTAL CLOSURE - INCHES
CENTIMETERS
AGE - DAYS
CENTRE-LINE
WEST RIB
0
5
10
15
20
0
10
20
30
40
50
0
250
500
750
1000
1250
1500

FIG. 15

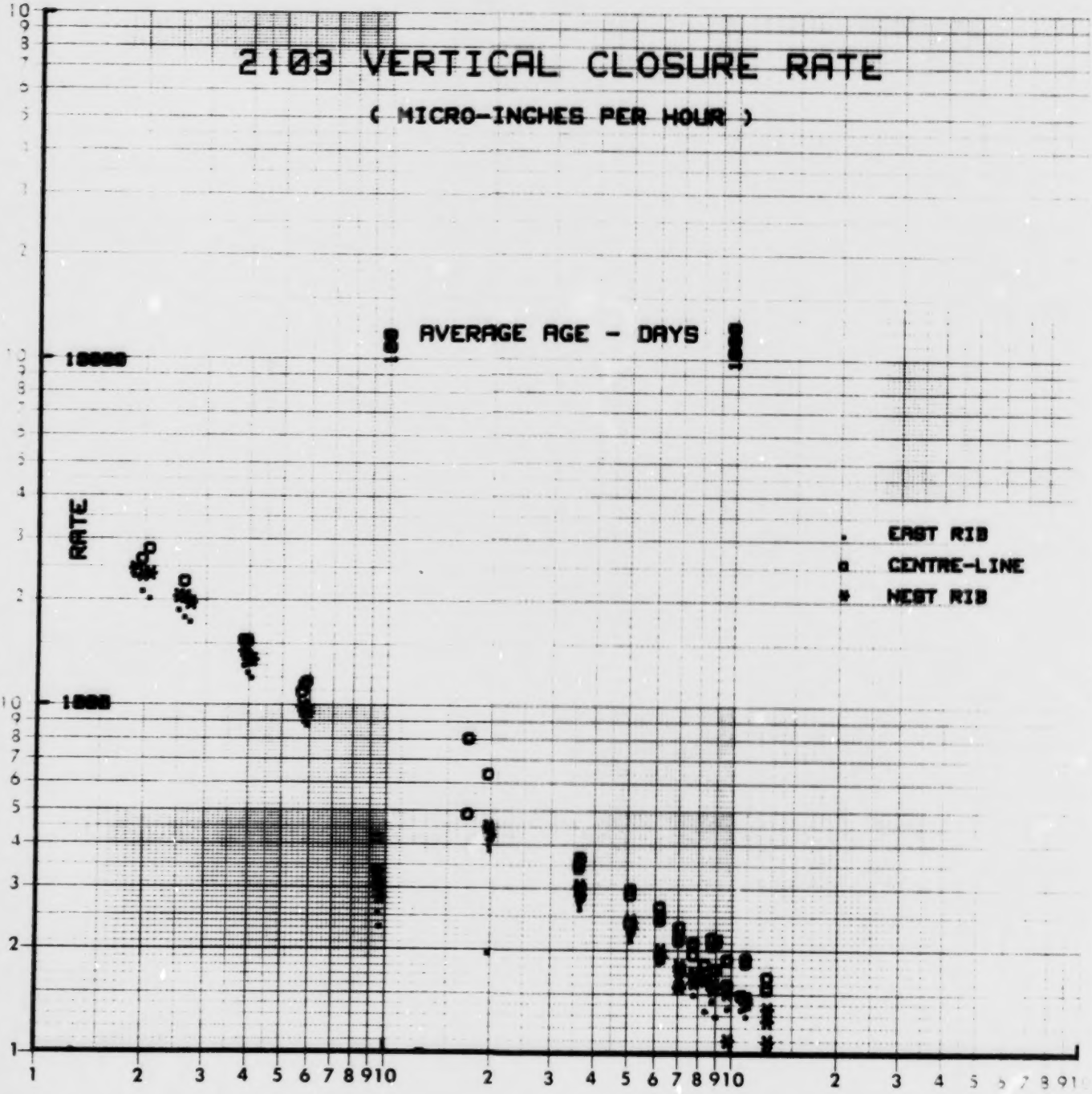
2103 VERTICAL CLOSURE RATE
(MICRO-INCHES PER HOUR)
AVERAGE AGE - DAYS
RATE
EAST RIB
CENTRE-LINE
WEST RIB

FIG. 16

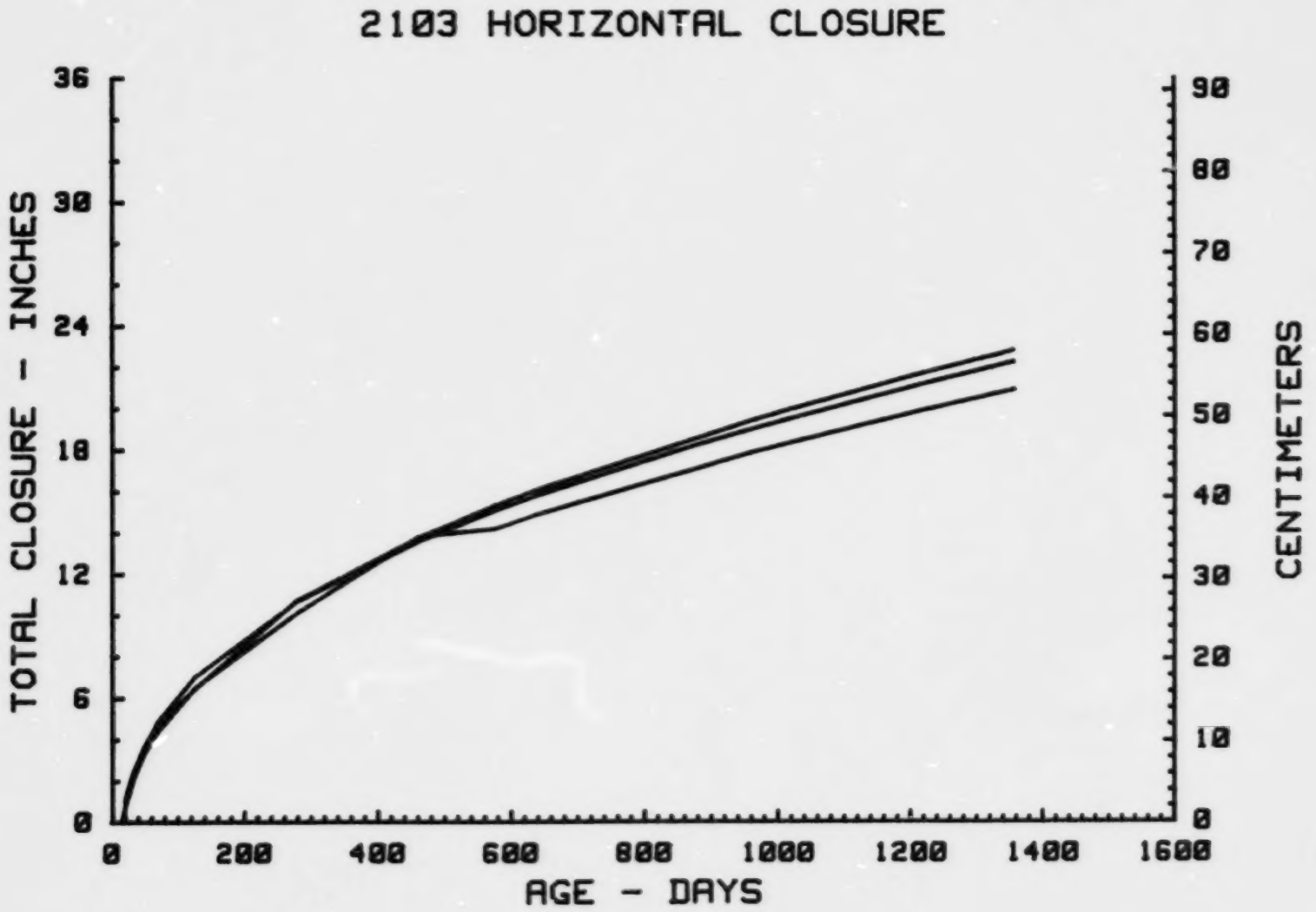
2103 HORIZONTAL CLOSURE
TOTAL CLOSURE - INCHES
0
6
12
18
24
30
36
CENTIMETERS
0
10
20
30
40
50
60
70
80
90
0
200
400
600
800
1000
1200
1400
1600
AGE - DAYS

FIG. 17

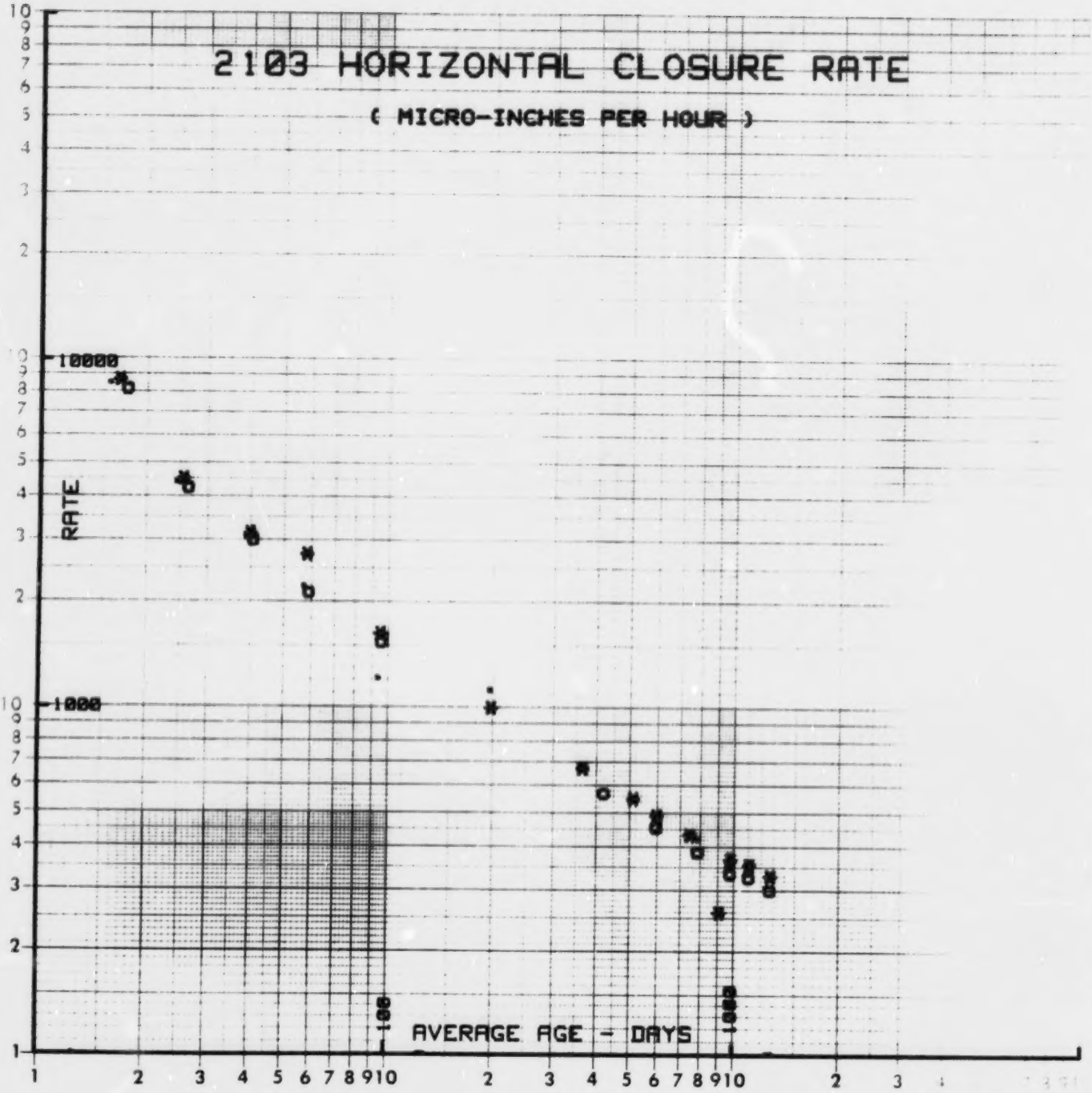
2103 HORIZONTAL CLOSURE RATE
(MICRO-INCHES PER HOUR)
RATE
10000
1000
100
AVERAGE AGE - DAYS
1 2 3 4 5 6 7 8 9 10 2 3 4 5 6 7 8 9 10 2 3

FIG. 18

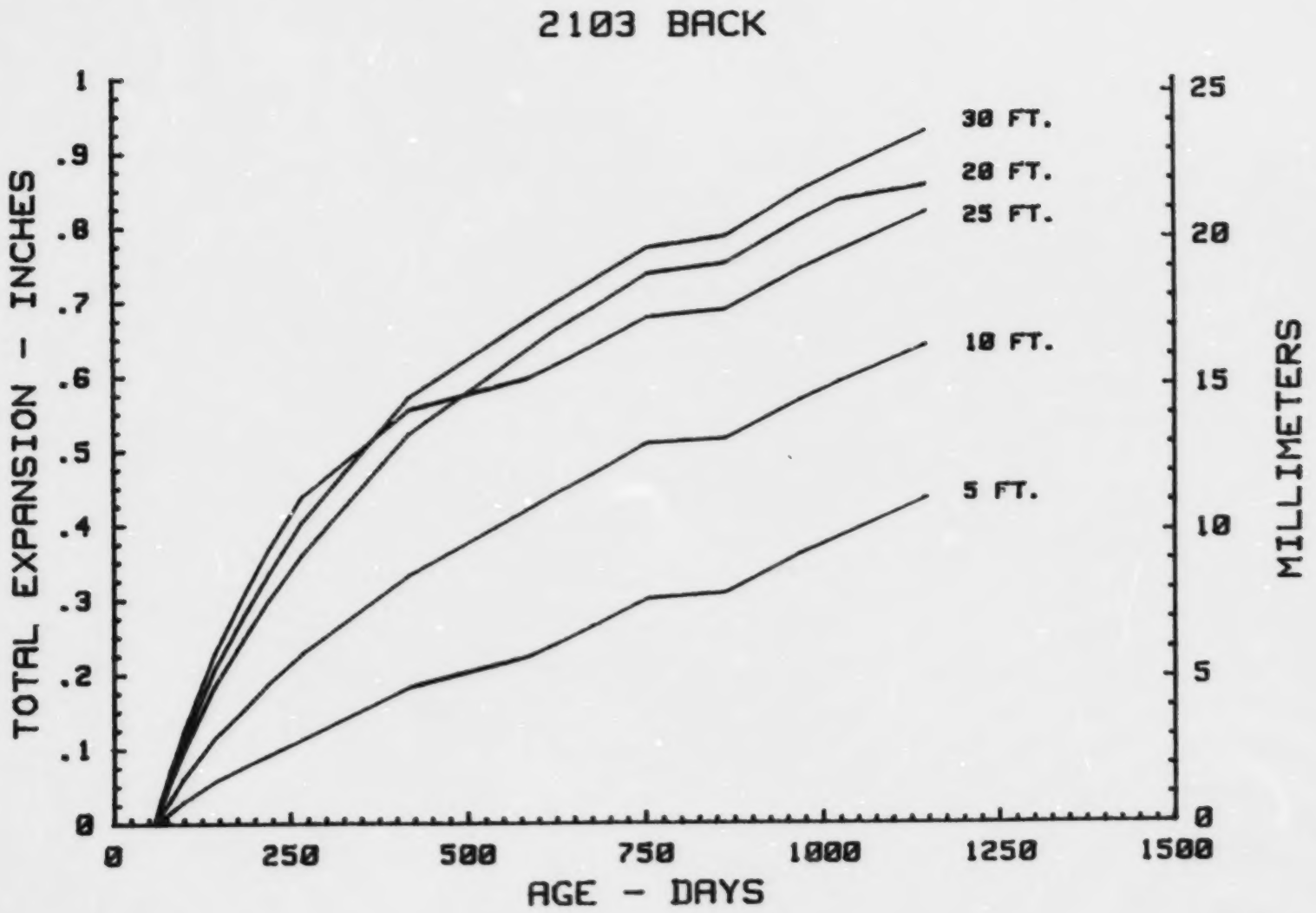
2103 BACK
TOTAL EXPANSION - INCHES
1
.9
.8
.7
.6
.5
.4
.3
.2
.1
0
MILLIMETERS
25
20
15
10
5
0
30 FT.
20 FT.
25 FT.
10 FT.
5 FT.
0
250
500
750
1000
1250
1500
AGE - DAYS

FIG. 19

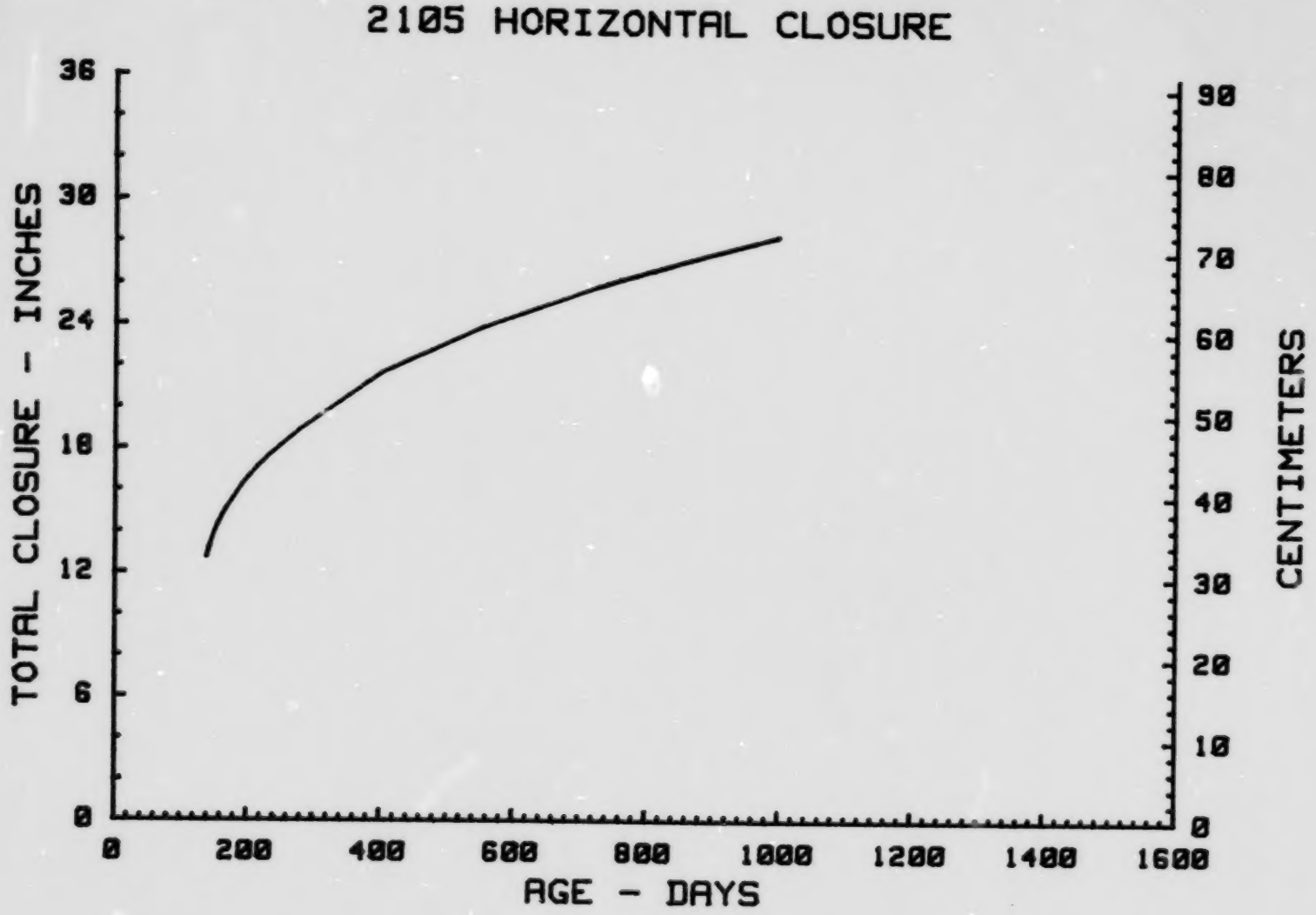
2105 HORIZONTAL CLOSURE
TOTAL CLOSURE - INCHES
0
6
12
18
24
30
36
CENTIMETERS
0
10
20
30
40
50
60
70
80
90
0
200
400
600
800
1000
1200
1400
1600
AGE - DAYS

FIG. 20

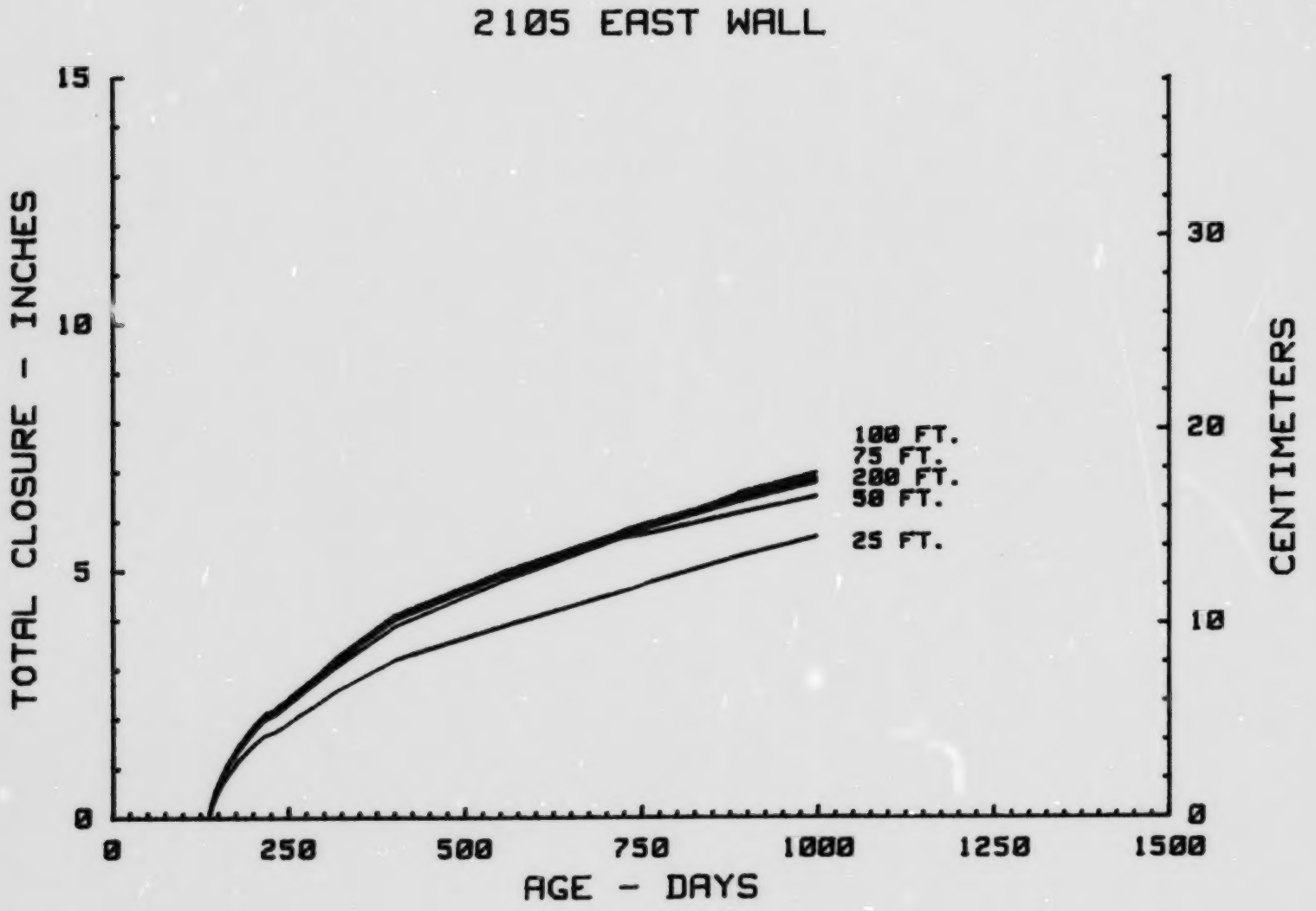
2105 EAST WALL
TOTAL CLOSURE - INCHES
CENTIMETERS
AGE - DAYS
100 FT.
75 FT.
200 FT.
50 FT.
25 FT.
0
5
10
15
0
10
20
30
0
250
500
750
1000
1250
1500

FIG. 21

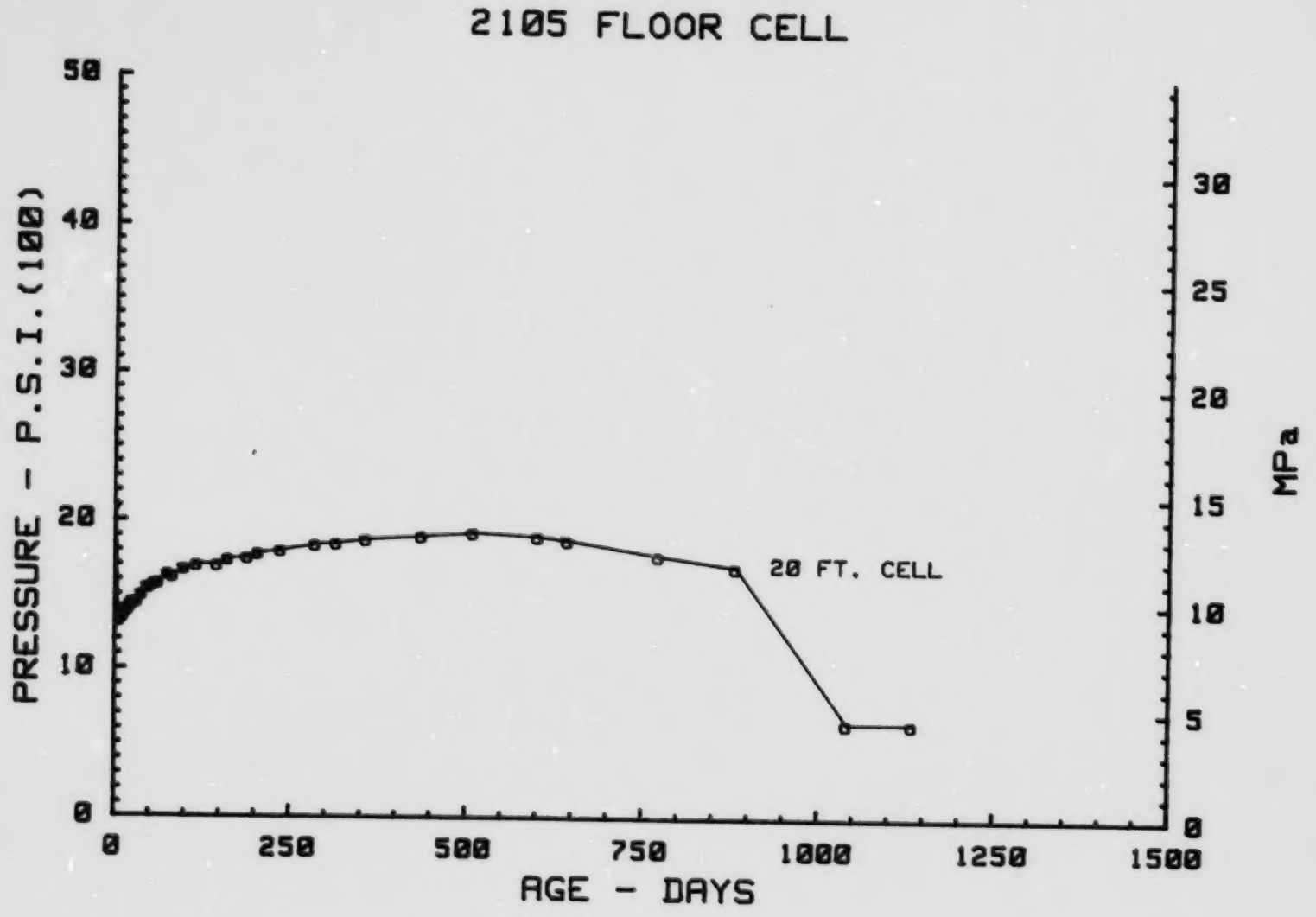
2105 FLOOR CELL
PRESSURE - P.S.I.(100)
50
40
30
20
10
0
MPa
30
25
20
15
10
5
0
20 FT. CELL
0
250
500
750
1000
1250
1500
AGE - DAYS

FIG. 22

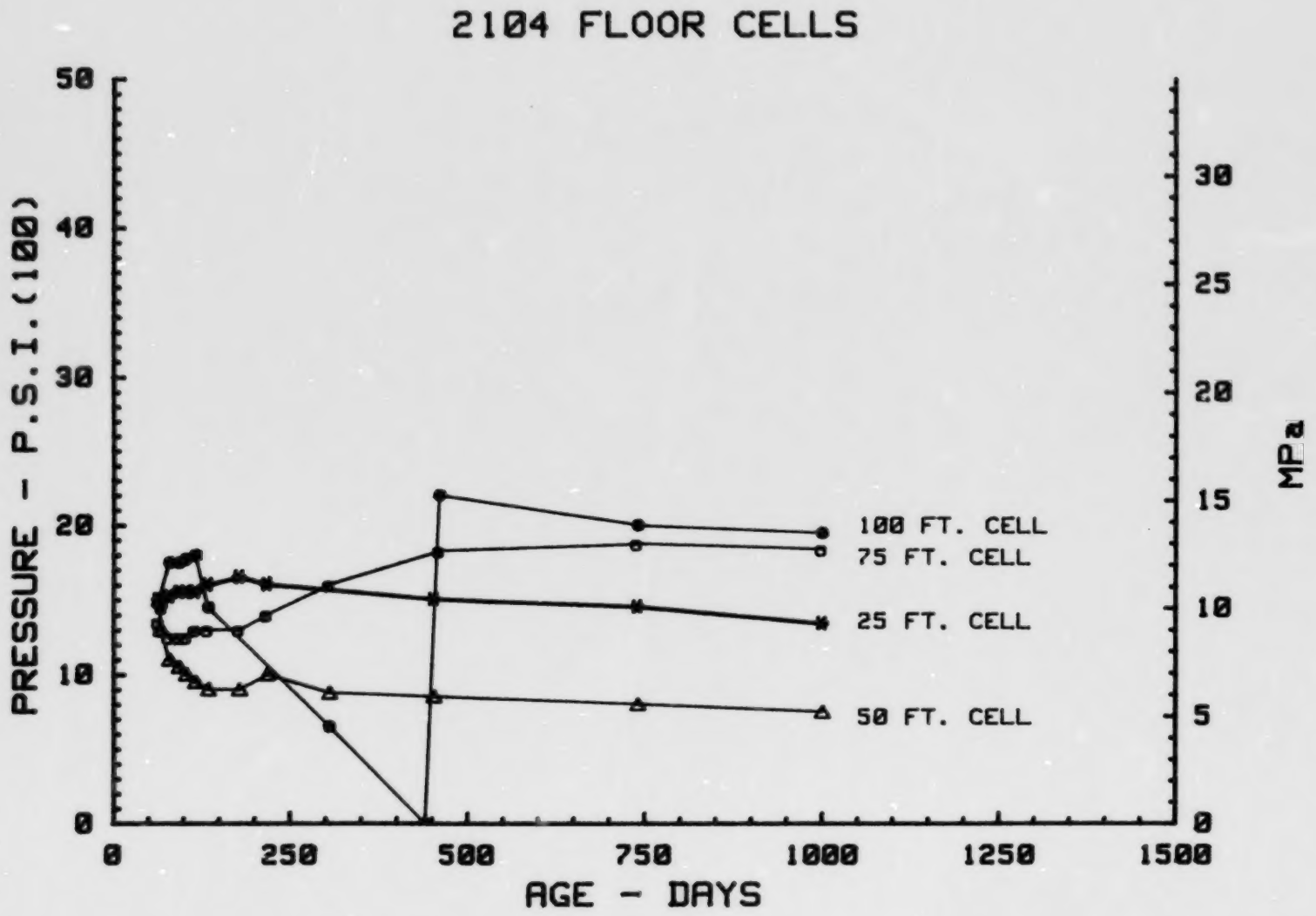
2104 FLOOR CELLS
PRESSURE - P.S.I.(100)
MPa
AGE - DAYS
0
10
20
30
40
50
0
5
10
15
20
25
30
0
250
500
750
1000
1250
1500
100 FT. CELL
75 FT. CELL
25 FT. CELL
50 FT. CELL

FIG. 23

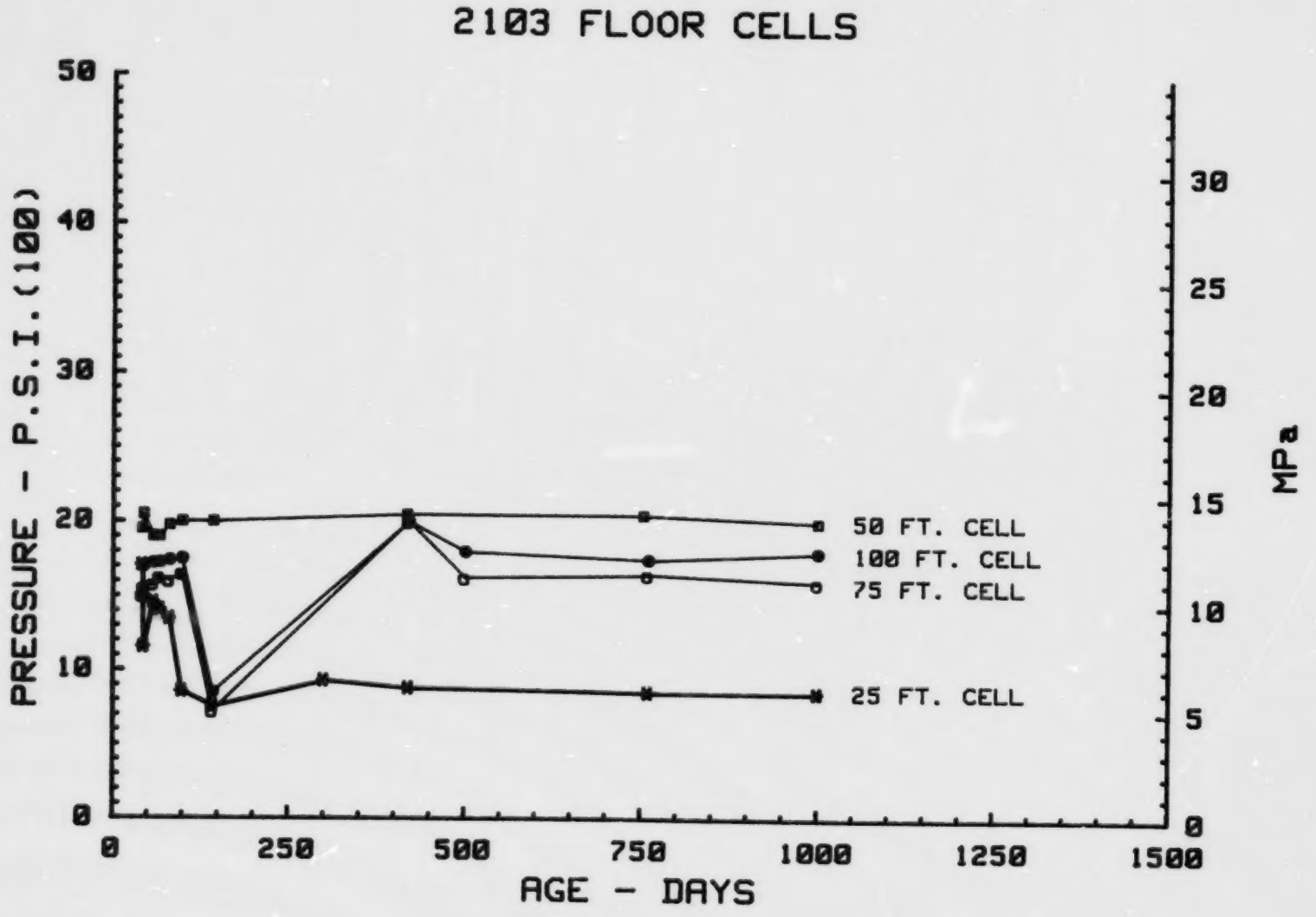
2103 FLOOR CELLS
PRESSURE - P.S.I.(100)
MPa
AGE - DAYS
50 FT. CELL
100 FT. CELL
75 FT. CELL
25 FT. CELL
0
10
20
30
40
50
0
5
10
15
20
25
30
0
250
500
750
1000
1250
1500

FIG. 24

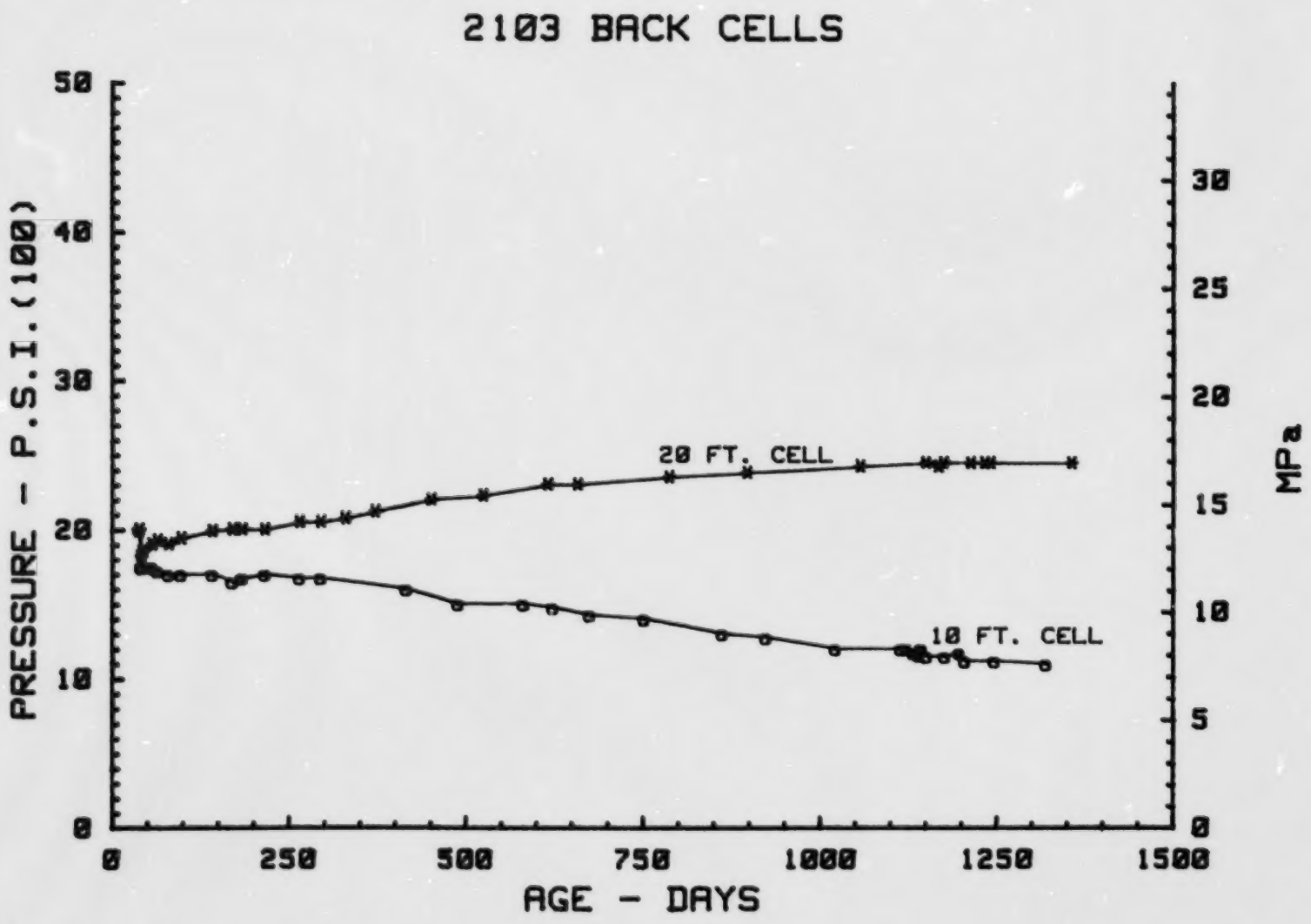
2103 BACK CELLS
PRESSURE - P.S.I.(100)
50
40
30
20
10
0
30
25
20
15
10
5
0
MPa
20 FT. CELL
10 FT. CELL
0
250
500
750
1000
1250
1500
AGE - DAYS

FIG. 25

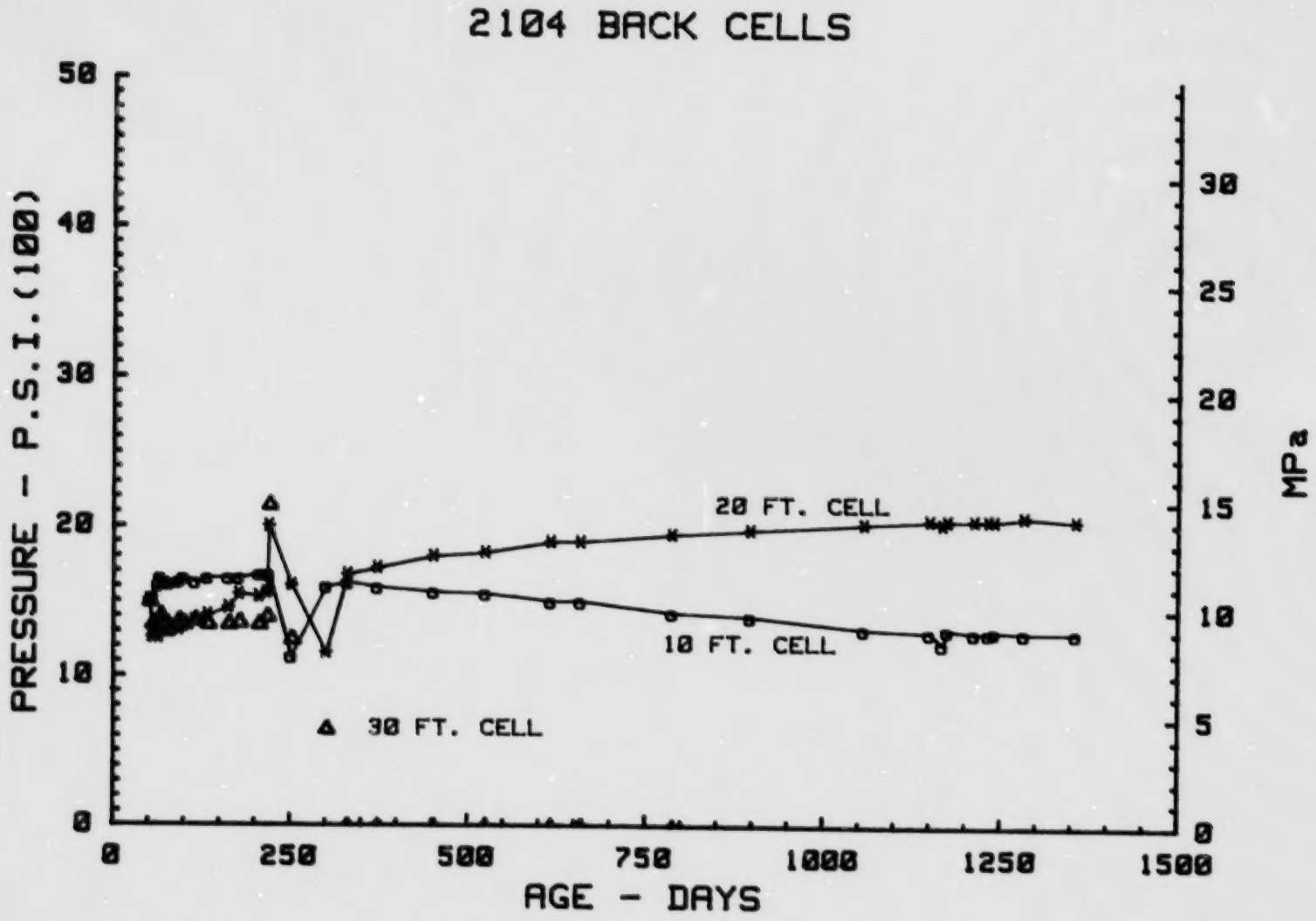
2104 BACK CELLS
PRESSURE - P.S.I.(100)
MPa
AGE - DAYS
20 FT. CELL
10 FT. CELL
30 FT. CELL
0
10
20
30
40
50
0
5
10
15
20
25
30
0
250
500
750
1000
1250
1500

FIG. 26

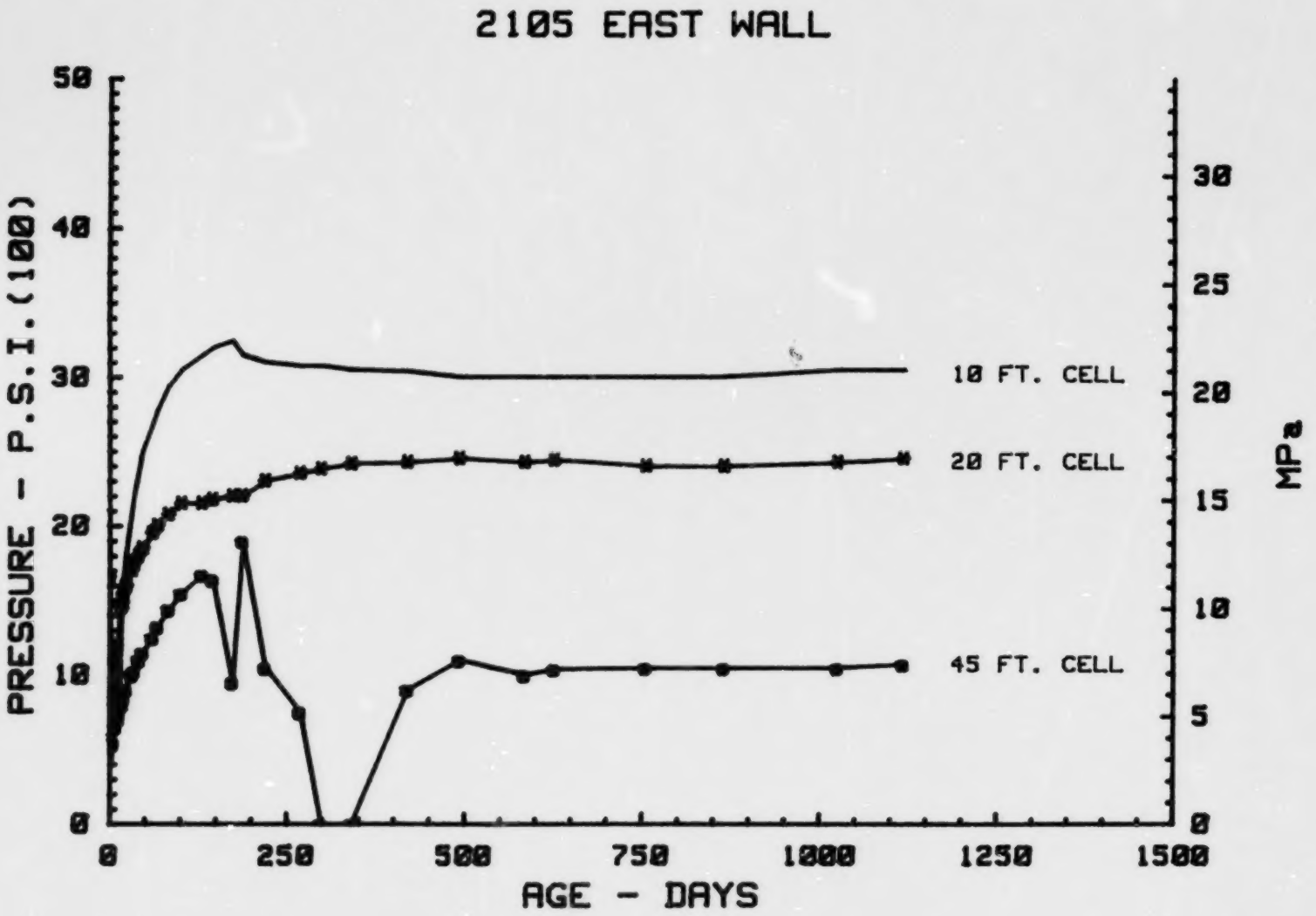
2105 EAST WALL
PRESSURE - P.S.I.(100)
50
40
30
20
10
0
30
25
20
15
10
5
0
MPa
10 FT. CELL
20 FT. CELL
45 FT. CELL
0
250
500
750
1000
1250
1500
AGE - DAYS

FIG. 27

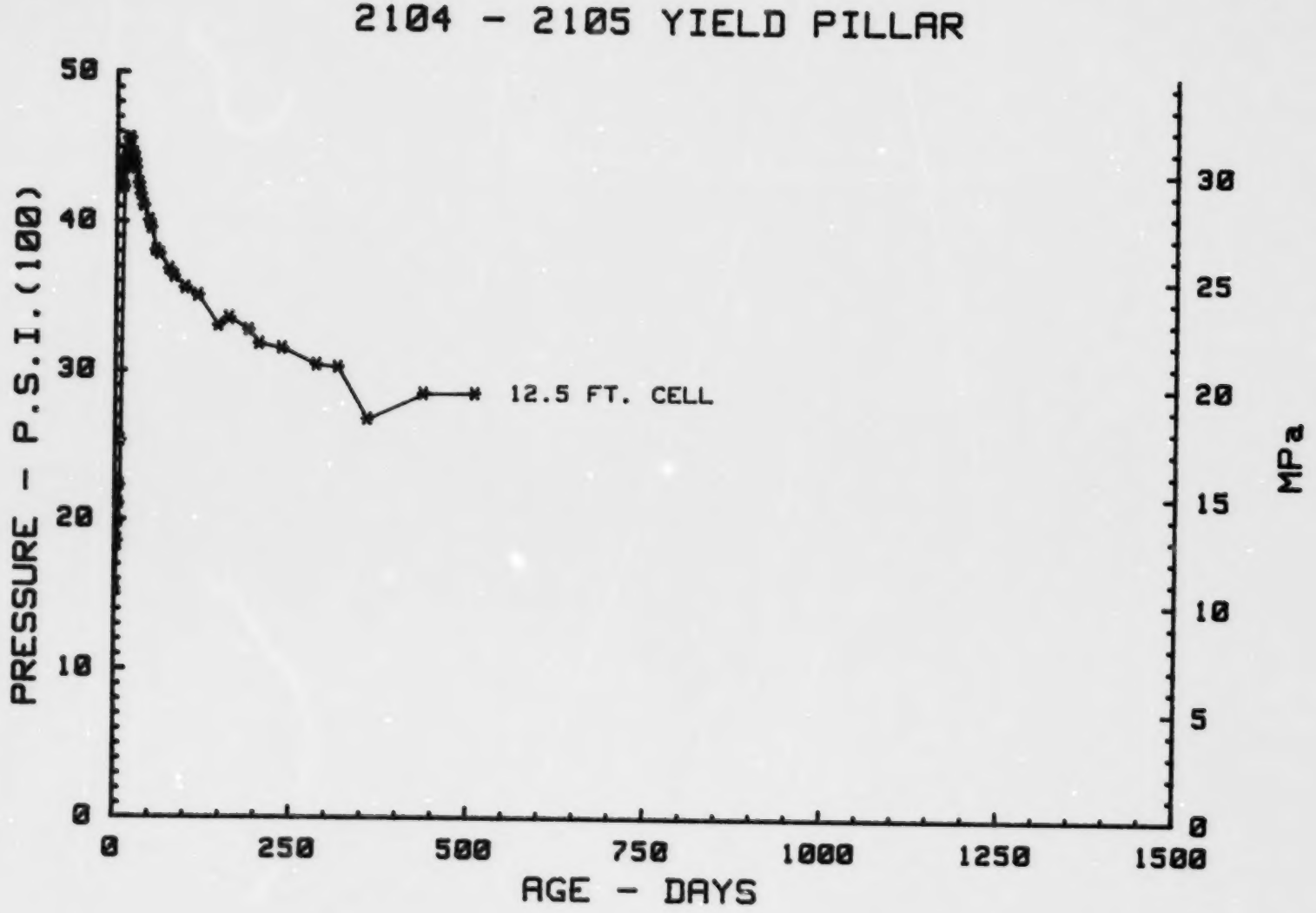
2104 - 2105 YIELD PILLAR
PRESSURE - P.S.I.(100)
50
40
30
20
10
0
12.5 FT. CELL
0
250
500
750
1000
1250
1500
AGE - DAYS
MPa
30
25
20
15
10
5
0

FIG. 28

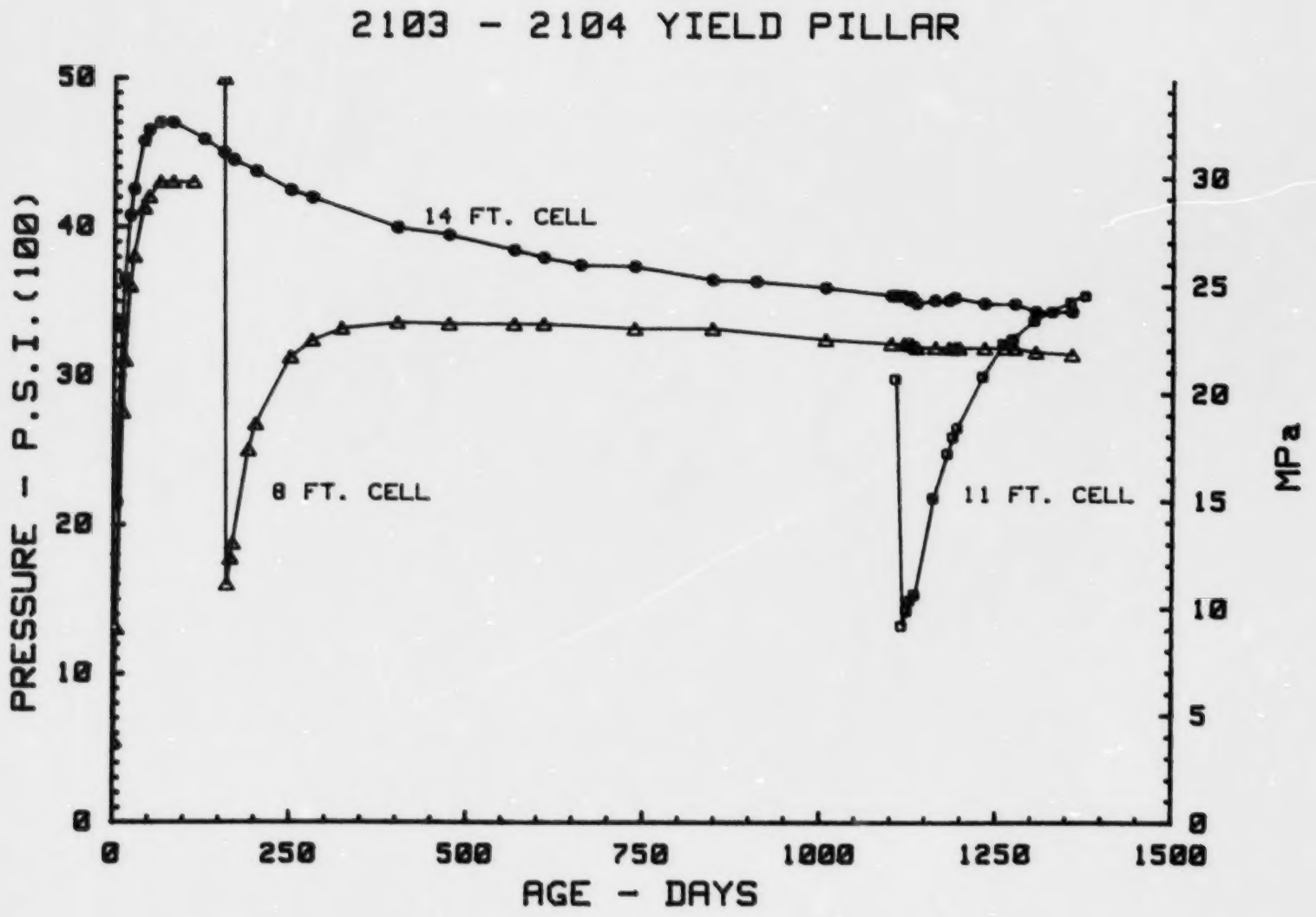
2103 - 2104 YIELD PILLAR
PRESSURE - P.S.I.(100)
MPa
AGE - DAYS
14 FT. CELL
8 FT. CELL
11 FT. CELL
0
10
20
30
40
50
0
5
10
15
20
25
30
0
250
500
750
1000
1250
1500

FIG. 29

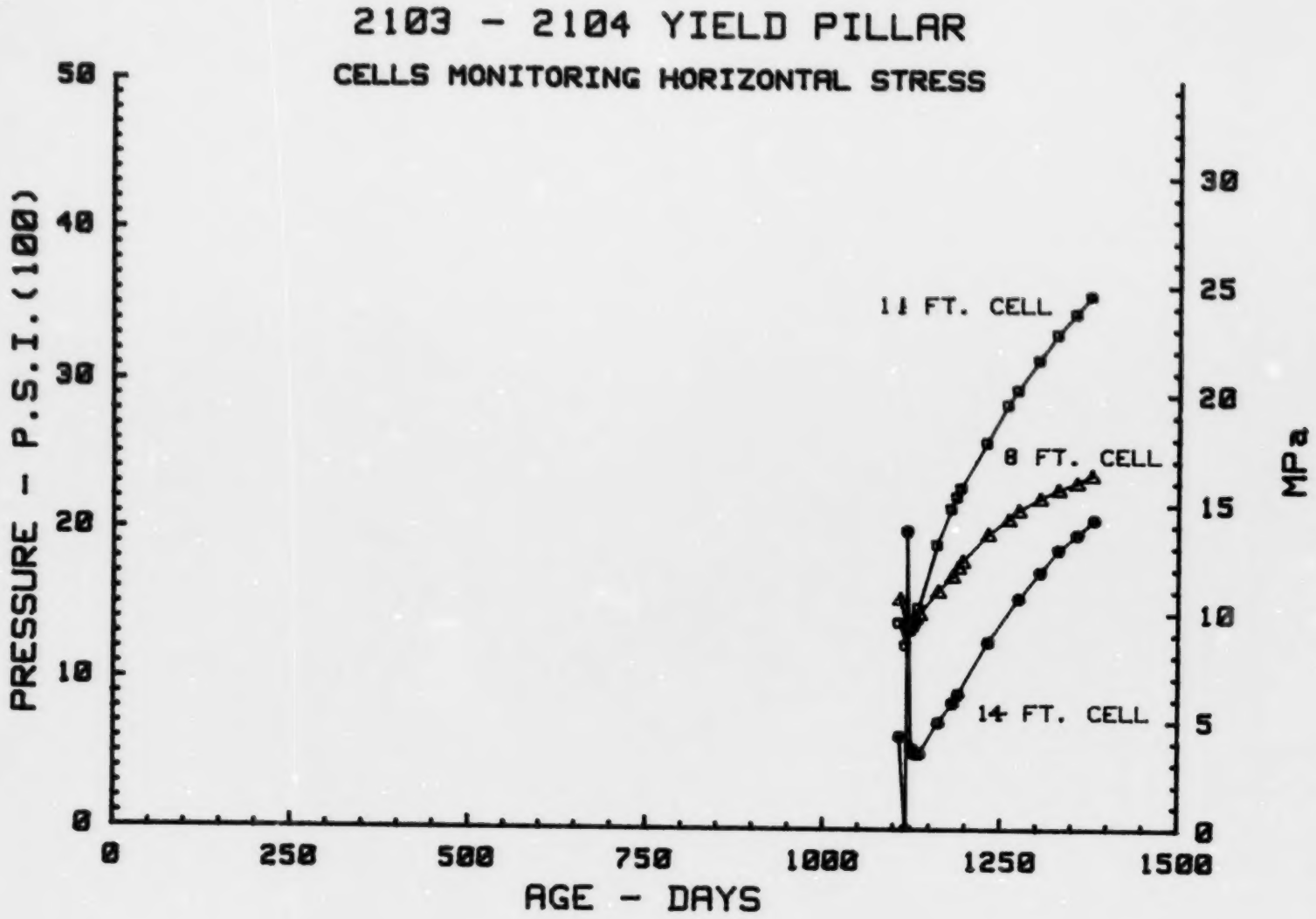
2103 - 2104 YIELD PILLAR
CELLS MONITORING HORIZONTAL STRESS
PRESSURE - P.S.I.(100)
50
40
30
20
10
0
MPa
30
25
20
15
10
5
0
11 FT. CELL
8 FT. CELL
14 FT. CELL
0
250
500
750
1000
1250
1500
AGE - DAYS

FIG. 30

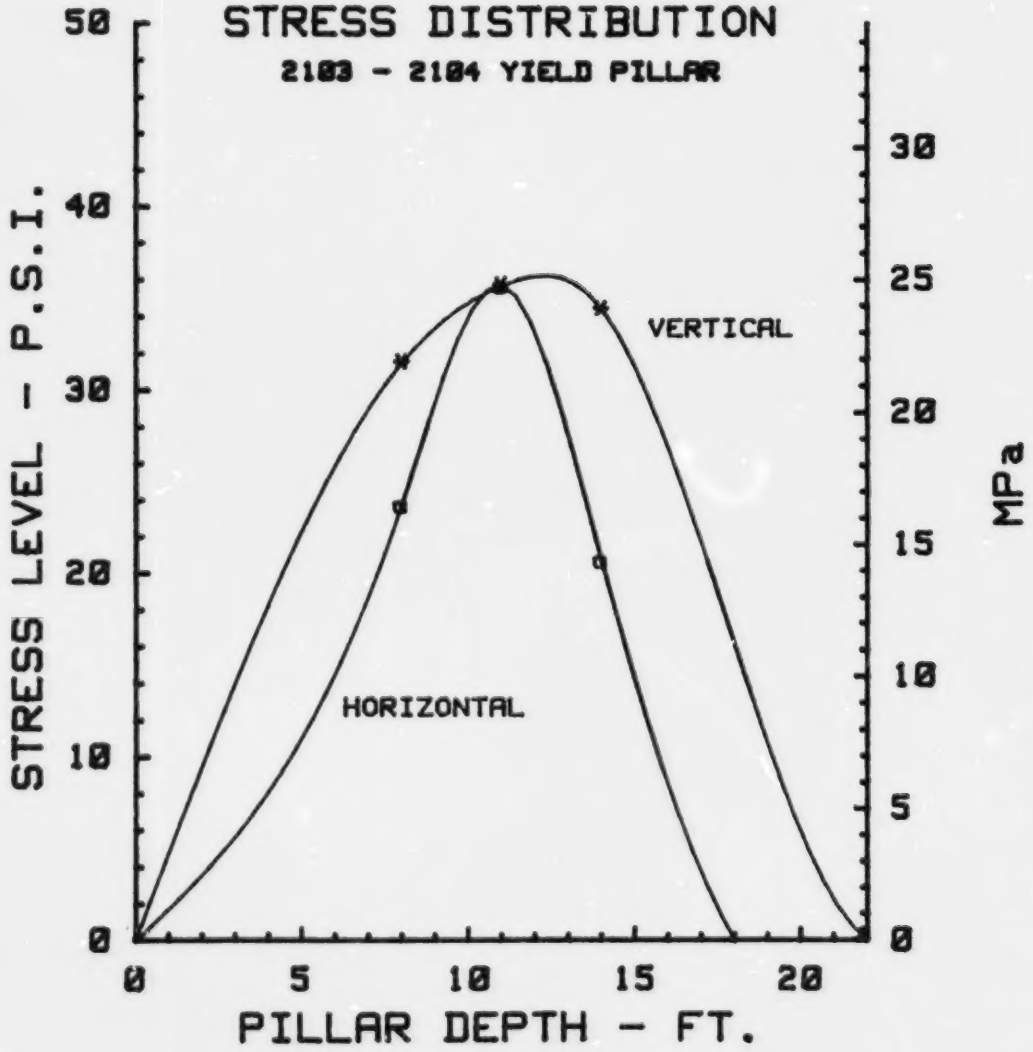
STRESS DISTRIBUTION
2103 - 2104 YIELD PILLAR
STRESS LEVEL - P.S.I.
50
40
30
20
10
0
30
25
20
15
10
5
0
MPa
VERTICAL
HORIZONTAL
0
5
10
15
20
PILLAR DEPTH - FT.

FIG. 31

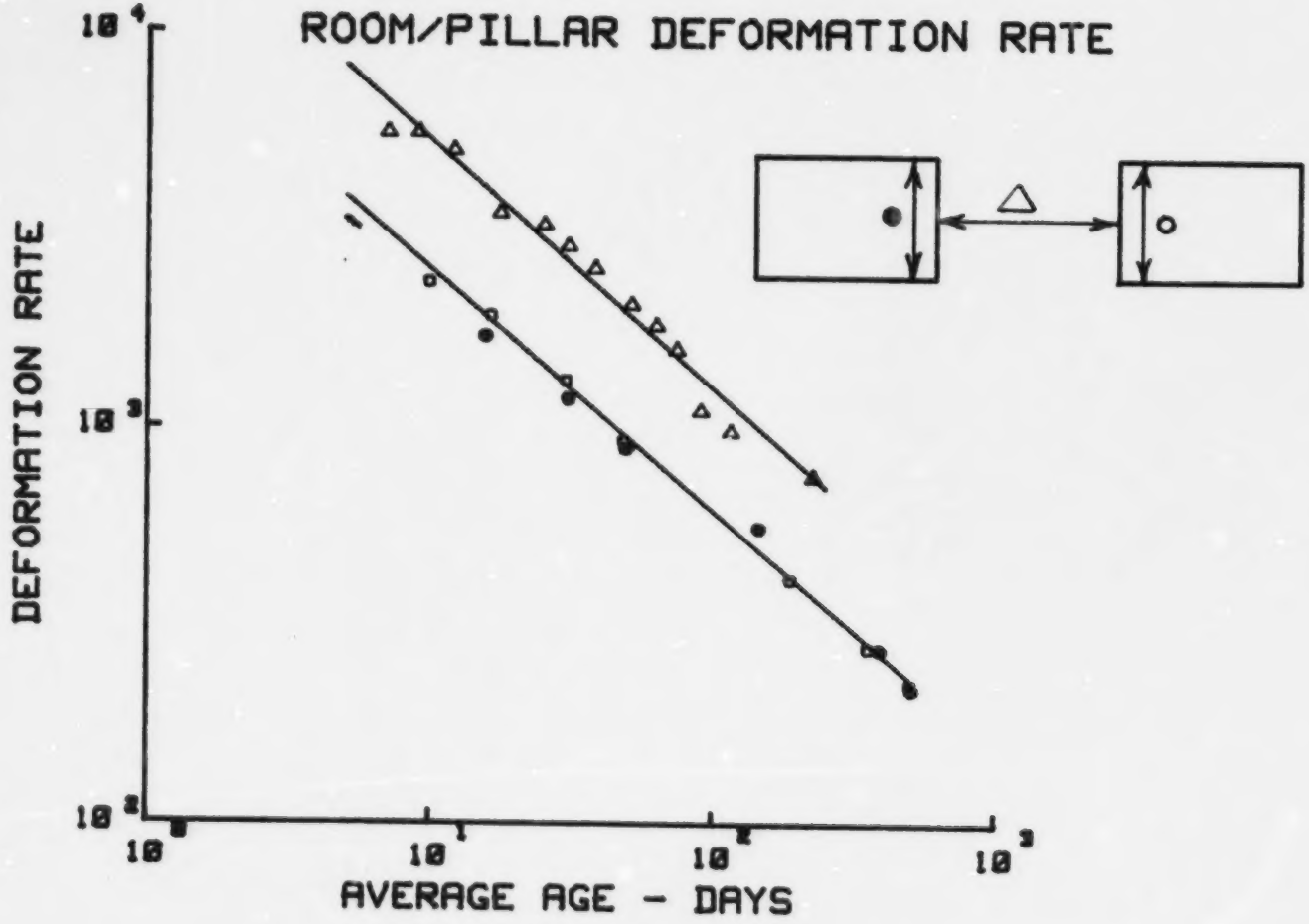
ROOM/PILLAR DEFORMATION RATE
DEFORMATION RATE
10 4
10 3
10 2
10 0
10 1
10 2
10 3
AVERAGE AGE - DAYS

FIG. 32

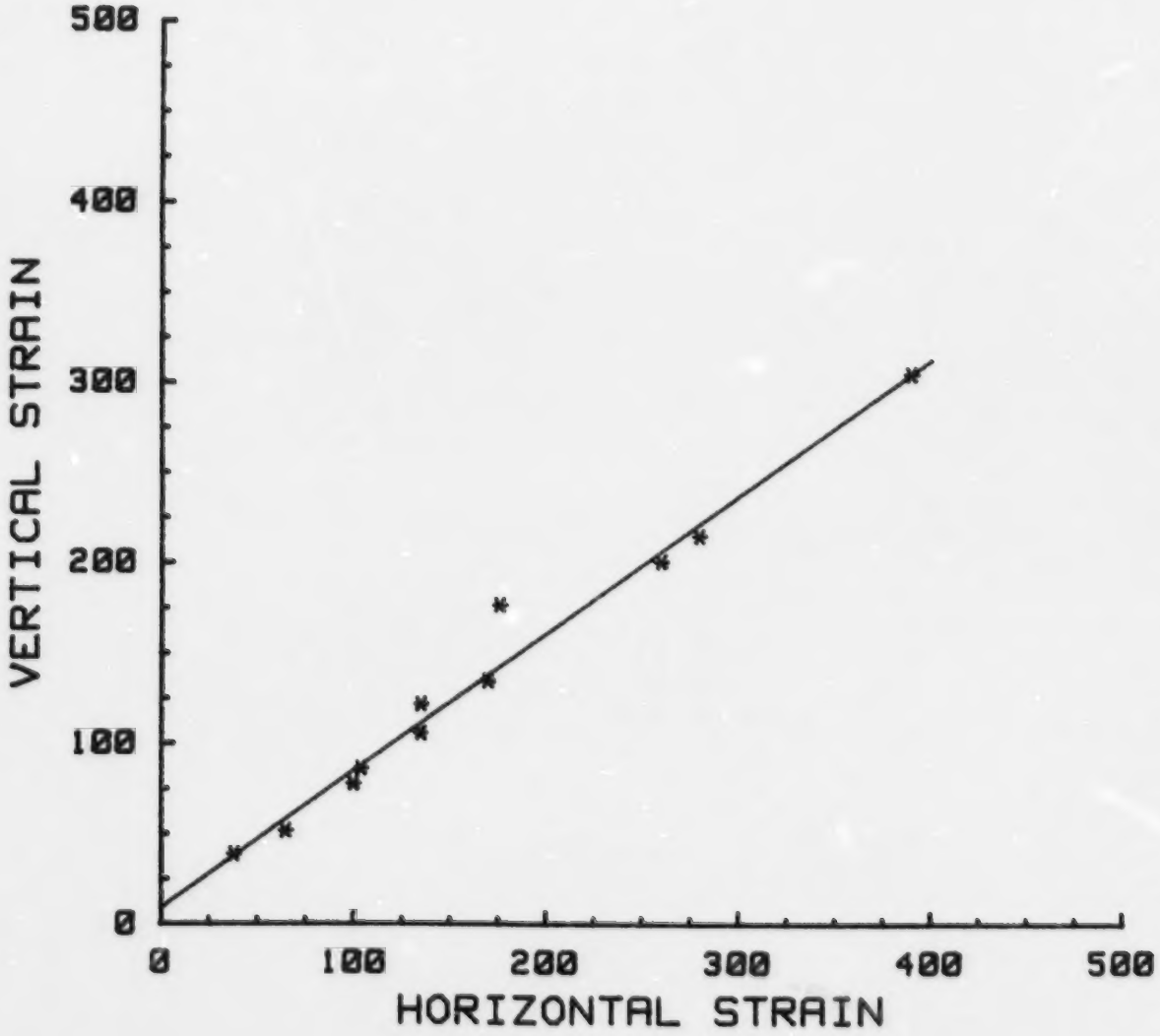
500
400
300
200
100
0
VERTICAL STRAIN
0
100
200
300
400
500
HORIZONTAL STRAIN

FIG. 33

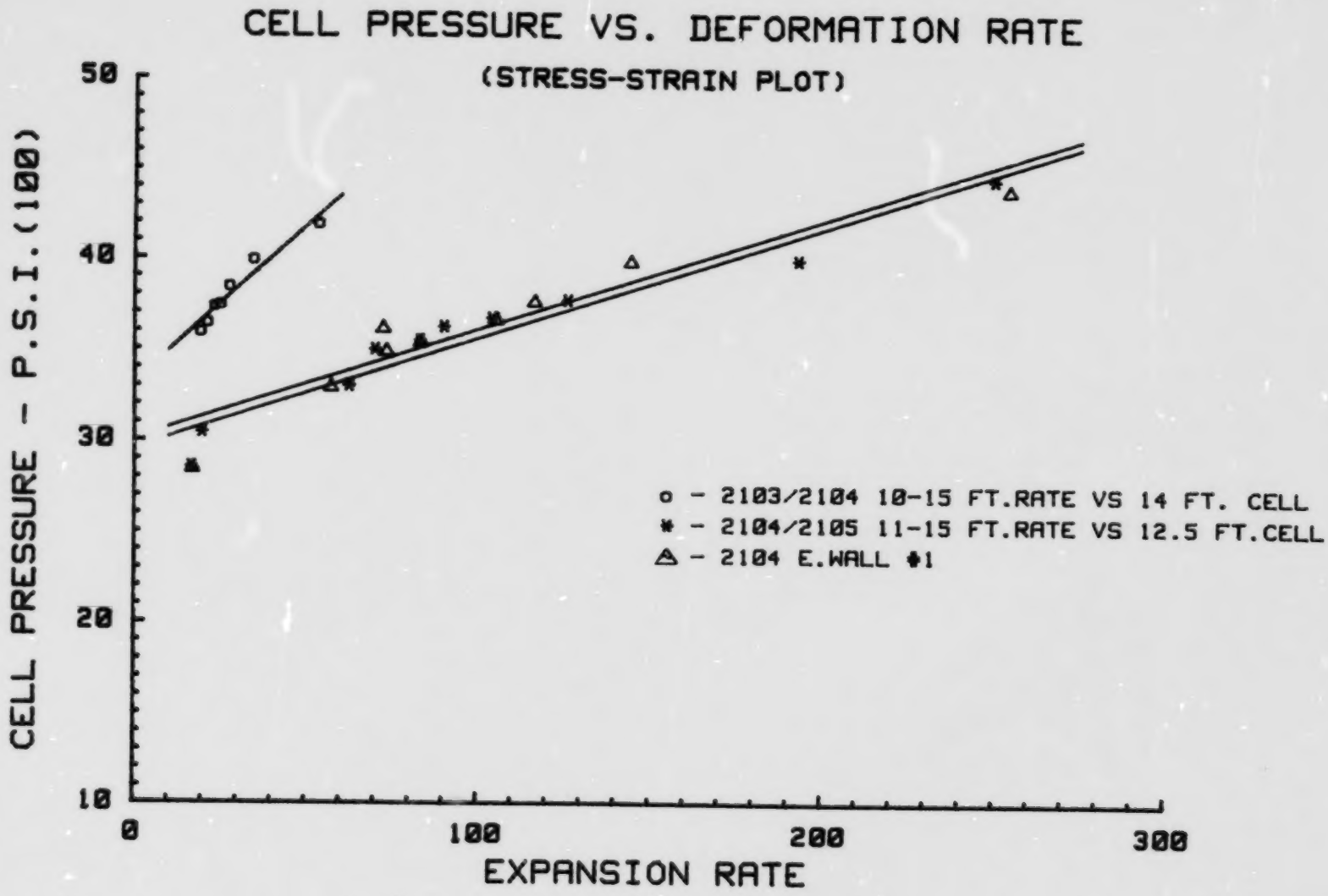
CELL PRESSURE VS. DEFORMATION RATE
(STRESS-STRAIN PLOT)
CELL PRESSURE - P.S.I.(100)
50
40
30
20
10
0
100
200
300
EXPANSION RATE
o - 2103/2104 10-15 FT.RATE VS 14 FT. CELL
* - 2104/2105 11-15 FT.RATE VS 12.5 FT.CELL
Δ - 2104 E.WALL #1

FIG. 34

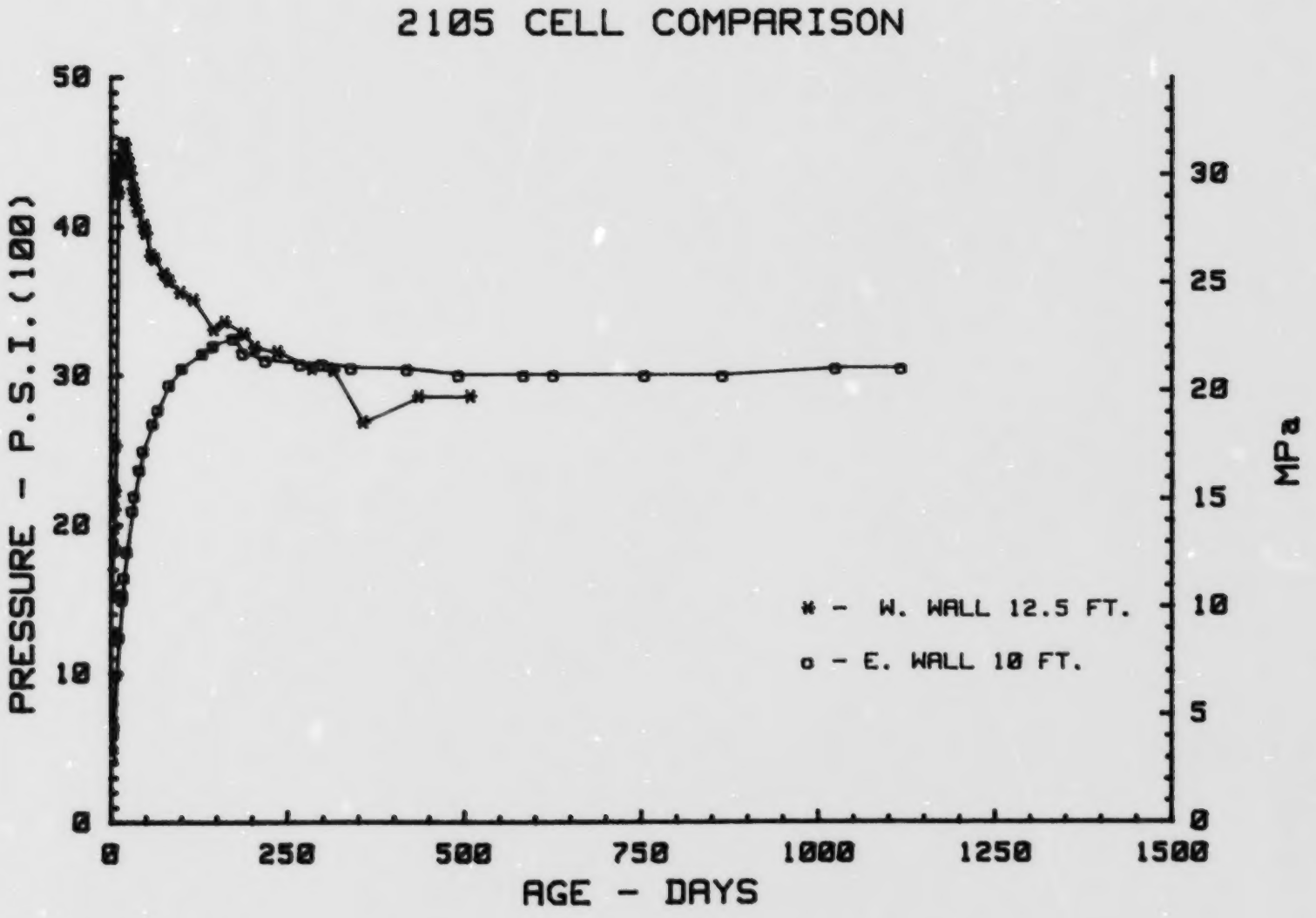
2105 CELL COMPARISON
PRESSURE - P.S.I.(100)
MPa
AGE - DAYS
* - W. WALL 12.5 FT.
o - E. WALL 10 FT.
0
10
20
30
40
50
0
5
10
15
20
25
30
0
250
500
750
1000
1250
1500

FIG. 35

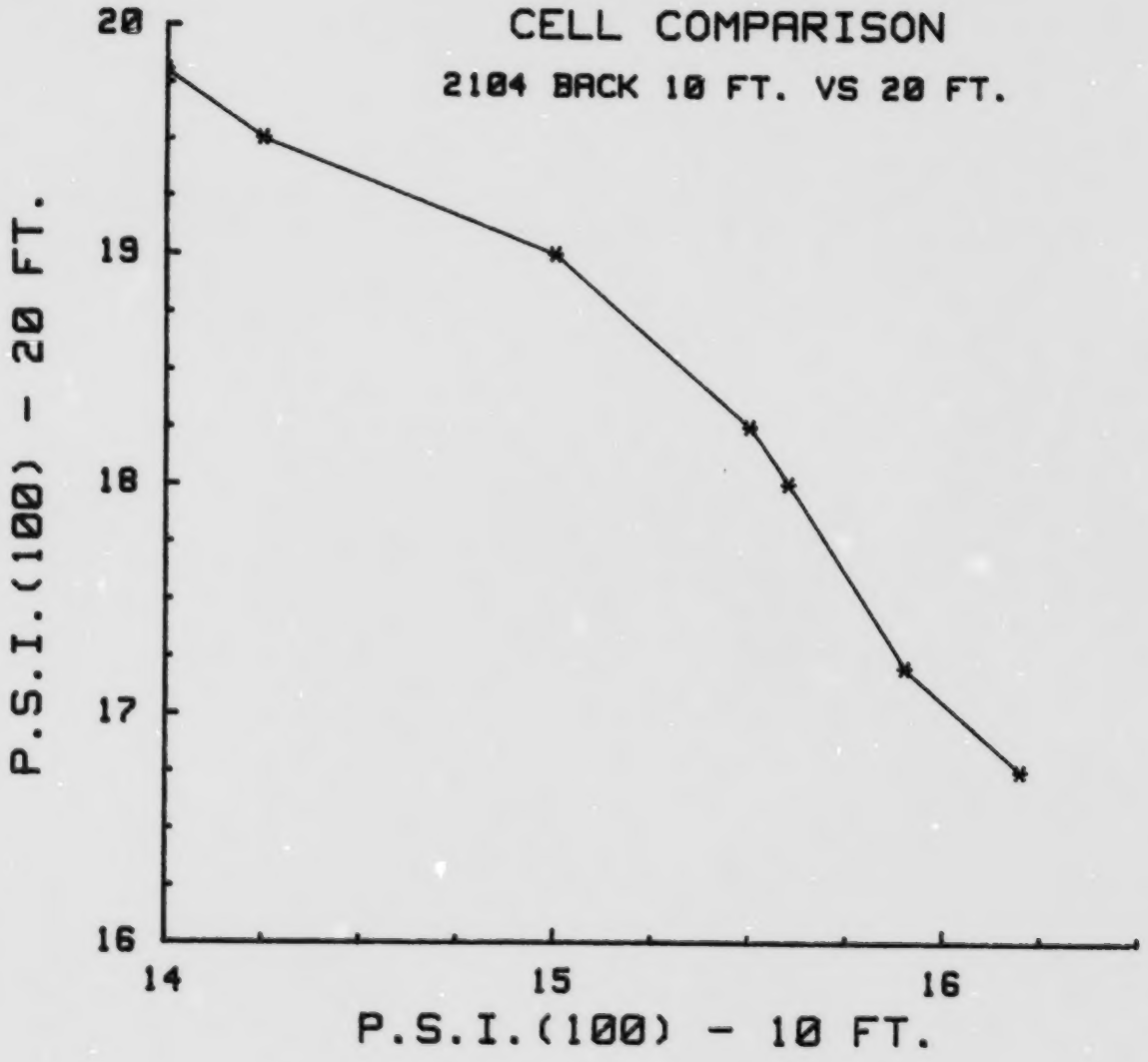
CELL COMPARISON
2104 BACK 10 FT. VS 20 FT.
P.S.I.(100) - 20 FT.
20
19
18
17
16
14
15
16
P.S.I.(100) - 10 FT.

FIG. 36

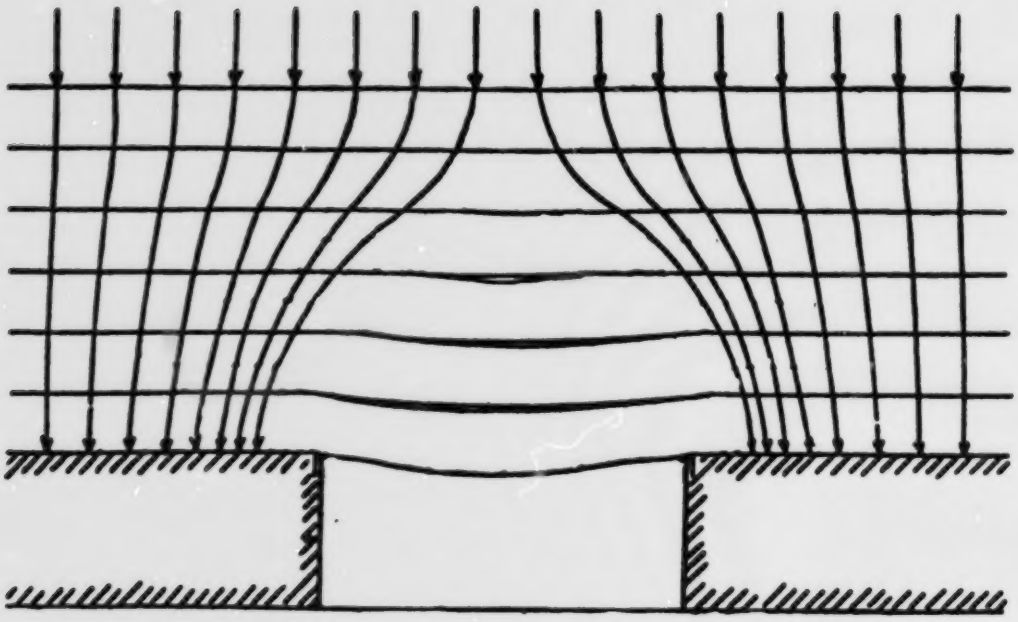

FIG. 37

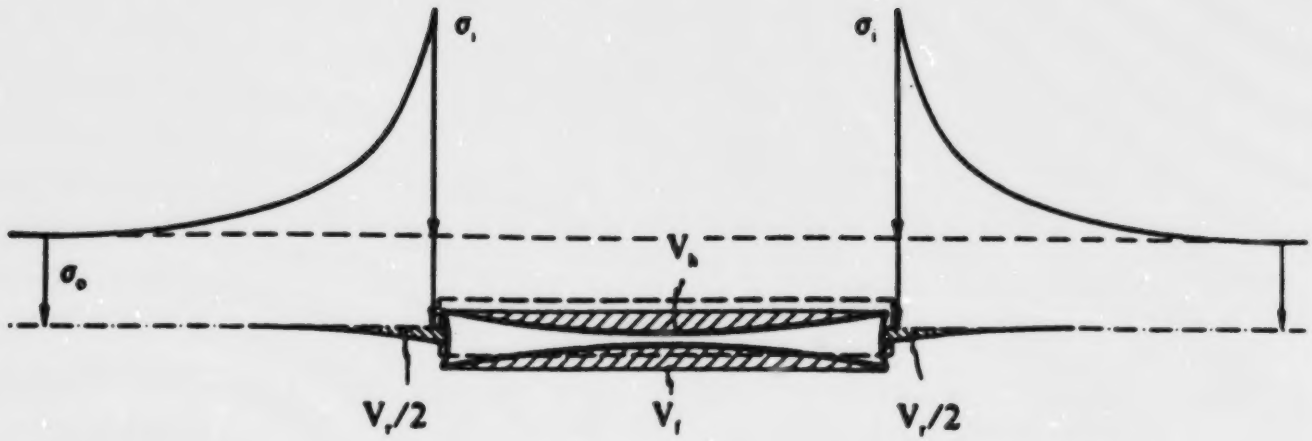

FIG. 38A

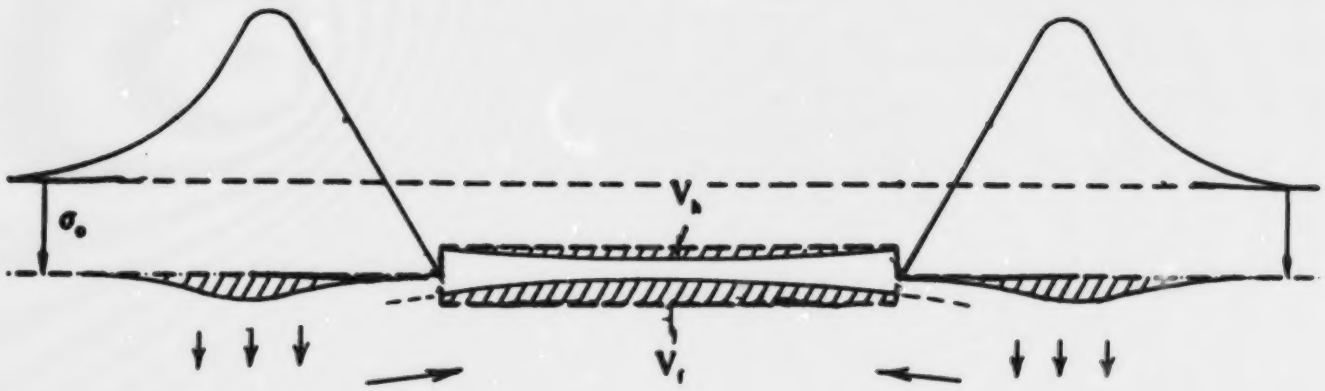

FIG. 38B

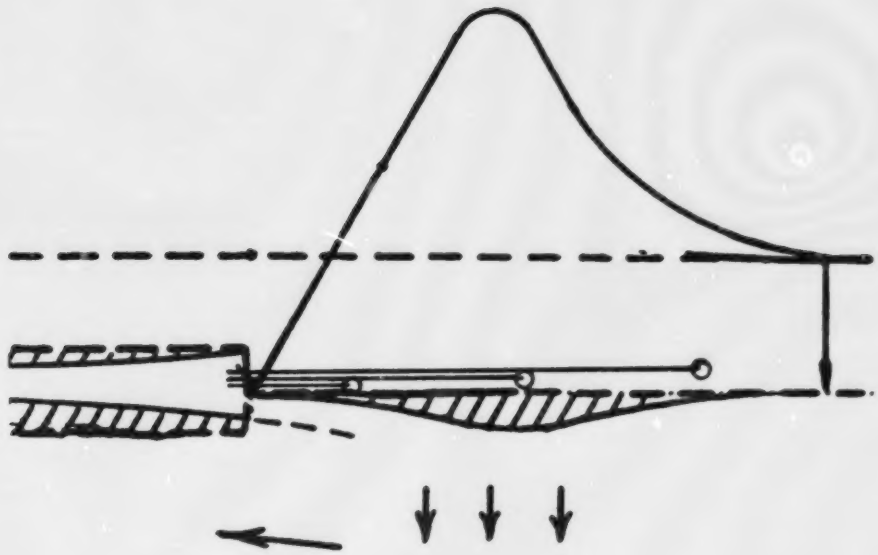

FIG. 39

LABORATORY TESTING

4.0 LABORATORY TESTING

4.1 UNCONFINED TESTS

Unconfined tests were carried out on various samples of salt and potash. Creep is clearly a problem even in the five minute duration of an unconfined test. An extremely low yield limit and great nonlinerarity over the range of anticipated loads make choosing values for analysis very difficult.

Fracturing due to stress relief and shipping damage was also a concern.

Young's Modulus for salt was also determined using sonic velocity under a variety of conditions. The method also provides some guidance as to a reasonable value for Poisson's ratio.

Tests were also carried out on samples of 2nd Red Beds and Dawson Bay limestone. Sample 1 was taken from the 2nd Red Beds. Samples 2 to 12 progress through the Dawson Bay from 57 feet (17 meters) to 113 feet (34 meters) above the mining horizon.

4.2 RESULTS AND CONCLUSIONS

Potash Young's Modulus

The Young's Modulus was found to be considerably lower than that of salt. Results may be anomalously low, but they fit reasonably well with those of Denison-Potacan (1987). It is suggested that a value of 5 MPa is used for modeling, although the creep component of numerical modeling is not particularly sensitive to Young's Modulus.

Potash Poissons Ratio

Initial values of Poisson's Ratio were very low. This may be interpreted as the closure of horizontal micro-cracks in early stages of the test. Values in the middle of the test - between the crack closure stage and the "damage" stage - may be most representative but because there is no region of constant Poisson's Ratio, it is difficult to justify the choice of any particular value. However, 0.2 is a reasonable choice from the tests although low according to most values in the literature.

Salt Young's Modulus

The tests gave inconsistent results, probably due in part to sampling damage (the effect of destressing) and shipping. A choice of 20 GPa is the best one since both the first test and the sonic velocity gave this value. Values of 25-30 (GPa are typically quoted for salt, so this is not to far removed. High creep rates at higher stresses invalidate the determination of Young's Modulus anywhere except during the first two MPa of load.

Salt Poissons Ratio

The best quality sample tested gave a Poisson's Ratio of approximately 0.2. The lower strength sample is dilitant throughout the test (increasing in volume) suggesting it is damaged and is yielding plastically. Using a volume of 0.2 in the determination of Young's Modulus from sonic velocity gives a value of 28.8 GPa which is probably reasonably realistic and is in line with the literature. The Poisson's Ratio is low compared to 0.35 often quoted but data for Poisson's Ratio is often poor and difficult to interpret.

POTASH CORE TESTS

SAMPLE	DESCRIPTION	INITIAL TANGENT MODULUS	POISSONS RATIO	ULTIMATE STRENGTH
1	Clean sylvinite, coarse crystals	4280 MPa	0.1	19.07 MPa
2	Sylvinite with approx. 10% shale	3430 MPa	Increasing 0.16 to 0.40 in early stages of test	15.45 MPa
3	Clean sylvinite, coarse crystals to 10 mm	1890 MPa	Approx. 0.1	21.0 MPa

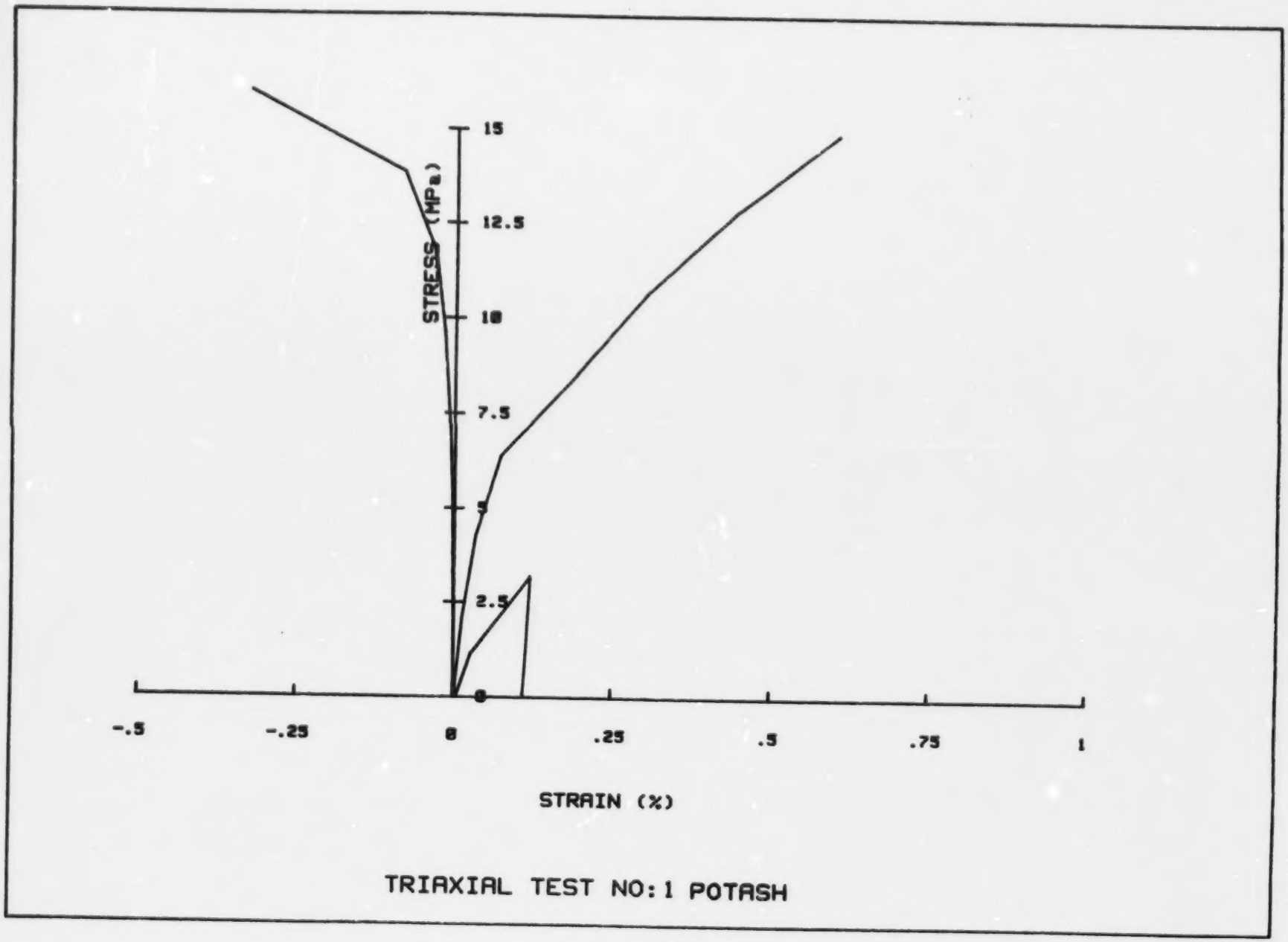

TRIAXIAL TEST NO: 1 POTASH

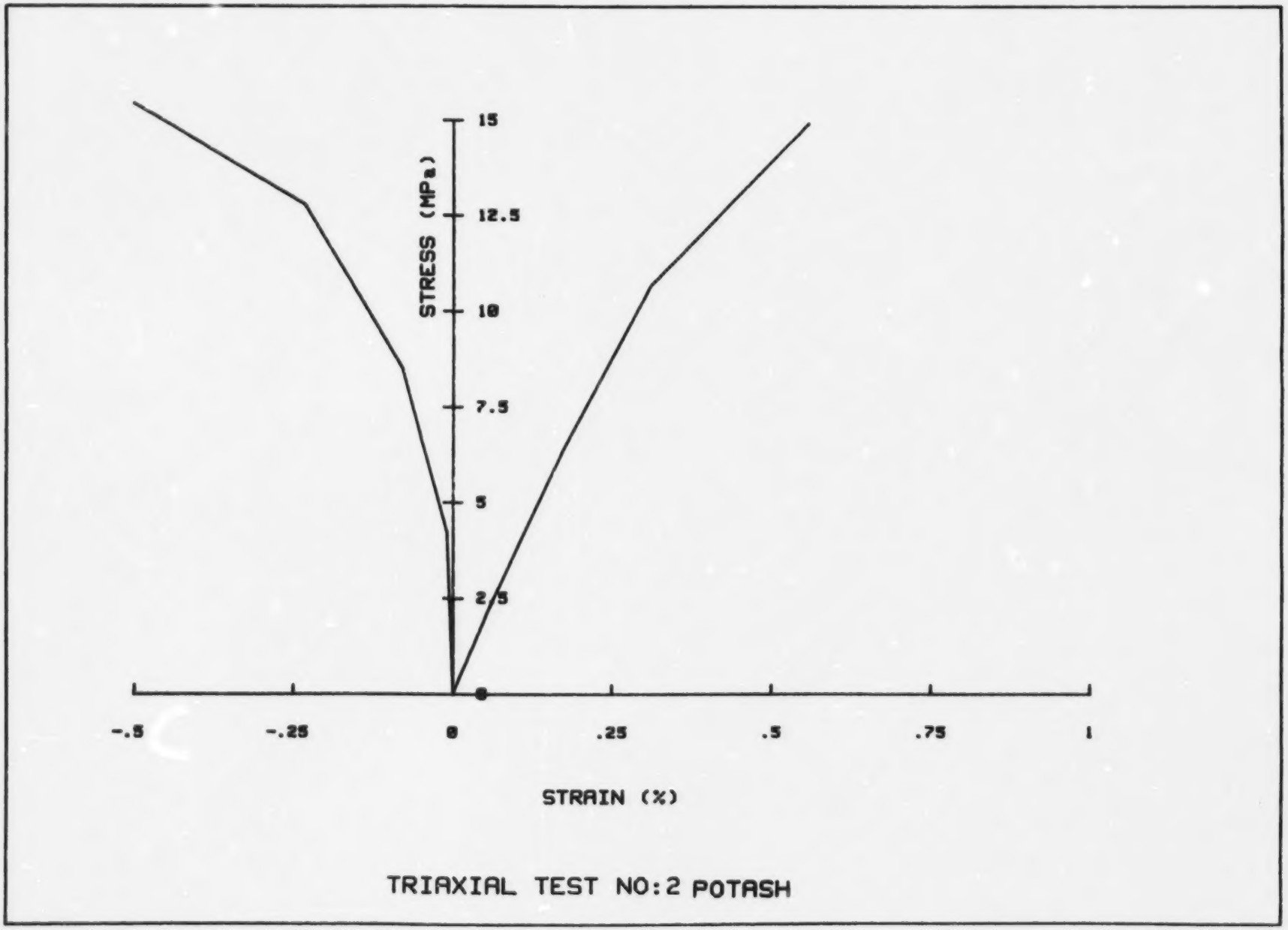
STRESS (MPa)
15
12.5
10
7.5
5
2.5
0
-.5
-.25
0
.25
.5
.75
1
STRAIN (%)
TRIAXIAL TEST NO:2 POTASH

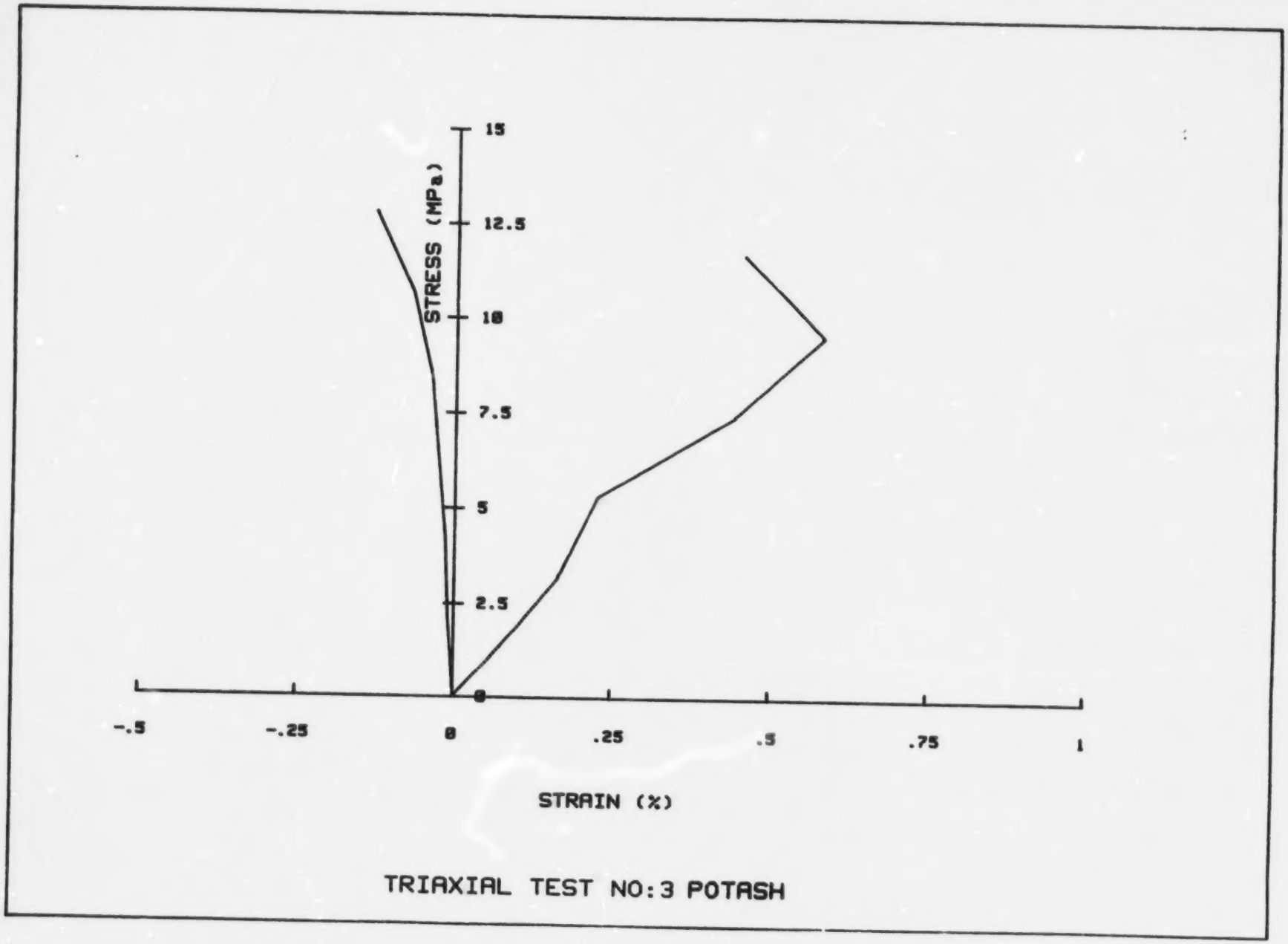

TRIAXIAL TEST NO:3 POTASH

Made in USA

AXIAL STRESS LEVEL PLOTTED VERSUS MODULUS OF ELASTICITY AND POISSONS RATIO FOR UNIAXIAL TESTS ON SALT

SAMPLE 1 Medium crystalline Dirty Salt
Sample length 14.9 mm
ultimate load 28.5 MPa

Sample 2 medium crystalline clean salt
Sample length 106mm
ultimate load 25.4 MPa

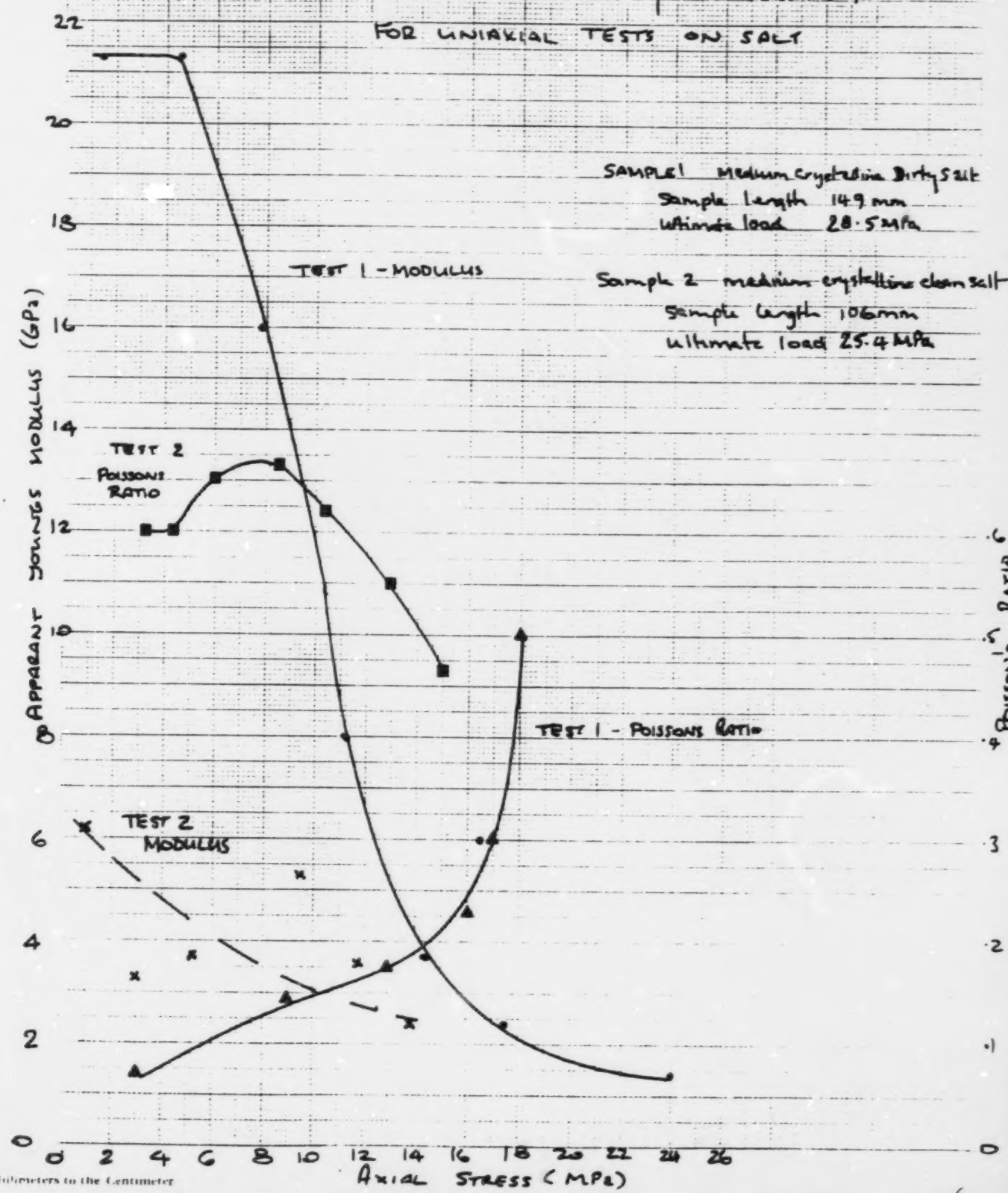

Millimeters to the Centimeter

Made in USA

YOUNGS MODULUS AFTER LOADING TO VARIOUS STRESS LEVELS MEASURED USING SONIC VELOCITY.

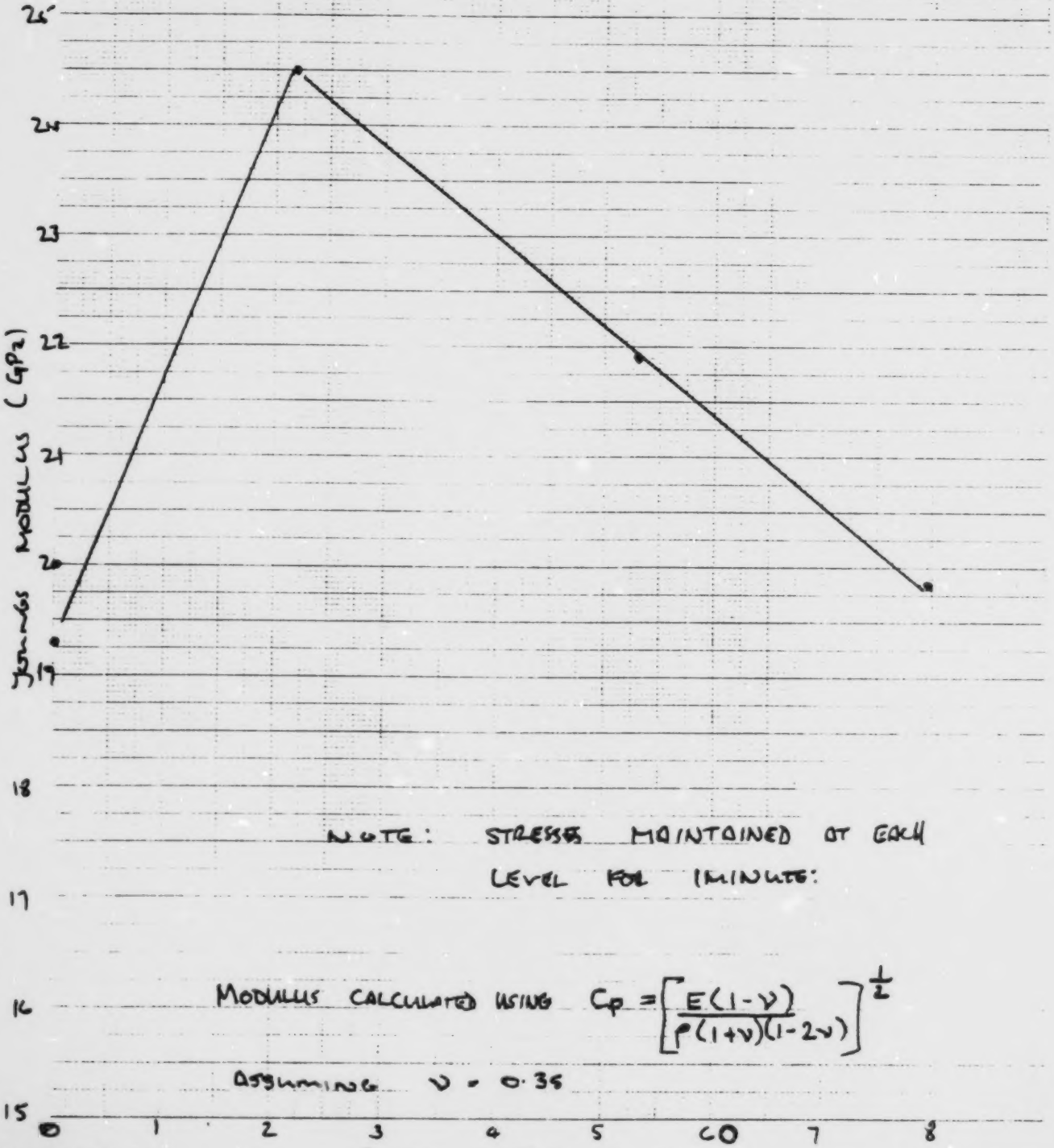

NOTE: STRESSES MAINTAINED AT EACH LEVEL FOR 1 MINUTE.

MODULUS CALCULATED USING $C_p = \left[\frac{E(1-\nu)}{\rho(1+\nu)(1-2\nu)}\right]^{\frac{1}{2}}$

ASSUMING $\nu = 0.35$

Millimeters to the Centimeter

Summary of Unconfined Compression and Sonic Velocity Tests on Dawson Bay Limestone Core

Sample Number	Density kg/m^3	u/c strength Mpa	Sonic Velocity m/s	Young's Modulus (sonic) GPa	Young's Modulus (u/c) Gpa	Poisson's Ratio
1	2547	32.1	4298	42.86	25.0	.19
2	2687	77.8	4854	56.98	35.3	.2(est)
3	2630	118.0	4739	52.75	34.0	.206
4	2604	88.0	4619	51.20	32.11	.192
5	2658	107.5	5519	72.86 *	81.0	.5
6	2628	111.0	5618	58.05 74.65 *	58.8	.322
7	2582	39.0	5628	73.60	43.6	.2(est)
8	2608	153.1	5522	73.43	49.86	.183
9	2632	127.0	5381	68.60	51.9	.20(est)
10 **	2615	58.0	5316	35.90 64.00 *	52.5	.396
11	2240	20.9	3225	20.58	14.93	.214
12	2439	57.8	3984	31.15	19.7	.268

* value of Young's Modulus based upon an assumed Poisson's ratio of 0.20

** sample failed prematurely due to uneven load application. This probably resulted in an inaccuracy in the measured Poisson's ratio

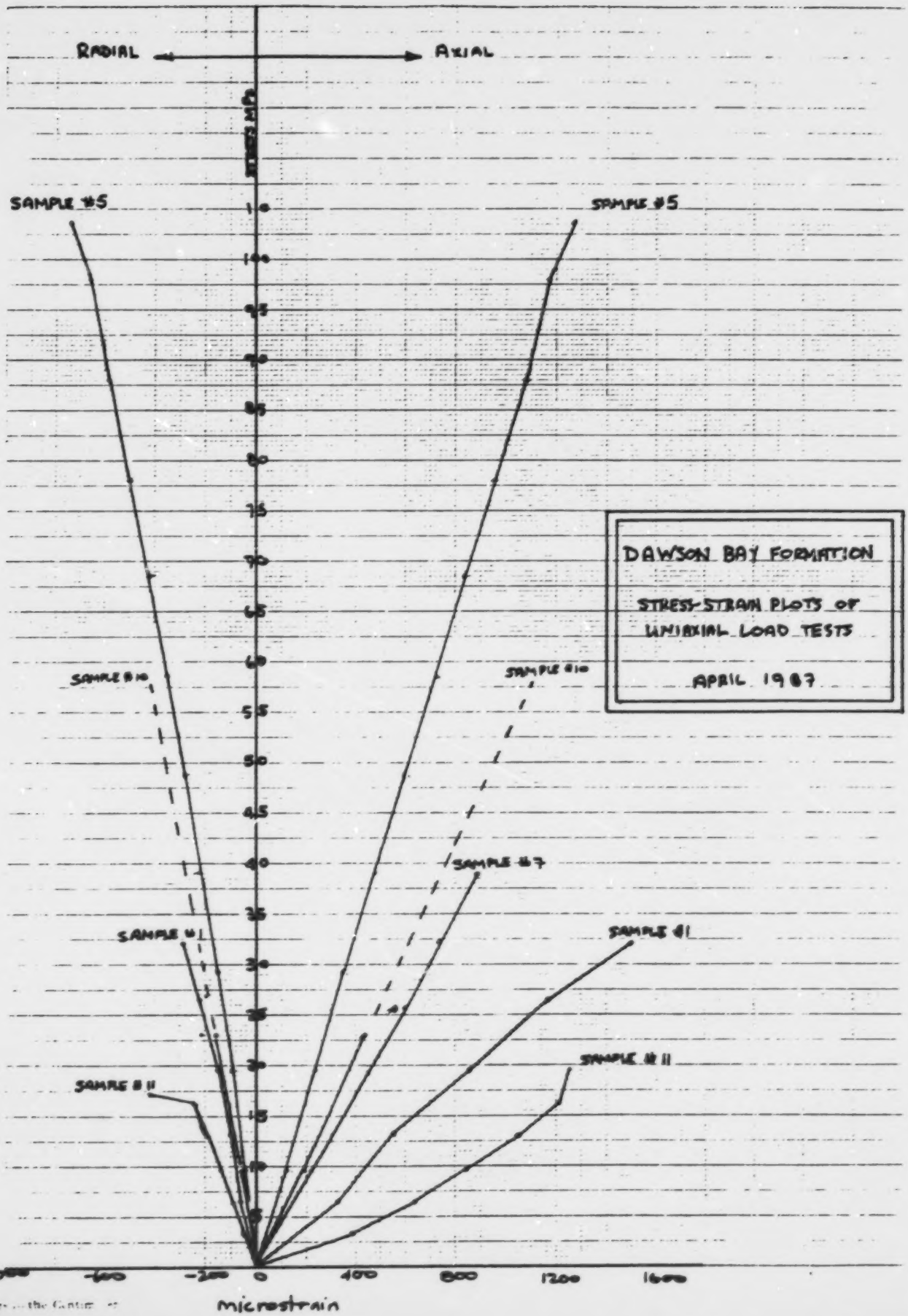
RADIAL
AXIAL
SAMPLE #5
SAMPLE #5
SAMPLE #10
SAMPLE #10
SAMPLE #7
SAMPLE #1
SAMPLE #1
SAMPLE #11
SAMPLE #11
DAWSON BAY FORMATION
STRESS-STRAIN PLOTS OF
UNIAXIAL LOAD TESTS
APRIL 1987
-600
-200
0
400
800
1200
1600
microstrain

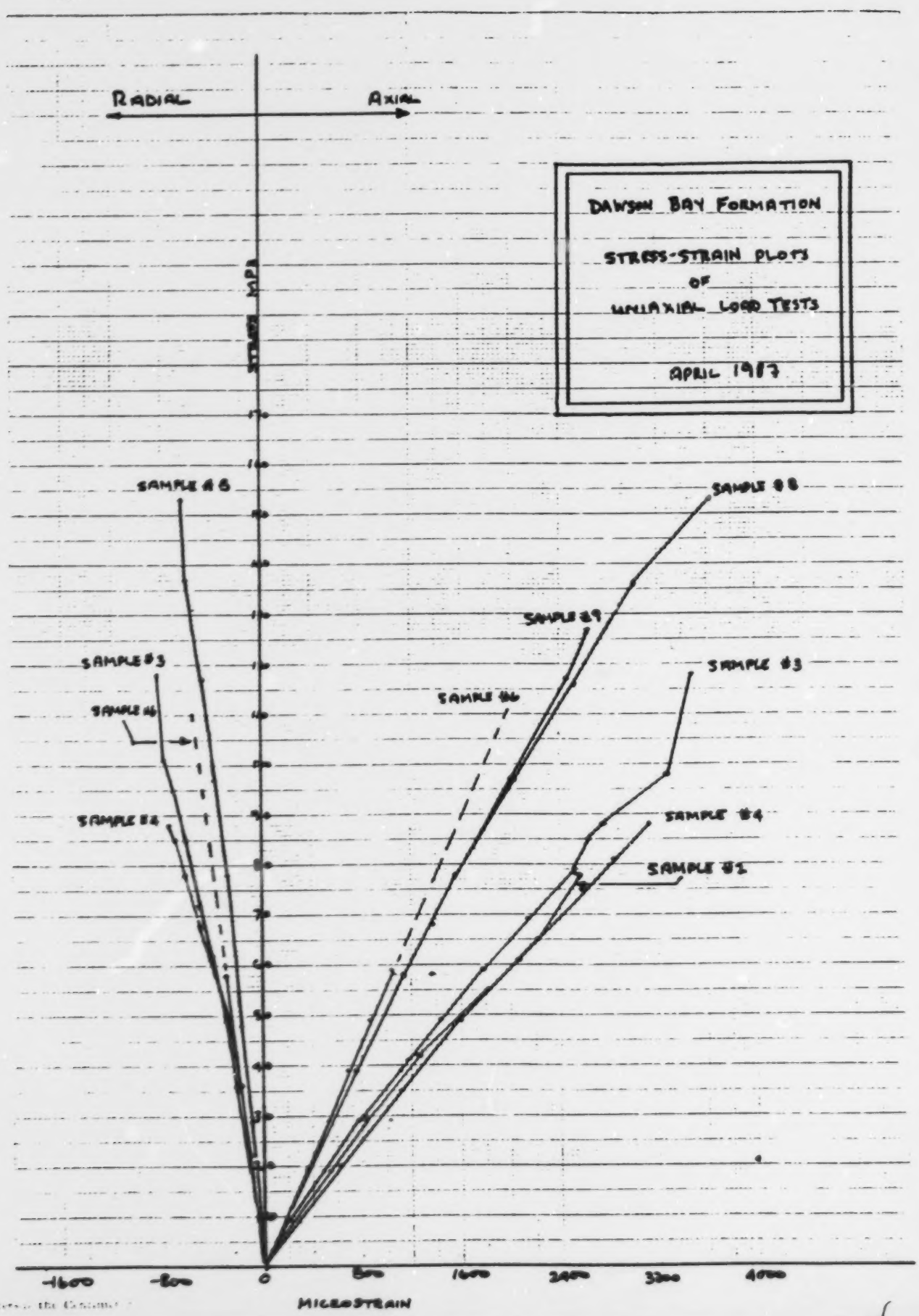
RADIAL
AXIAL
DAWSON BAY FORMATION
STRESS-STRAIN PLOTS
OF
UNIAXIAL LOAD TESTS
APRIL 1987
MPa
SAMPLE #5
SAMPLE #8
SAMPLE #9
SAMPLE #3
SAMPLE #6
SAMPLE #3
SAMPLE #6
SAMPLE #4
SAMPLE #4
SAMPLE #1
-1600
-800
0
800
1600
2400
3200
4000
MICROSTRAIN

TRIAXIAL TESTING OF COMINCO POTASH CORE SAMPLES BY THE SASKATCHEWAN RESEARCH COUNCIL

by

Joe Jones

and

John Unrau

April 6, 1988

POTASH CORE SAMPLES

The samples, as received, were in generally good condition with the exception that they were tapered from one end to the other. Refer to Table I for sample diameter data.

Table I. Sample Diameter Data.

Sample	Cominco 02	Cominco 03	Cominco 04	Cominco 05	Cominco 06
Top diameter (mm)	201.6	204.0	203.6	199.9	202.4
Bottom diameter (mm)	194.8	198.0	198.0	195.5	197.1
Diameter difference (mm)	6.8	6.0	5.6	4.4	5.3

It was agreed that SRC would proceed to test these samples as specified by COMINCO.

The samples were sealed in plastic bags until they were prepared for testing.

SAMPLE PREPARATION

As each sample was required for testing it was first cut to ~405 mm in length using a rotary diamond saw. The ends of the sample were then lapped using a disc sander with 80 and 100 grit sanding discs. Metal bands of varying thickness were fastened around the sample to help compensate for the sample taper in order that the sample ends could be made parallel.

Each sample was instrumented with three linear potentiometers, to measure axial strain, four strain gauges and a diametral strain measurement band with strain gauges, to measure diametral strain. Three threaded metal pads were cemented 120° apart on the sample circumference ~10 mm from the sample end on both ends of the sample. These pads are used to attach the linear potentiometers to the sample.

The samples were then jacketed with highly elastic polyurethane of ~7 mm thickness. This is done by placing the sample in a metal mould with the platens in place. The polyurethane mix is prepared and poured into the mould around the sample. The mould is left on ~one day to allow the jacket to cure.

After the mould was removed from the sample, the linear potentiometers were attached to the sample using threaded rod sections threaded into the metal pads.

The instrumented and jacketed samples were then loaded into the triaxial test cells. Sensor signal connections and hydraulic pressure line connections were then made.

INSTRUMENTATION

Two pressure transducers are used on each test cell to measure the applied pressures, axial and confining.

The pressure transducers and linear potentiometers were calibrated prior to test commencement. Linear regression analysis was carried out on each set of sensor data to obtain a slope and intercept for each.

The strain gauge conditioning unit was adjusted to provide correct excitation for the strain gauges.

A Fluke 2240B data logger in conjunction with an IBM PC computer was used for data acquisition and applied stress maintenance during the tests. A digital output interface in the IBM PC was used to control a 110 volt AC controller board which in turn controlled solenoid valves supplying air to high pressure air operated hydraulic valves. These hydraulic vales, 4 per cell, are used to adjust the applied hydraulic pressure in the cell axial and confining circuits.

TEST MEASUREMENT AND CONTROL

Software written for the IBM PC / Fluke data logger combination provides continuous monitoring and control of up to four triaxial test cells simultaneously. Data for each sample under test can be independently stored on a diskette at selected intervals and common data for all samples can be printed out at the desired time interval.

The software allows continuous monitoring of all sensors for the samples on test, stress and strain calculation are performed and digital output provides a means of adjusting the applied axial and confining stresses on each sample.

SAMPLE TESTING

Each sample was consolidated under hydrostatic stress conditions equal to the test confining stress until the change in axial strain became less than 10 microstrains per day.

Each sample was tested for a minimum of 120 days at the original specified conditions, stage 1. Refer to Table II. Various stages of loading were applied to samples 3, 5 and 6.

Please refer to Table III for sample description and comments.

TEST RESULTS

Strain and time data for each sample were extracted from the original data files.

Strain versus time plots were then made for each sample from this extracted data.

Table II SAMPLE CONSOLIDATION AND TEST CONDITIONS

SAMPLE	COMINCO-2	COMINCO-3	COMINCO-4	COMINCO-5	COMINCO-6
Cell #	2	1	3	4	5
Consolidation:	Aug. 3/87 @ 15:50	Aug. 3/87 @ 15:50	Aug. 23/87 @ 14:50	Oct. 5/87 @ 17:15	Oct. 5/87 @ 17:40
Applied Pressure					
axial (MPa)	5	10	5	5	10
confining (MPa)	13	20	15	15	20
Test Conditions:					
Stage 1	Aug. 12/87 @ 16:50	Aug. 8/87 @ 9:41	Sep. 3/87 @ 10:35	Oct. 19/87 @ 16:44	Oct. 13/87 @ 14:10
Axial stress (MPa)	20	30	25	25	30
Confining stress (MPa)	13	20	15	15	20
Stage 2	—	Jan. 18/88 @ 8:17	—	Feb. 17/88 @ 17:03	Jan. 31/88 @ 10:45
Axial stress (MPa)		45		20	25
Confining stress		20		15	15
Stage 3	—	—	—	Feb. 18/88 @ 17:36	Mar. 2/88 @ 16:30
Axial stress (MPa)				30	30
Confining stress (MPa)				15	15
Stage 4	—	—	—	Mar. 2/88 @ 17:00	Mar. 10/88 @ 00:45
Axial stress (MPa)				25	25
Confining stress (MPa)				15	15
Completion	Dec. 14/87 @ 13:25	Jan. 20/88 @ 18:35	Jan. 11/88 @ 17:20	Mar. 16/88 @ 16.43	test in progress

Table III

SAMPLE DESCRIPTION AND COMMENTS

SAMPLE	COMINCO-2	COMINCO-3	COMINCO-4	COMINCO-5	COMINCO-6
DIMENSIONS: (average)					
Before Test					
Length (mm)	401.3	403.2	406.4	408.0	406.3
Diameter (mm)	198.0	201.0	200.8	197.7	199.7
L/D	2.027	2.006	2.024	2.064	2.035
End Parallelism (mm)	0.75	0.75	0.75	0.75	0.80
After Test					
Length (mm)	398.5	341.0	388.5	387.5	
Diameter (mm)	199.5	232.5	210.0	207.0	test in
L/D	1.997	1.467	1.850	1.872	progress
End Parallelism (mm)	0.25	0.84	0.48	0.51	
DESCRIPTION: (general for all samples)	50 - 70 mm zone of finer crystals (up to 10 mm) with clay. 120 - 150 mm zone of coarse crystals (up to 40 mm) with traces of clay. 30 - 40 mm zone of finer crystals (up to 5 mm). 120 - 140 mm zone of coarse crystals (up to 40 mm) with clay. 60 - 70 mm zone of finer crystals (up to 10 mm).				
COMMENTS:	No problems with test.	No problems with test.	Strain rate was fairly high. Strain gauges were lost early in test. Oil was found in sample after the test was completed.	No problems with test.	Test in progress.

COMINCO-2
STRAIN vs. TIME

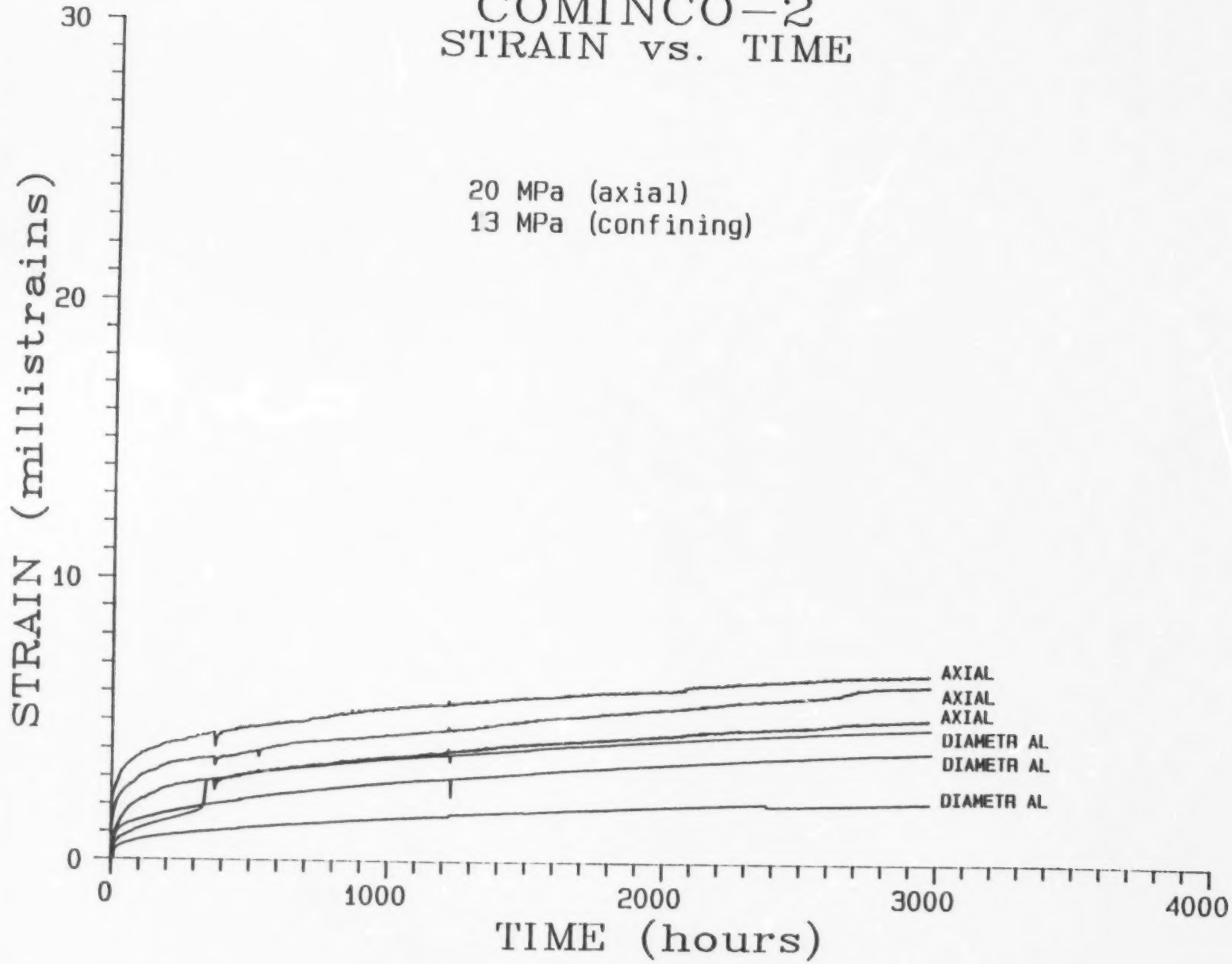

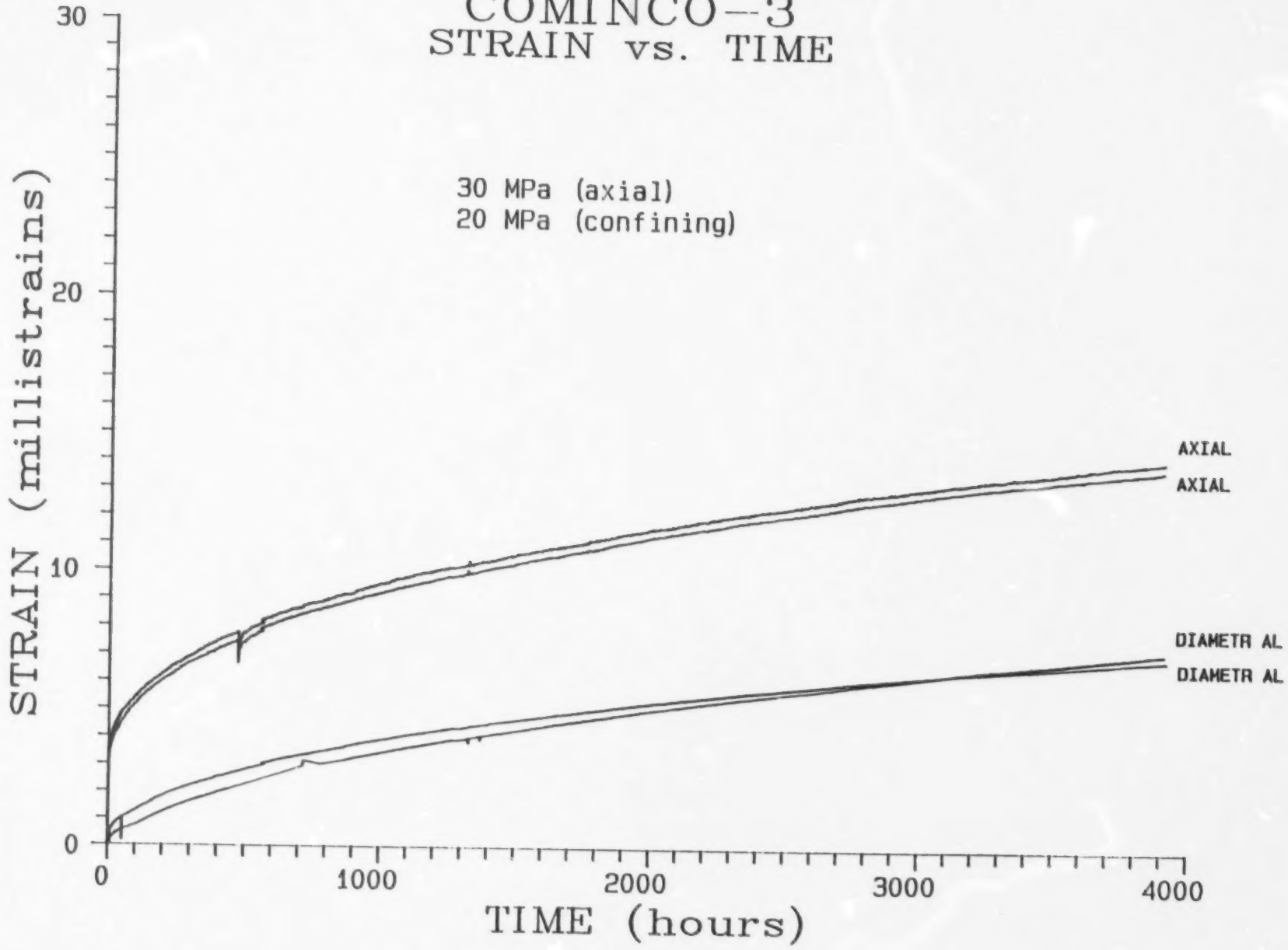
COMINCO-3
STRAIN vs. TIME
30 MPa (axial)
20 MPa (confining)
STRAIN (millistrains)
30
20
10
0
0
1000
2000
3000
4000
TIME (hours)
AXIAL
AXIAL
DIAMETR AL
DIAMETR AL

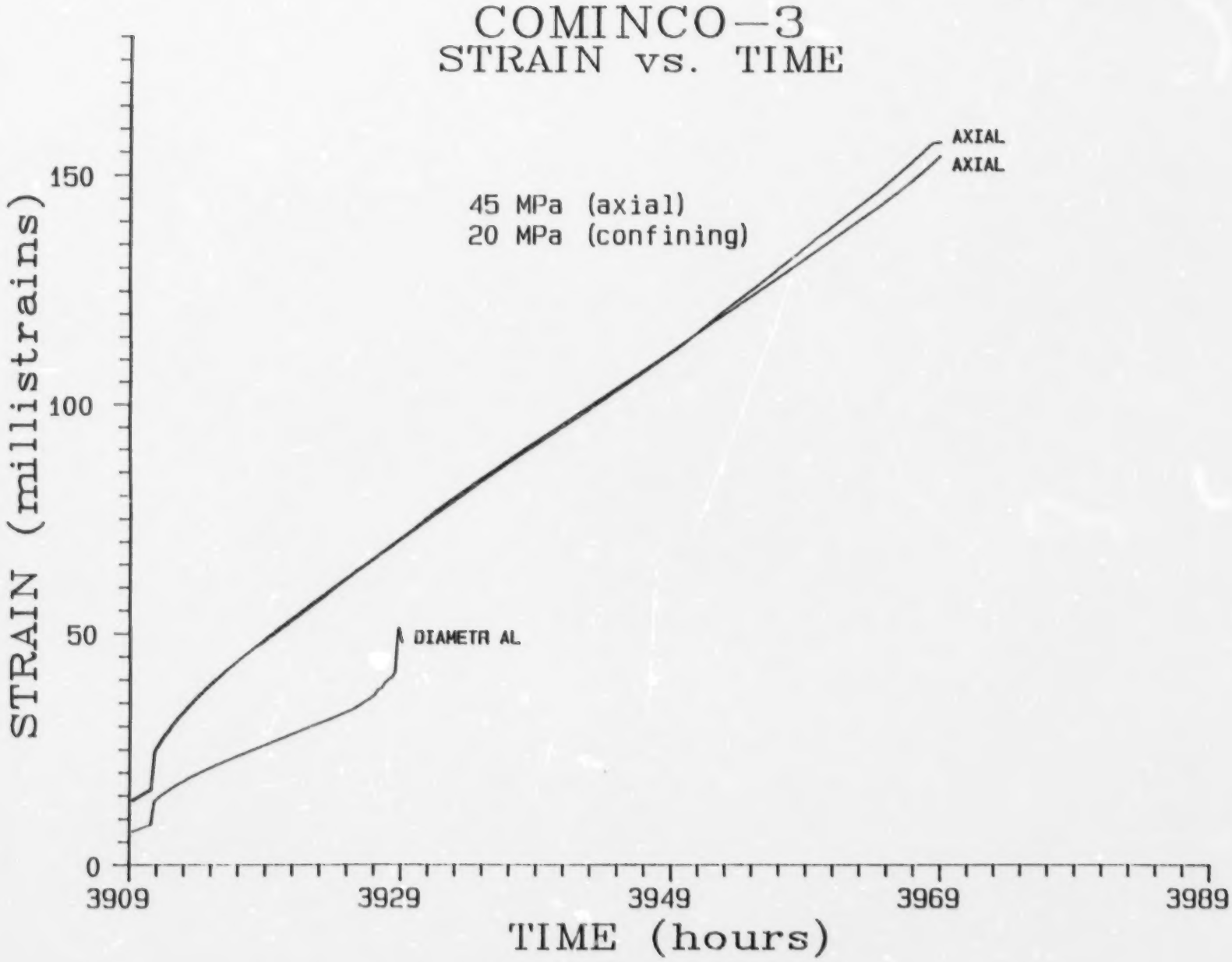
COMINCO—3
STRAIN vs. TIME
45 MPa (axial)
20 MPa (confining)
AXIAL
AXIAL
DIAMETR AL
STRAIN (millistrains)
0
50
100
150
3909
3929
3949
3969
3989
TIME (hours)

COMINCO–4
STRAIN vs. TIME

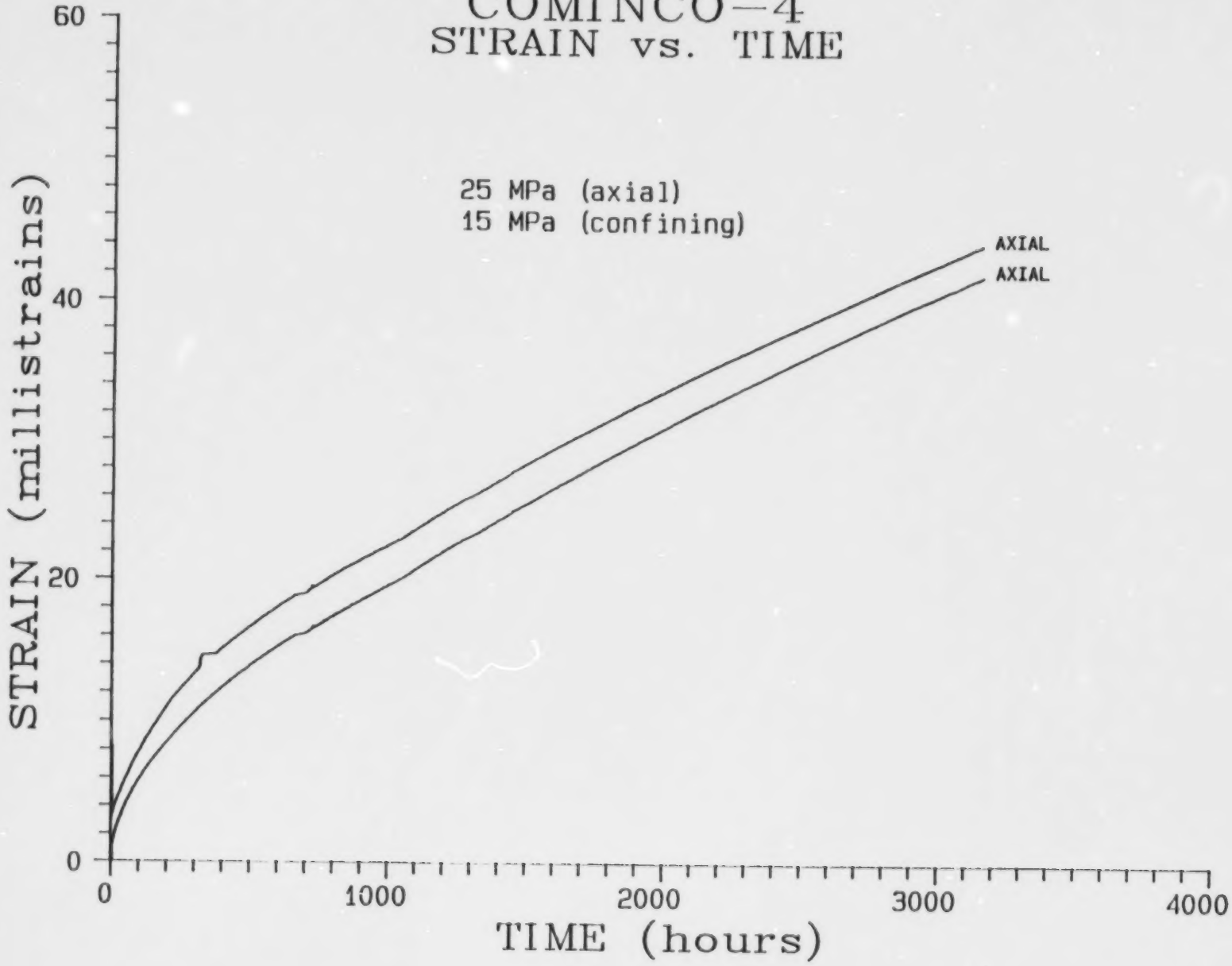

COMINCO–5
STRAIN vs. TIME

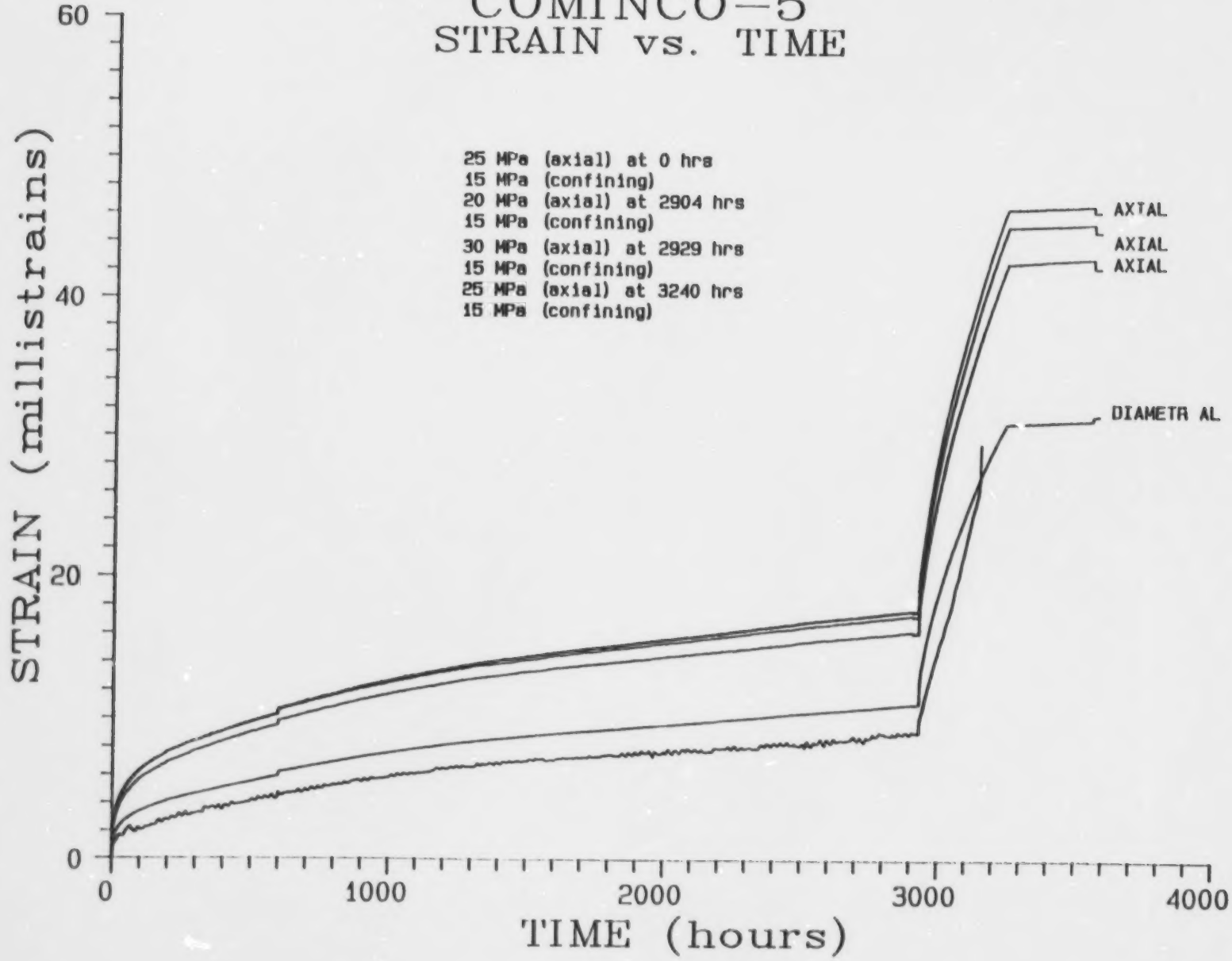

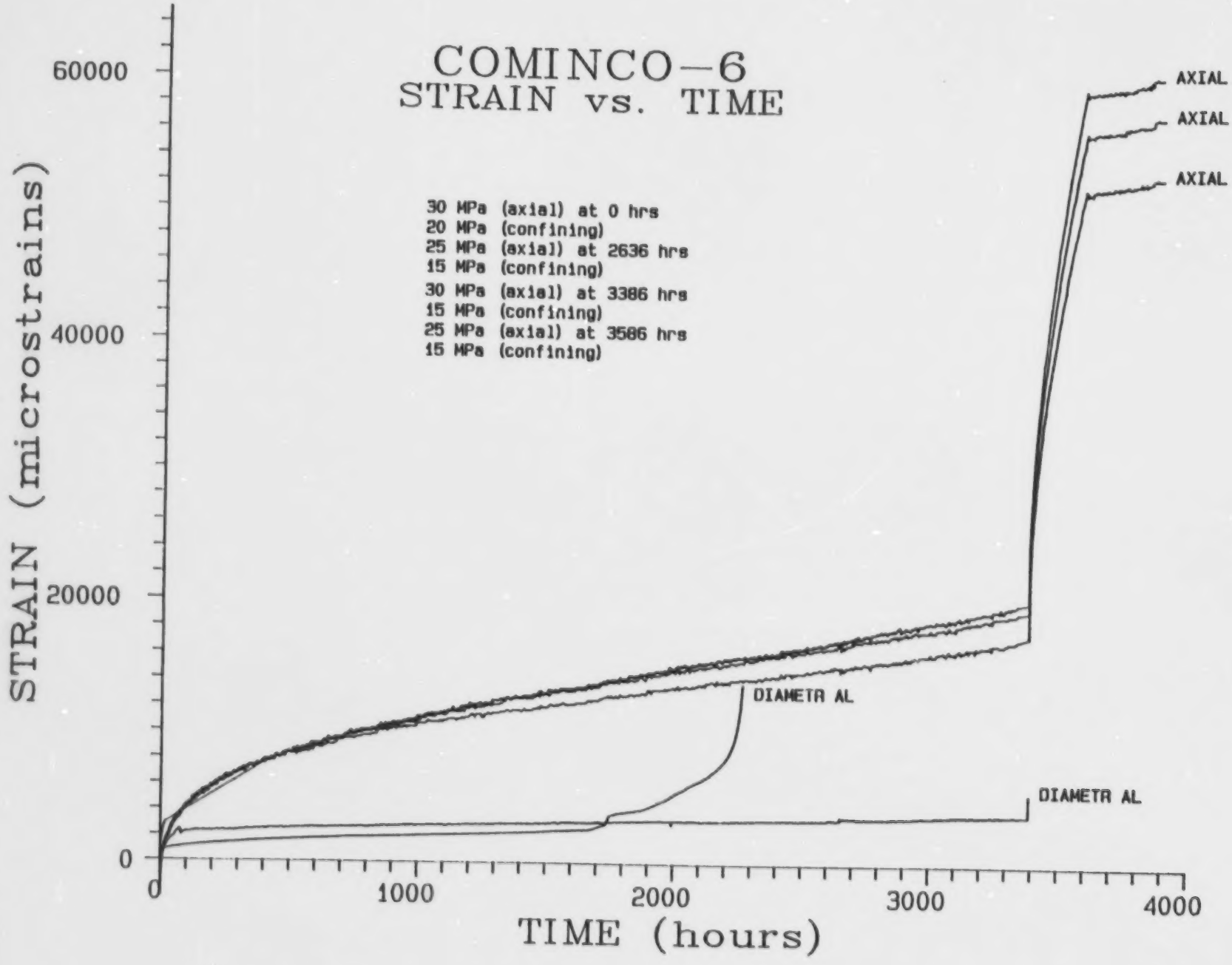
COMINCO-6
STRAIN vs. TIME
30 MPa (axial) at 0 hrs
20 MPa (confining)
25 MPa (axial) at 2636 hrs
15 MPa (confining)
30 MPa (axial) at 3386 hrs
15 MPa (confining)
25 MPa (axial) at 3586 hrs
15 MPa (confining)
AXIAL
AXIAL
AXIAL
DIAMETR AL
DIAMETR AL
60000
40000
20000
0
0
1000
2000
3000
4000
STRAIN (microstrains)
TIME (hours)

NUMERICAL MODEL

5.1 INTRODUCTION

The numerical analysis portion of this project was divided into 3 tasks. The first was to take GEOROC in the form it was originally developed for CANMET and improve its ease of use by adding pre and post processors and posting the program to micro-computer. The second task was to analyse a series of simple models for the purpose of determining the influence of variations in mesh size, opening geometry and material properties on the ability of the program to match observed behavior. Thirdly, a large model of the instrumented 5-entry system was analysed and its predictions compared with field measurements. The last task incorporated an analysis of laboratory test data generated during the project and the derivation of suitable constitutive laws to describe the stress-deformation-time behavior of the major stratigraphic components.

50% of the funding for the numerical analysis on this project was expended on a parametric study by RE/SPEC Ltd. of Calgary, whose office is now closed. This work is not reported here, though has been previously described in project progress reports. The work was undertaken without benefit of laboratory data and thus the variations in constitutive low parameters serve as a rough guide as to the effects of each parameter on the shape of the creep curve but do not assist greatly in choosing reasonable values for realistic models.

5.2 DEVELOPMENTS TO GEOROC

Like most large finite element programs, and particularly those developed primarily for internal use by specialist consultants, GEOROC is relatively complicated to use. It also requires considerable computer resources and may be prohibitively expensive for a company which has to buy time on outside computer systems. For instance, a moderately complex problem comprising 1,000 nodes may take 3 hours on a large mini computer which, at 10¢ per cpu second, would cost around $1,000. Thus, even a limited suite of analyses could be prohibitively expensive.

The two difficulties outlined above led to the primary aim of the developments undertaken to make Georoc more accessible to potential users. The approach taken was to make the program avalable on micro-computer and to prepare pre and post processors to guide the user through input preparation and output analysis.

The IBM PC AT and compatible machines are the primary class of machines chosen for the implementation of GEOROC. They were chosen, not because of any inherent suitability for the task, but because they are ubiguitous in mining engineering offices. In general, technical staff are familiar with their operation and the necessary additions to the hardware are economical. Other micro-computers will readily accept the IBM at version of GEOROC, requiring only a handful of input/output changes. A decision was made to remain with the MS/DOS operating system because only staff employed specifically for numerical analysis/computing will wish to learn the UNIX or XENIX operating systems available for micro-computers. MS-DOS places unnecessary restrictions on program size, but the advent of OS/II will circumvent this difficulty.

The MS-Fortran code of GEOROC is UNIX compatible and should also be OS/II compatible once a Fortran compiler is introduced. Under MS-DOS, the program of course runs on any member of the PC family.

The changes to GEOROC involved a certain amount of code reorganization to allow for lower limits on argument list length and continuation lines. Output was all reformatted to 80 column width to permit viewing on standard screens

and narrow carriage printers. Input was changed to permit separate data and mesh files to be generated, which is a convenience when many different analyses are performed with the same mesh. Subroutines were added for two additional creep laws (Denison-Potacan, Mraz Project Consultants 1987 and Day & Beddoes 1988). A manual is included as Appendix A of this report and should be read in conjunction with the original users manual (RE/SPEC 1985), replacing Chapter 5 in the latter.

The user is guided through the preparation of an input file by an interactive program which allows limited editing and writes a completed input file to disk. The beginning user will find this helpful as it avoids some of the confusing choices between options presented by the manual, and suggests default answers to many questions. As with most programs of its type, the expert will find it faster to use an editor to create the input file.

The rather limited post processor available for the mini-computer version of GEOROC has been replaced by a programmable database interrogation system which gives the user great flexibility in manipulating output data and writing it to files suitable for creating graphs and plots. The tabular ASCII files it produces can be read by most spreadsheet and graphics software packages available for the IBM PC. A manual for this program is also included in the Appendix.

All software described in this section is available on 102 Mb floppy disk with this report. Instructions for compiling source cost with microsoft Fortran compilers are on the disk, along with an example problem.

5.3 MATERIAL LAWS FOR FINITE ELEMENT MODELLING

In order to use the results of laboratory tests for numerical modelling it is necessary to formulate a "constitutive law" describing the response of the material to a range of stress states. Many constitutive laws are available in the literature, and, because in general none exactly match observed material behavior for all conditions, it is necessary to choose the most useful one for a particular purpose. GEOROC, in its present form, permits the use of four material models. These are:

1) Linear Elasticity. Classical Hookes Law behavior is an acceptable idealization for the Dawson Bay Limestone which is sufficiently far from the mine excavations to be in a stress range below its yield point.

2) Power Law. The Power Law takes the form;

$$E = A\sigma^m t^n$$

Where A,m,e, and n are constants
E = total strain
σ = stress
t = time under load

This law describes creep strain as a decaying function of time, but can also be rearranged to give creep rate as a decaying function of total creep. These two forms are commonly known as time hardening and strain hardening creep laws. As a special case n = 1 yeilds a steady state of Norton type creep law. The power law is entirely empirical but has been found to give reasonable results when modelling a variety of rock types. It has been chosen to model the salt and potash because it has wide acceptance and because it is best able to match the decaying rate of deformation observed both in the laboratory and in-situ. Better creep formulations are undoubtedly available, but none has so far emerged as a clear historical and practical favourite.

3) Denison-Potacan. Dusseault in Denison Potacan 1987, proposes a law consisting of two steady state Norton type relationships which meet at a state boundary surface called the PrandtL limit. There is some laboratory evidence that slow, diffusion creep rates at low stress may

be linearly related to stress while at higher stresses the creep rate is proportional to higher powers of stress. Laboratory tests performed for this project do not clearly demonstrate the truth of this hypothesis. While its use in the future cannot be ruled out, the loss of the ability to fit early deformation response was considered to be a negative aspect for this project.

4) Rate Spectrum Theory. This law is based upon the probability of any potential creep "location" moving at a particular energy level. By defining a density spectrum which describes the likelihood of a creep "event" over a range of energies, it is possible to model various creep mechanisms in a realistic way. While this model offers some theoretical attractions it is relatively untried and was not applied for this project.

5.4 MATERIAL PROPERTIES

DAWSON BAY LIMESTONE

The properties of the Dawson Bay Limestone are extremely variable, although all the samples tested behaved in a approximately elastic manner. A mean value for Young's Modulus of 40 MPa and a poissons ratio of 0.22 were chosen for modelling. Although rock stiffnesses are usually decreased below their laboratory value for modelling purposes, scoping analyses suggested this was unnecessary for the Dawson Bay. If Youngs Modulus was significantly reduced, the observed predominance of floor heave over roof sag in room closure was not predicted.

POTASH

Elastic properties for potash have been discussed previously. Values of Young's Modulus of 5,000 MPa and of poisson's ratio of .25 were chosen for modelling. It should be noted that the deformation is independent of Youngs Modulus so predicted strains are not sensitive to the value chosen. However, the solution scheme involved the application of equivalent model forces to cause the creep deformations, thus the stress changes occuring during creep are sensitive to Young's Modulus.

Least squares methods were used to fit the Power law relationship to laboratory creep data. The following relationships were obtained.

Power Law $\varepsilon = 5.65 \times 10^{-9} \sigma^{2.76} t^{0.5}$

Norton Law $\varepsilon = 1.2 \times 10^{-12} \sigma^{2.76}$

SALT

A Young's Modulus in the range 20 GPa - 28 GPa was found from laboratory tests. The lower value was chosen for modelling. Further reduction of the value was considered unnecessary due to the homogeneity and lack of fracturing in the salt mass. A poisson's ratio of 0.25 was chosen. A back analysis was performed on field data which shows that the horizontal to

vertical ratio of pillar deformation is 0.78. This value gives poisson's ratio equal to 0.28 assuming plane strain conditions.

The large difference between the moduli of potash and salt appear justified in the light of field observations of the behavior of the two materials.

Creep tests were not performed on the salt, so the power law is based solely on the observations of relative deformation rates in the two materials.

Power Law $\varepsilon = 2 \times 10^{-9} \sigma^{2.76} t^{0.5}$

Norton Law $\varepsilon = .6 \times 10^{-12} \sigma^{2.76}$

MODEL ANALYSIS

6.0 ANALYSIS OF NEAR-FIELD ROCK BEHAVIOR

The objective of this project is as much to explore and demonstrate the value of numerical modelling to potash mining as it is to back fit the data gathered in the field. The finite element method is a powerful tool for gaining an insight into many aspects of rock mass behavior and some simple models can give useful results. Two aspects of the behavior of the rock mass in the immediate vicinity of the entry system were chosen to illustrate the use of relatively simple models. These are discussed in the following sections. The analysis of a simple single room model are then presented before describing the larger model used for the 5 room entry system.

6.1 ANALYSIS OF YIELD PILLARS

Field measurements indicate that the outer pair of the three yield pillars in an entry system have an eccentric vertical stress distribution.

Observations clearly indicate that peak vertical stresses are skewed towards the protected room side of the pillar. One possible cause of this is the loss of support on the stress relief side due to buckling of the floor and roof beds.

A finite element analysis of a pillar with unequal unrestrained height on either side demonstrates that the hypothesis given above leads to the observed stress distribution. The mesh shown in Figure 1 was used for the analysis. Horizontal restraint was provided to all vertical surfaces except for the pillar; vertical restraint was given to the bottom edge. Dimensions are such that a 6 m pillar with 5.5 m room on either side is modelled, making use of symmetry about both vertical edges. A load of 25 MPa was applied to the upper surface.

Figure 2 illustrates the elastic and steady state creep distribution of vertical stress, using the material properties for potash from Section 5.4. The elastic stress distribution is the classical one with peak abutment stresses near the pillar faces. Creep relieves stresses at the abutment and transfer more stress towards the centre of the pillar. The maximum stress is found to be approximately 1/3 pillar thickness from the protected room. The maximum stress is twice that near the stress relief face but only 40% more than that near the protected face. The steady state distribution was established after approximately 10 days of loading, suggesting that in-situ instrumentation would not register the period of load redistribution in small pillars.

Figure 3 is included to illustrate the capability of the GEOROC post processor to generate plots of mesh deformations at any time step. This graphical representation of the results can sometimes be an aid to their interpretation.

This analysis has demonstrated that the hypothesis that pillar stress distributions are influences by loss of support on the stress relief side is plausible.

This analysis has demonstrated the hypothesis that pillar stress distributions are influenced by loss of support on the stress relief side. It also increases confidence in the validity of field measurements. The results obtained from this pillar analysis are in contrast to initial analysis with the large 3 entry mesh which indicated that if restraint is not removed from the relief drift side the load centre of the piller is skewed towards that side.

6.1 ANALYSIS OF ROOF BEAMS

A major cause of failure in the stress relief rooms is buckling of roof and floor slabs. These beams or slabs become completely detached from the strata above them (below them in the case of the floor) and thus carry only their self weight at the time of failure. The thickness of roof slabs is such that self weight above is unlikely to be sufficient to fail them, particularly if no longitudinal cracks or joints are present as is usually the case. It is a reasonable assumption, then, that high horizontal stresses contribute to instability of the roof beams. A elastic analysis of an axially loaded plate was performed using the equations given by Hoek and Brown (1980). This indicated that a plate with an axial load of 20 MPa should be stable with a thickness as low as 0.1 m if it is firmly clamped at the abutments and 0.2 m if it is pinned at the abutments. Thus an elastic analysis does not explain the failure of beams of .6 m thickness or greater. The conclusion is that creep of the beam decreases its stability and increases the probability of buckling.

If instability of a roof beam can be predicted from a finite element analysis, it would be possible to incorporate into GEOROC an algonthm which checks the status of roof and floor elements and decides when they should be removed to simulate collapse or buckling failure. With this aim, a series of analyses of beams under self-weight and with initial imposed deflections were performed.

A number of different mesh configurations similar to that shown in Figure 4 were analyzed. The axial load was provided by edge loads on the right hand side of the support (pillar) and the centre of the beam was fixed horizontally to provide symmetry. Self weight was the only vertical loading. Unlike elastic behavior, the beam maintained a constant stress across its depth while the rate of sag of the mid-point decayed with time according to the power law used. A steady state constitutive law gave rise to a constant stress and constant sag rate. The magnitude of sag was very small, being only a few millimeters for beams 0.2 to 0.9 m thick. The sags were considerably less than those observed, and the sag rates were insufficient to exceed the

rate of closure of the back in general, and thus to permit separation between the beam and the continuum above it. The effect of gravity on the formation and failure of beams would appear to be negligible - it is only a significant factor in the final stage of collapse of the roof. This conclusion is in accord with field observation that both floor and roof buckling take place together and that gravity is a stabilizing rather than a driving force in the case of the latter.

Although horizontal slabs, even with eccentric loading, are quite stable, this is not the case if the slab has an initial deflection at the centre of its span. Such a situation can occur as the roof and floor creep as a continuum into the excavated room, eventually causing a slab to become detached due to shear along a plane of weakness. Once detached, this slab is eccentrically loaded and has an initial deflection. It can then creep and sag rapidly as the abutments more inwards. As shown in Figure 5 an initial deflection of 0.1 m (4 inches) has increased to 0.2 m (8 inches) over 60 days. This sag rate is about 10 times that of the same beam with no initial deflection. The load eccentricity does not redistribute to a constant load across the depth of the beam as it does with no initial deflection and the resulting high stress gradient is likely to permit crushing of the top face and tension cracks on the lower face, with eventual collapse.

Since the roof slabs are strong enough to support their own weight and only fail due to the combination of high axial loads and an initial deflection, slotting to relieve axial load (as practised at the mine) is effective in their stabilization. The resulting cantilevers, even though separated from the back, are self-supporting if they are of the order of 0.5 m thick or greater. Thinner slabs may require bolting.

6.3 ANALYSIS OF SINGLE ROOMS

Using a large, complex mesh, it is time consuming and costly to perform large numbers of parametric variations. It is also often difficult to interpret the results when the influences from several excavations interact at a point. For this reason, a series of analyses were performed using single room meshes. The parameters of interest were the mesh refinement required around an opening, the influence of very weak elements in the back, and the effects of changing the relative stiffness and creep properties of the rock mass.

1) Variation of Mesh Refinement Around Rooms.

Choosing the correct size and shape of elements is of critical importance in finite element analysis. Since elements must deflect into a shape controller by the mathematics of their formulation, they may not conform readily to the deformed shape of a mine opening and as a result behave in an artificially stiff manner. Both elements which are too large and those which are skewed far from rectangular can cause this type of problem. Conversely, elements which are too small may also cause problems in some instances by producing ill conditioned matrices which cannot be solved accurately.

The other side to choosing element size is economy. The solution time, thus the cost, for an analysis increases linearly with the number of elements. (this is true for creep, not a full equation solution as occurs during an elastic analysis). Keeping the number of elements to the minimum necessary for the desired degree of accuracy saves time and money and the effort expended looking through the results.

The analysis performed for this purpose used a 5.5 m by 3 m room typical of the Cominco entries. Two and four elements were used in the back to determine the influence of element size. Figure 6 shows the deformed shape of the back after 1 year of creep. The differences between the deformed shapes of the back with 2 and 4 elements clearly illustrate the effect of element stiffness.

The two element back has a greater deformation at the pillar and a smaller deformation at the centre of the room, just as would be expected if the back were stiffened. There is also an anomaly in the shape caused by the element trying to deform in a way for which it is not designed. Note that the centre deformation is slightly less than the deformation 1 m towards the pillar, a result which is intuitively unreasonable.

The four element back is clearly more flexible and deforms into the anticipated shape without anomalies.

In conclusion, a room surrounded on all sides with 4 elements per face will perform well and experience has shown that unless very localized affects are being studied it is unnecessary to increase the mesh refinement beyond this level. If processing time or computer memory are inportant restrictions, two elements per face can be used but interpretation should take into account some anomalous effects and that errors in deflection production of 5-10% can be anticipated.

2) Influence of Weak Elements in the Back.

The back strata at the Vanscoy mine contain clay partings which are persistent enough to be used as a marker horizons. The nature of abutment and pillar deformation indicate that these partings act as slip surfaces along which considerable deformation can take place without causing significant failures of the pillar/back intersection. The back in the stress relief drifts tend to separate at the clay partings, with the lower strata buckling into the opening.

Some difficulty is encountered when trying to model this behavior realistically using GEOROC. The program allows for no "jointing, slip between elements, or plastic yeilding, thus restrains pillar elements from deforming independently of the back elements. A possible way of alleviating this problem is to have a layer of thin, very soft elements in the back which shear extremely readily. Although, ideally, these

elements should be only a few centimeters thick, this is impractical because they would become extremely distorted and behave anomalously. As a result, the test was performed with the first layer of elements in the back 1 meter thick, with their modulus reduced to one tenth of that of the surrounding salt and with their creep constant increased by a factor of 10. (The creep constant referred to is parameter A in the time power law).

Figure 7 shows the deformed shape of the rib after one year with and without the soft elements in the back. The addition of the soft elements has the affect of increasing the displacement at mid-height by 30% and that at the top of the rib by 80%. The deformed shape is still dictated by the continuity which is maintained between the rib and the back and as a result it does not closely match the 90° joint between rib and back seen in practice. However, the desired effect of increasing horizontal expansion of the abutment preferentially near the top has been achieved and this may be a useful technique to use when studying very local stress distributions such as those within a pillar. However, a joint element would clearly be more suitable for the purpose and the addition of such an element is one development to GEOROC worth considering in the future.

3) Influence of Material Properties on Room Deformation.

Sensitivity analyses were performed at three stages in the project - once during the parametric study by RE/SPEC Ltd., again with a single room mesh during the testing and verification of PC version of GEOROC and finally after laboratory data had been analyzed. The first two series of analyses were educational in nature rather than of direct practical value. They provided some experience with the program and gave some idea of the effect of changing various parameters. They also showed that it is possible to generate solutions which are superficially reasonable while using material constitutive laws quite unlike these derived from laboratory testing. This demonstrated that a good fit to some subset of field data is not necessarily adequate

justification for claiming the validity of a model and using it for predictive analyses. As an example, a power law for potash $\varepsilon = 4 \times 10^{-14} \sigma^{6} t^{.6}$ gives a reasonable fit to room 2105 closure, as does $\varepsilon = 5.5 \times 10^{-9} \sigma^{2.75} t^{.6}$. The power on time is the same, hence the shape of the creep curve is the same, but the predicted stress distributions are completely different. Consider that if the exponent of stress is 6, creep rate at a stress of 10 MPa is one million times greater than that of a stress of 1 MPa, whereas with an exponent 2.75 it is only 562 times greater. Thus, for the same deformation at the face of an opening, a far greater volume of salt must be mobilized at the lower value of exponent.

The most useful analyses were performed after analysis of the SRC creep test data, discussed in Section 4. At this point, there was good data for the elastic properties of the Dawson Bay Limestone and the creep of potash, and a few tests on elastic constants for the salt and potash. However, creep test had not been performed on the salt and no data was available for the Red Beds. Both these needed to be estimated from the finite element sensitivity analyses.

The Red Beds were dealt with by incorporating them as part of a single elestic unit with the Dawson Bay Limestone. The limestone was shown by laboratory tests to be highly variable in strength and stiffness, so there was little justification for treating the Red Beds separately.

The salt was assigned a constitutive law identical to that of potash and it was then adjusted to decrease its creep rate until a good match to field data was achieved for the ratio of horizontal to vertical closure of the 2105 room. This does not necessiarily give the best fit, and other measurements could have been used for comparison. The exponent of stress was maintained the same as that for potash simply because there is no evidence to the contrary and because variation of the creep constant gives much more direct control of creep rates.

The Young's modulus of the Dawson Bay Limestone was not decreased below its laboratory value because it was found that a high value was needed in order to induce floor closures as great as, or greater than back closures, which is the pattern observed in the mine.

Although a good fit to 2105 closure data is achieved using the power law derived from laboratory data, there is no guarantee that the fit will be reasonable in the long term since both sets of data extend for only a few months. For this reason, the steady state creep law (exponent of time equals one) must also be considered for predictive modelling, and its results compared with those from the time power law. Comparisons between the single room model and field results for the first 90 days of deformation in room 2105 are shown in Figures 8 and 9.

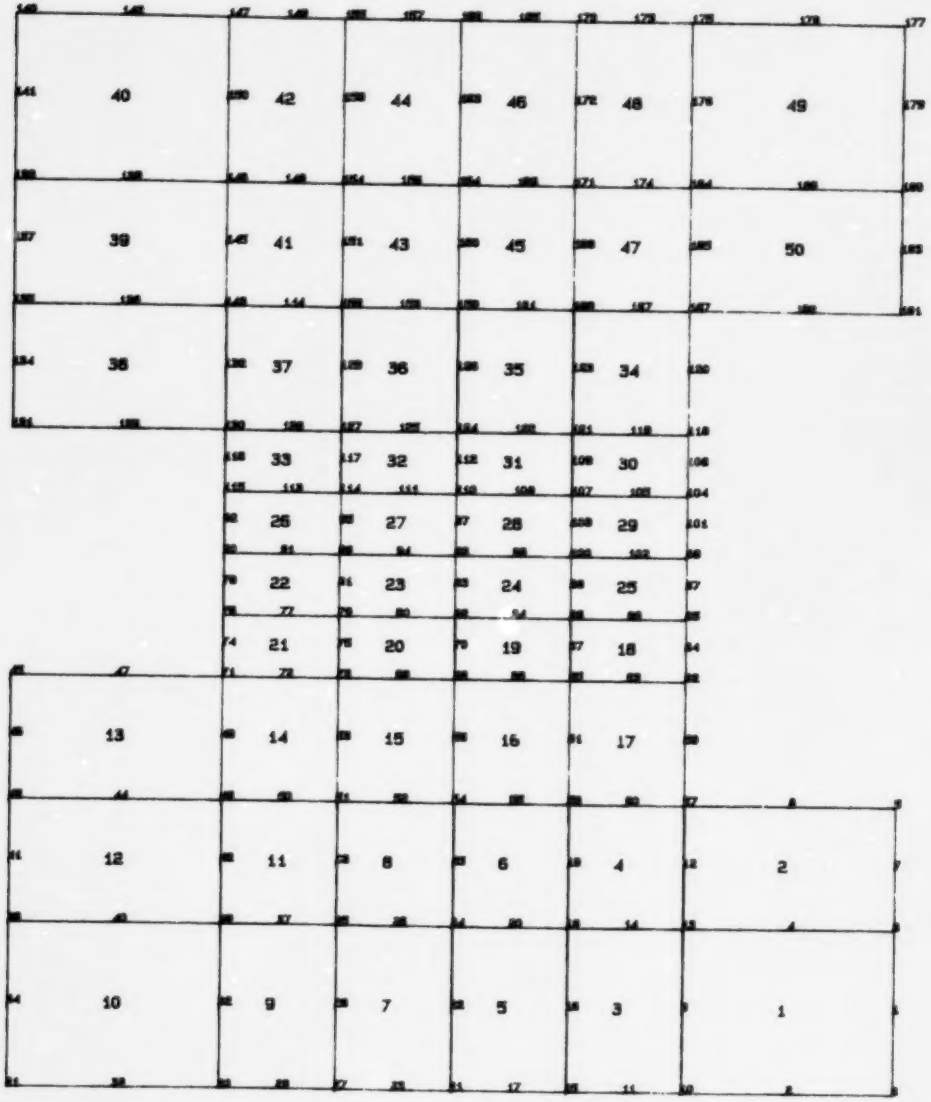
40
42
44
46
48
49
39
41
43
45
47
50
38
37
36
35
34
33
32
31
30
26
27
28
29
22
23
24
25
21
20
19
18
13
14
15
16
17
12
11
8
6
4
2
10
9
7
5
3
1

FIG. 1

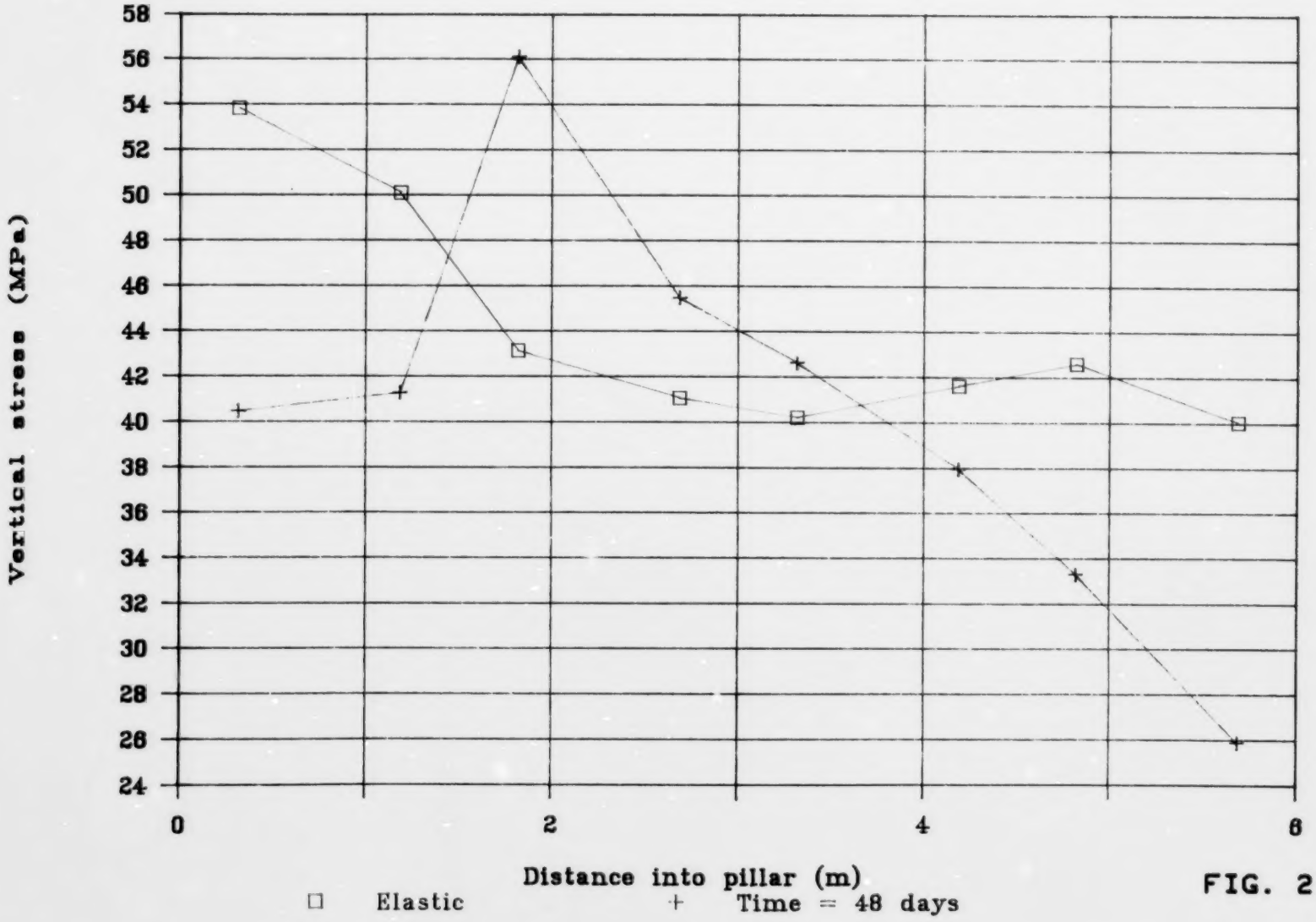
Vertical stress (MPa)
58
56
54
52
50
48
46
44
42
40
38
36
34
32
30
28
26
24
0
2
4
6
Distance into pillar (m)
□ Elastic
+ Time = 48 days

FIG. 2

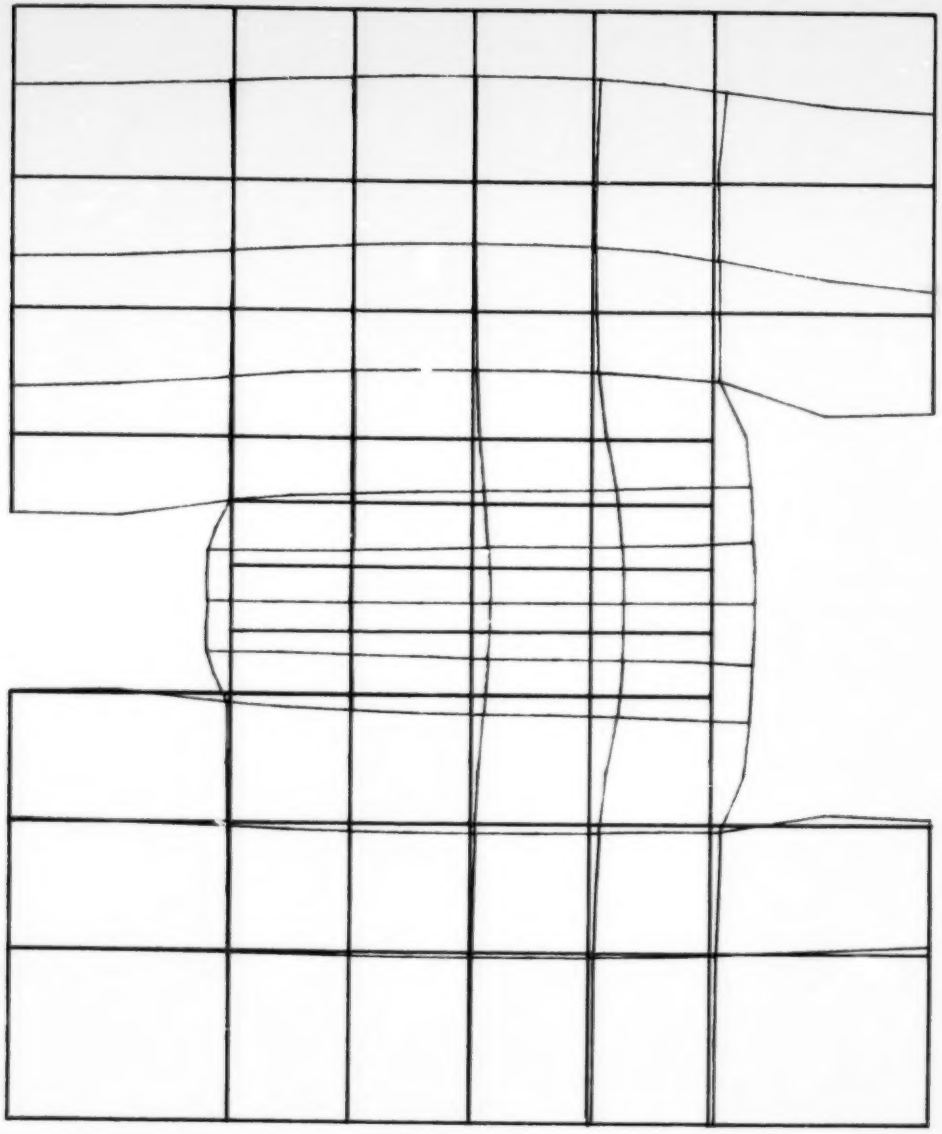

FIG. 3

36	35	28	25	24	22	20
34	33	29	26	23	21	19
32	31	30	27	18	17	16
				15	14	13
				12	11	10
				9	8	7
				6	5	4
				1	2	3

FIG. 4

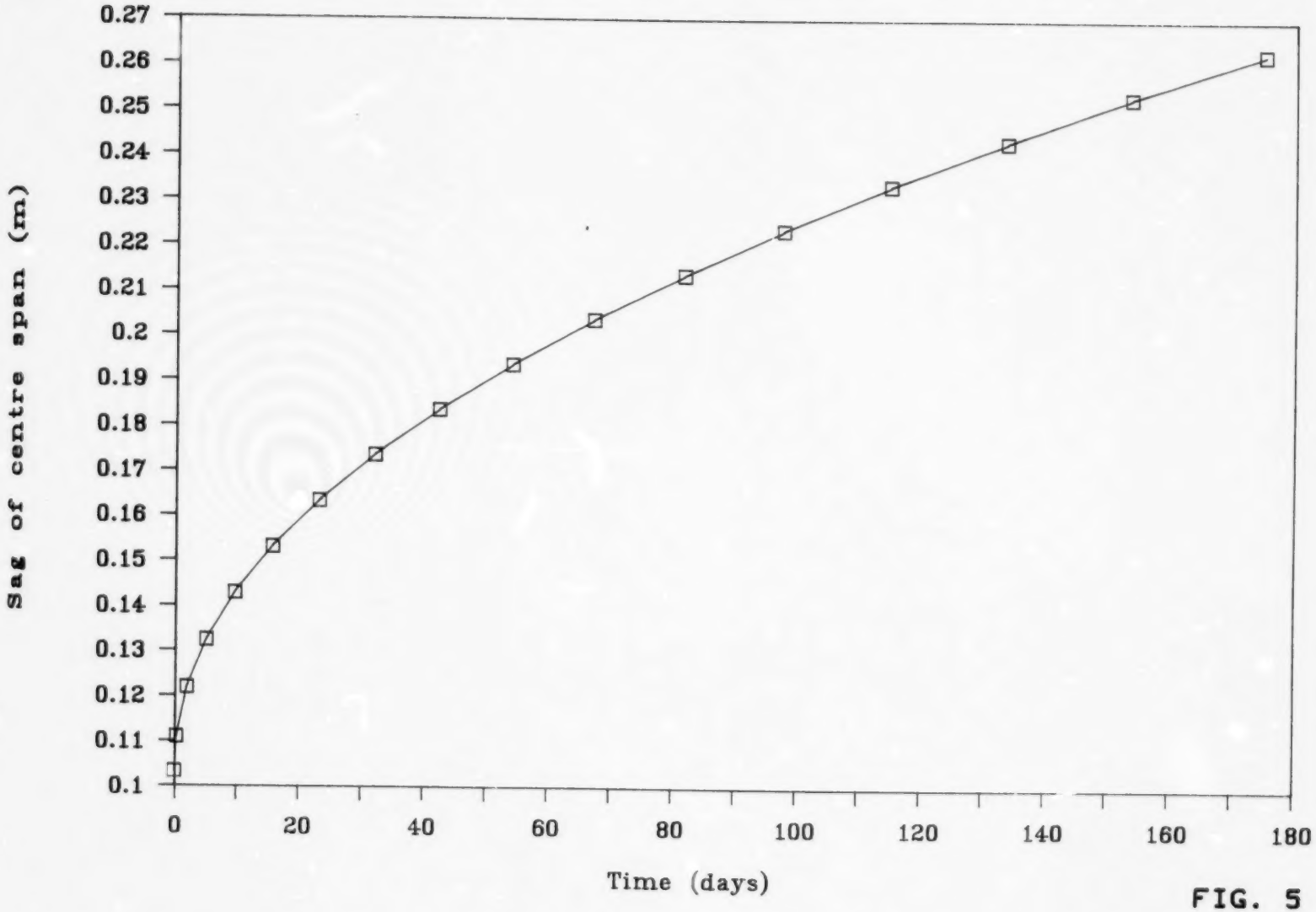
Sag of centre span (m)
0.27
0.26
0.25
0.24
0.23
0.22
0.21
0.2
0.19
0.18
0.17
0.16
0.15
0.14
0.13
0.12
0.11
0.1
0
20
40
60
80
100
120
140
160
180
Time (days)

FIG. 5

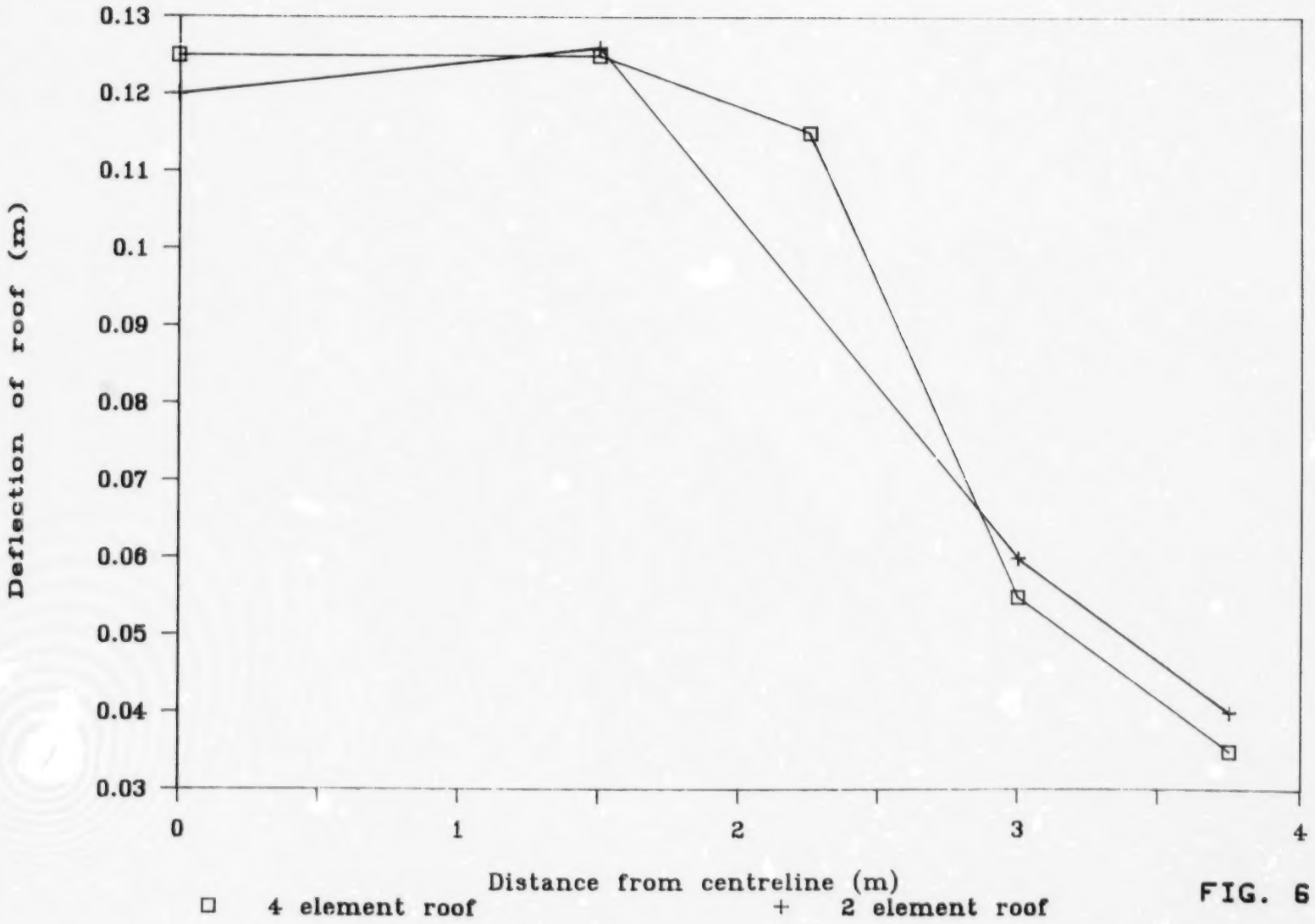
0.13
0.12
0.11
0.1
0.09
0.08
0.07
0.06
0.05
0.04
0.03
Deflection of roof (m)
0
1
2
3
4
Distance from centreline (m)
□ 4 element roof
+ 2 element roof

FIG. 6

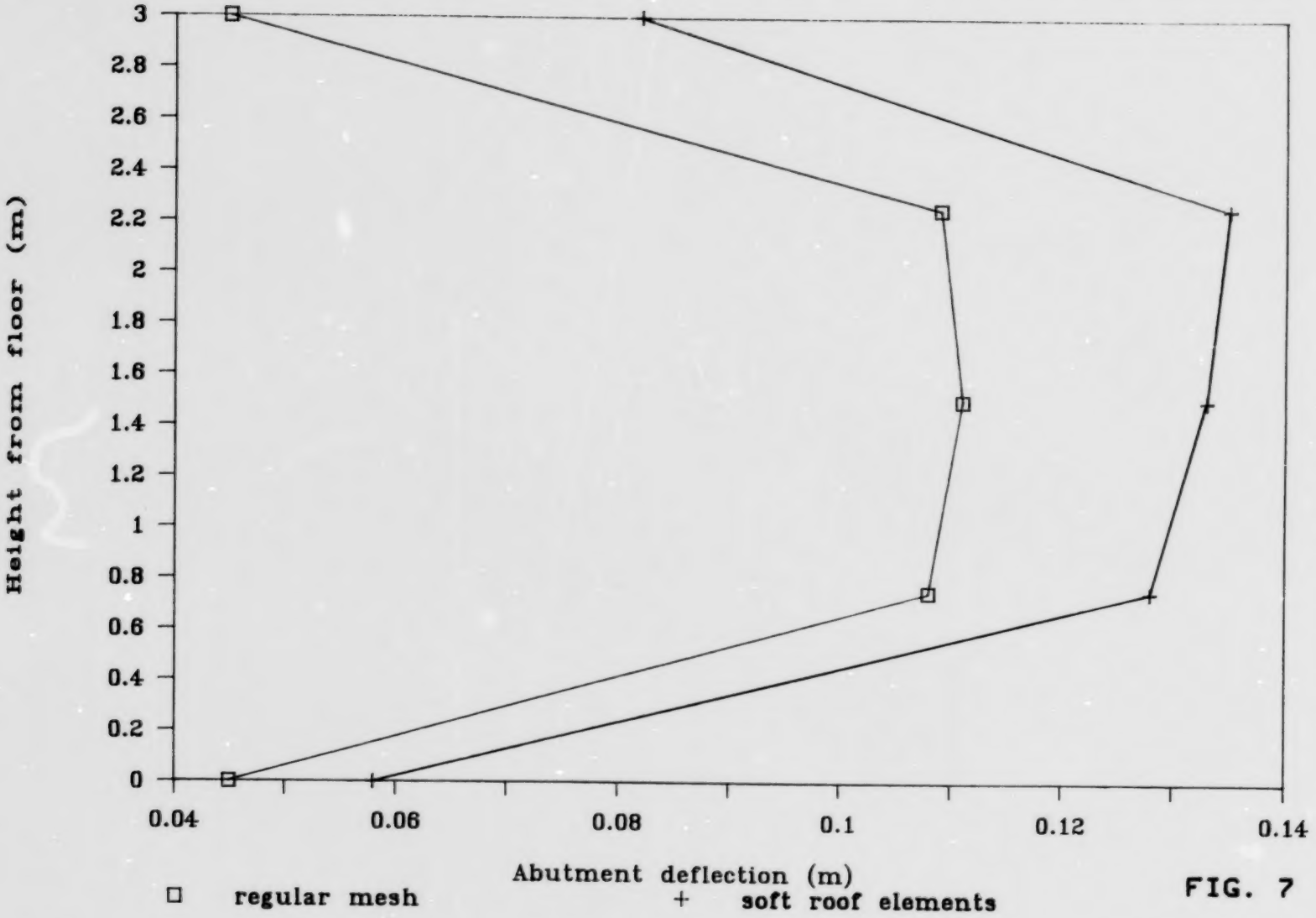
Height from floor (m)
3
2.8
2.6
2.4
2.2
2
1.8
1.6
1.4
1.2
1
0.8
0.6
0.4
0.2
0
0.04
0.06
0.08
0.1
0.12
0.14
Abutment deflection (m)
□ regular mesh
+ soft roof elements

FIG. 7

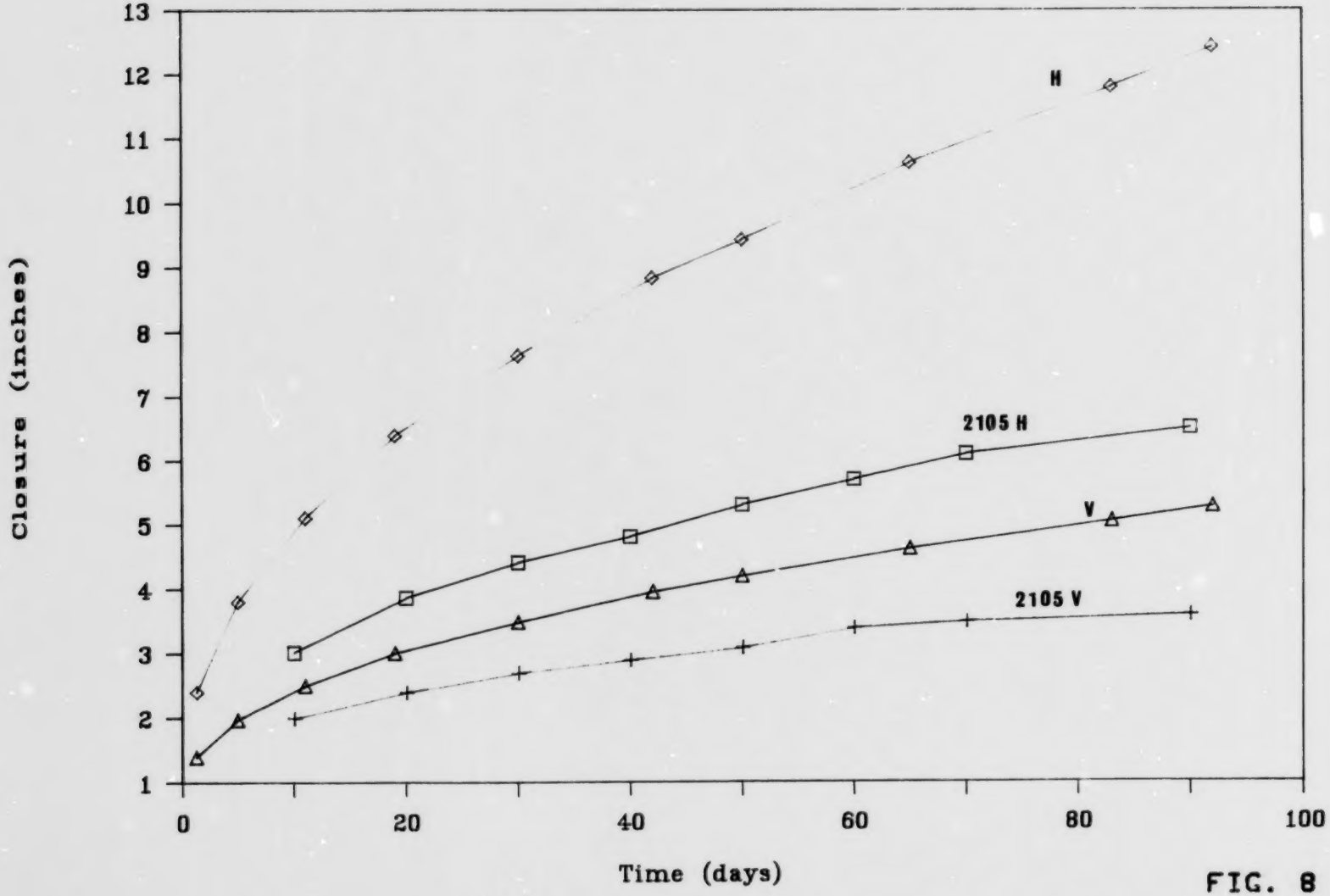
Closure (inches)
13
12
11
10
9
8
7
6
5
4
3
2
1
0
20
40
60
80
100
Time (days)
H
2105 H
V
2105 V

FIG. 8

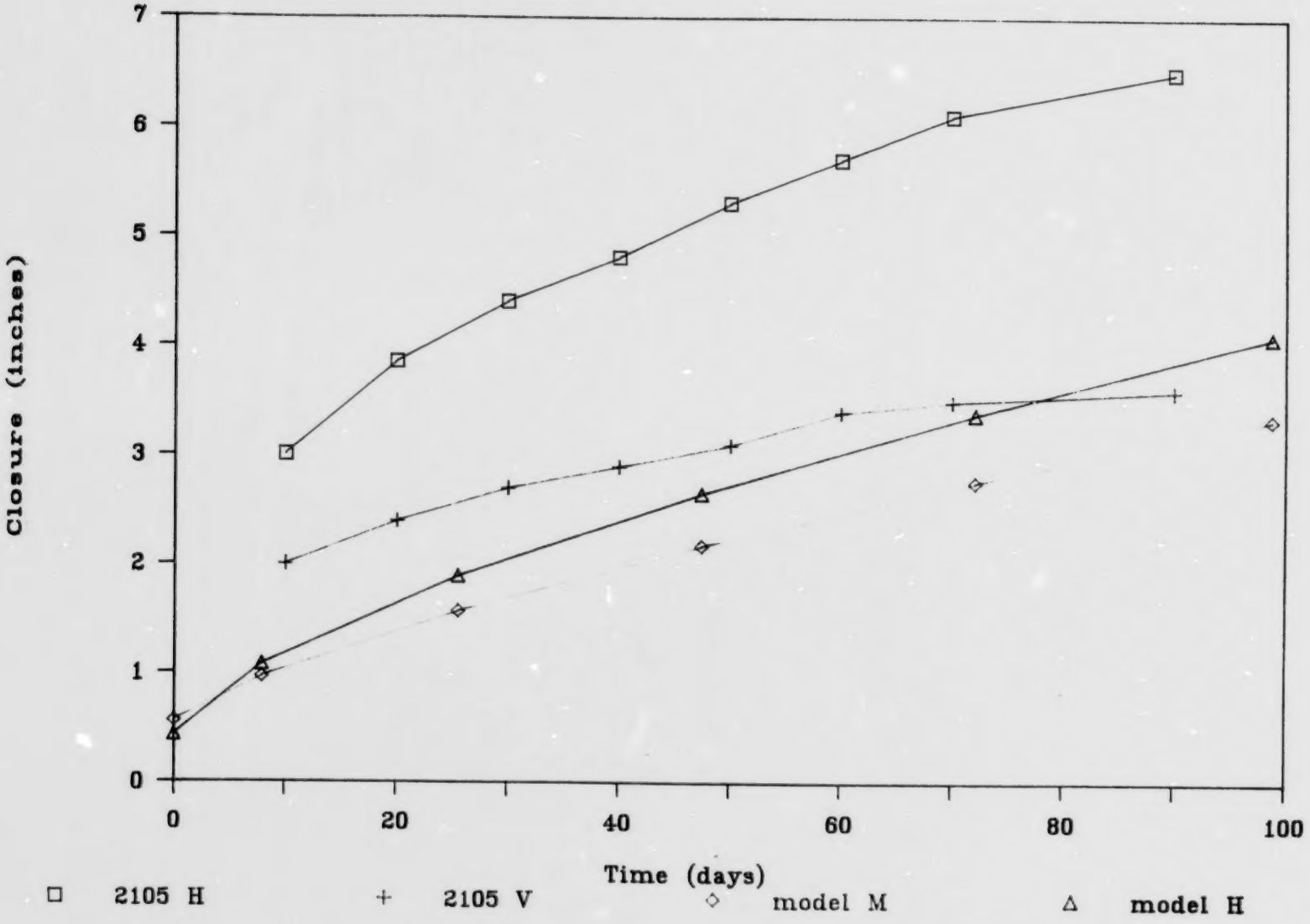
Closure (inches)
0
1
2
3
4
5
6
7
0
20
40
60
80
100
Time (days)
2105 H
2105 V
model M
model H

6.4 ANALYSIS OF THE FIVE ROOM ENTRY SYSTEM

6.4.1 MODEL DESCRIPTION

The five room entry system was modelled with a mesh comprising 238 elements and 777 nodes as shown in Figure 10 (DWG. #1T03). The upper two rows of elements form a stiff elastic beam, simulating the Dawson Bay Limestone and Red Beds. The potash member is 3.0 meters thick and is modelled as a layer 2 elements deep. The remaining elements are salt. Symmetry about the left edge of the mesh is used to allow only half the system of entries to be modelled. The right hand boundary is also restrained against horizontal deformation, but is sufficiently remote from the excavations to have no influence on them. The entries are excavated in a time sequence, closely following the mining sequence. The outer room (and its mirror image, the other side of the axis of symmetry) was excavated at "time zero", as part of the elastic solution. The next room was excavated after 90 days and the final central room after 120 days. The outer rooms are all 5.5 meters in width; the central room is 7 meters wide. The pillars are all 6 meters thick. At the time the central room was excavated, two elements were also removed from the roof of the outer entry to simulate roof failure.

Loading on the model was by in-situ stress. An overburden load of 23.5 MPa was applied to the upper surface and was distributed throughout the model by earth pressure coefficients of 1.0 in both horizontal axis. A body force component of .02 MPa per meter depth was added to the in-situ stress to account for gravity within the model.

Severe numerical instability when using the constitutive law derived from laboratory testing forced the use of a single excavation stage for some steady state simulators. This was unfortunate but does not invalidate the stress distributions predicted. They are believed to accurately model conditions a year or more after the mine entries were driven. The source of numerical instability is still being investigated, but has only been observed on the larger UNIX version, not on the MS DOS version of GEOROC.

6.4.2 STRESS DISTRIBUTION AROUND THE ENTRY SYSTEM

The stress distributions described in this section are those existing 45 days after the final excavation using the steady state material properties discussed previously. Intermitent numerical instability problems prevented longer runs with this material model although other material models derived from incomplete laboratory data behaved stabley. Since this is believed to be a hardware/operating system problem, complete runs will be reported once it is solved.

1. Pillars and Abutments

The distribution of vertical stress through the pillars at mid height is shown in Figure 11. The inner pillar (2103-2104) is symmetrically loaded, with a peak stress of 36 MPa (5,220 PSI). The outer pillar (2104-2105) is asymmetrically loaded due to the removal of support in the back of 2105. The peak stress is again 36 MPa. The abutment has a lower stress adjacent to the room (23 MPa) than have either of the pillars and the peak load of 34 MPa (4930 PSI) is also lower than in the pillars. The abutment stress peak is very broad and with time broadens further and moves away from the entry. Stresses compare well with those measured by pressure cells in the pillars. The peak stress of 32 MPa (4700 PSI) in the 2104-2105 pillar and the stress of 23 MPa (3,335 PSI) at a depth of 3 meters (10 feet) in the abutment are examples. The model predicts stress relaxation in both of the pillars and close to the face of the abutment so there appears to be good comparison between the model and field behaviour. The stress peak in the abutment does not match well and the reasons for this are not clear. The presence of a peak stress somewhat greater than the original in-situ stress is anticipated but pressure cells indicate that the peak is only 3 meters into the abutment and reaches maximum values below the in-situ stress. It may be that higher stresses were attained before the cell reached equilibrium, but the expected evidence of stress

transfer away from the entry is not provided by other cells placed up to 30 meters into the wall. One possible reason is that the pressure cells in locations where creep is very slow do not reach a true equilibrium due to creep of the resin encasing material. Other explanations pertaining to modelling errors will be sought.

2. Stresses Above and Below the Rooms

Above and below the rooms is a large stress relieved zone. The effect of vertical load reduction can be observed at least 30 meters below the middle room and horizontal stress are reduced to a depth of about 20 meters. The stress field above the middle room is almost a mirror image of that below it despite the presence of the Dawson Bay Limestone. Figure 12 illustrates the vertical and horizontal stresses above and below the 2103 room. The overburden, or in-situ, stress gradient is included for reference.

The outer rooms do not cause such a depth of stress relief. Horizontal and vertical floor stresses for both these rooms are shown in Figure 13. Horizontal stresses below 2105 peak at a stress of 26 MPa (slightly above the overburden pressure) 6 meters below the floor. They then reduce to remain slightly below the overburden pressure to depths greater than 20 meters. In 2104, there is a small peak about 2 meters below the floor and then below 5 meters there is a steady increase towards the overburden pressure, which is not exceeded.

Vertical stresses below both rooms remain below 20 MPa for a depth of at least 20 meters. As expected, the stresses increase more rapidly with depth below the 2105 room.

The stress profiles correspond, at least qualitavely very well with those produced by pressure cells. The locations of the peaks and relative magnitudes of stresses are encouraging results. Note that only the horizontal stresses can be compared since the vertical

stresses cannot be measured by borehole cells. Absolute stress magnitudes, like those in the abutment pillars, do not compare favourably. Stresses measured in the field are in the range of 7 to 14 MPa (1,000 - 2,000 PSI) or only about 60% of those predicted by the model. Again, the possibilities for the cause of this error are poor model behaviour, a very poor estimate of the overburden pressure and in-situ stress ratio, or the pressure cells equilibrating at a stress below the actual stress.

6.4.3 DEFORMATION DISTRIBUTION AND ROOM CLOSURE

The fit of the steady state and time power laws derived from laboratory tests to the closure of the first cut room (2105) has been presented earlier. Very encouraging fits were given by the steady state law; the power law for potash would benefit from a decrease in the exponent of time to 0.5 from 0.6. The vertical closure rate of room 2103 is shown superimposed on the field data in Figure 14., illustrating the close match of vertical closures. The ratio of centre to ribside vertical closures was predicted to be 0.7, somewhat lower than the value of 0.8 found in the field data. The distribution of deformation into the back of room 2103 is shown in Figure 15.

A difficulty was encountered when trying to match the relative closure of the three instrumented rooms during the first year after development. Even the rapidly decaying time-power law does not adequately differentiate between the early closures of the rooms. However, this may not be particularly important with regards to the behaviour of the entry system. Field data indicates that after about 100 days there is very little difference between the vertical closure rates of the 2103 and 2104 rooms. The model also gave this result and showed that 2105 had closure rates about 15% higher up to 1,000 days.

A prediction of the model which is less readily explained is that of approximately equal contributions to vertical closure by the back and the floor. Despite assigning a very high stiffness to the Dawson Bay, the field observation that a majority of closure comes from the floor is not matched. Since this field data cannot be questioned, modelling errors must be to blame. The back salt is either rather stiffer than the floor salt (ie. it creeps at a lower rate due to different impurity or moisture content) or the overburden acts as a even more rigid beam that has been supposed. In either case, the problem can be readily overcome if there is field evidence to support hypothesis.

6.4.4 CONCLUSIONS

Finite element analysis has been used to accurately model the five room entry system and several components of that system. While the models were not without their failings, they demonstrated the potential power of numerical modelling in the study of new opening geometries and in the interpretation of field observations. Perhaps most important was the fact that constitutive laws derived directly from laboratory testing were used, and were not adjusted or "calibrated" to fit the field data. This demonstrates the value of a multi-faceted rock mechanics study and should provide encouragement to others to utilize the large diameter core testing facilities in Saskatchewan.

1	3	7	13	70	84	98	112	126	140	154
2	4	8	14	69	83	97	111	125	139	153
5	6	9	15	68	82	96	110	124	138	152
10	11	12	16	67	81	95	109	123	137	151
17	18	19	20	66	80	94	108	122	136	150
21	22	23	24	65	79	93	107	121	135	149
25	26	27	28	64	78	92	106	120	134	148
29	30	31	32	63	77	91	105	119	133	147
33	34	35	36	62	76	90	104	118	132	146
37	38	39	40	61	75	89	103	117	131	145
41	42	43	44	60	74	88	102	116	130	144
45	46	47	48	59	73	87	101	115	129	143
49	51	53	55	58	72	86	100	114	128	142
50	52	54	56	57	71	85	99	113	127	141

FIG. 10

Cominco 5-room entry (Dwg #1)

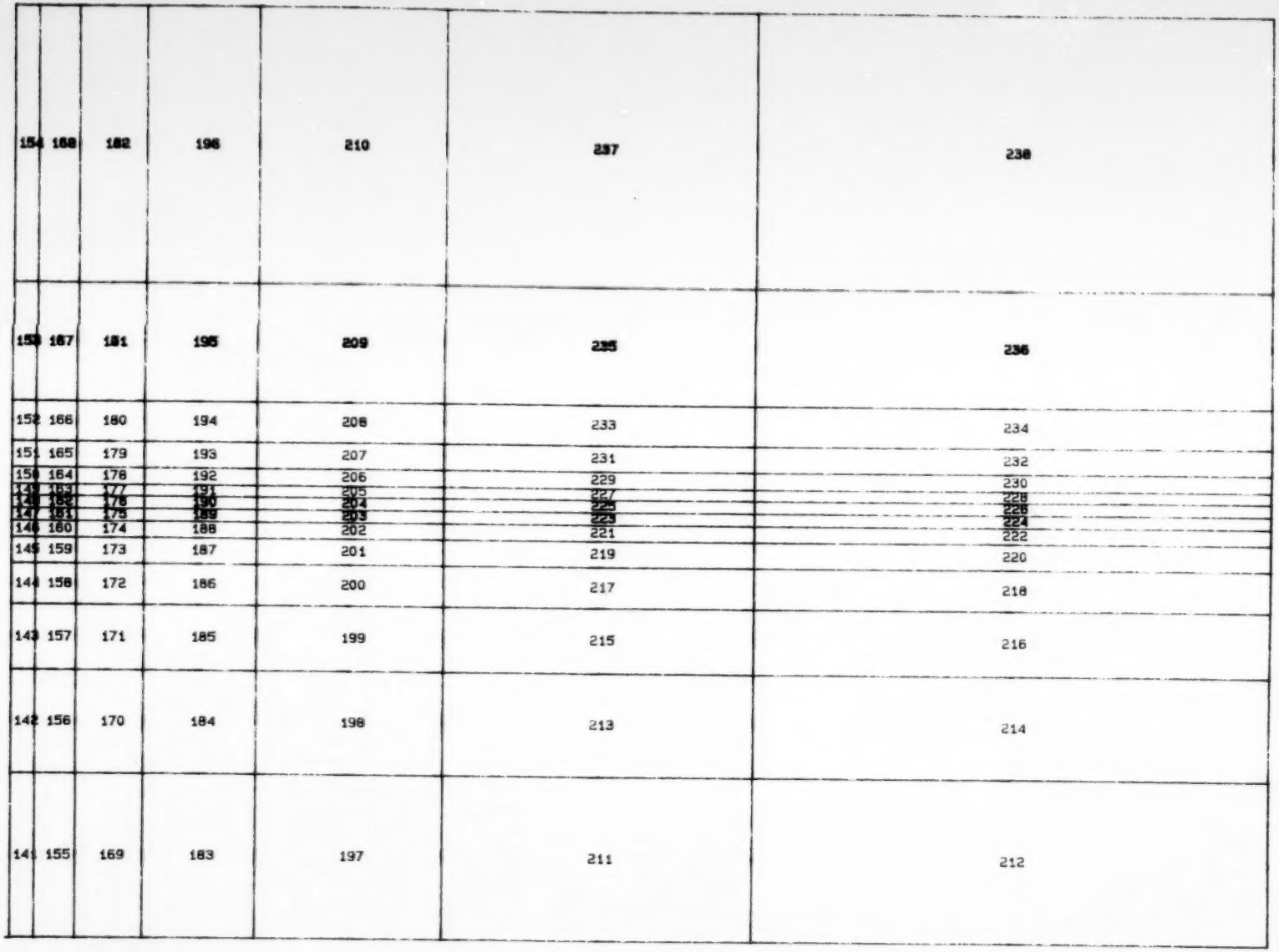

FIG. 10

Cominco 5-room entry (Dwg #2)

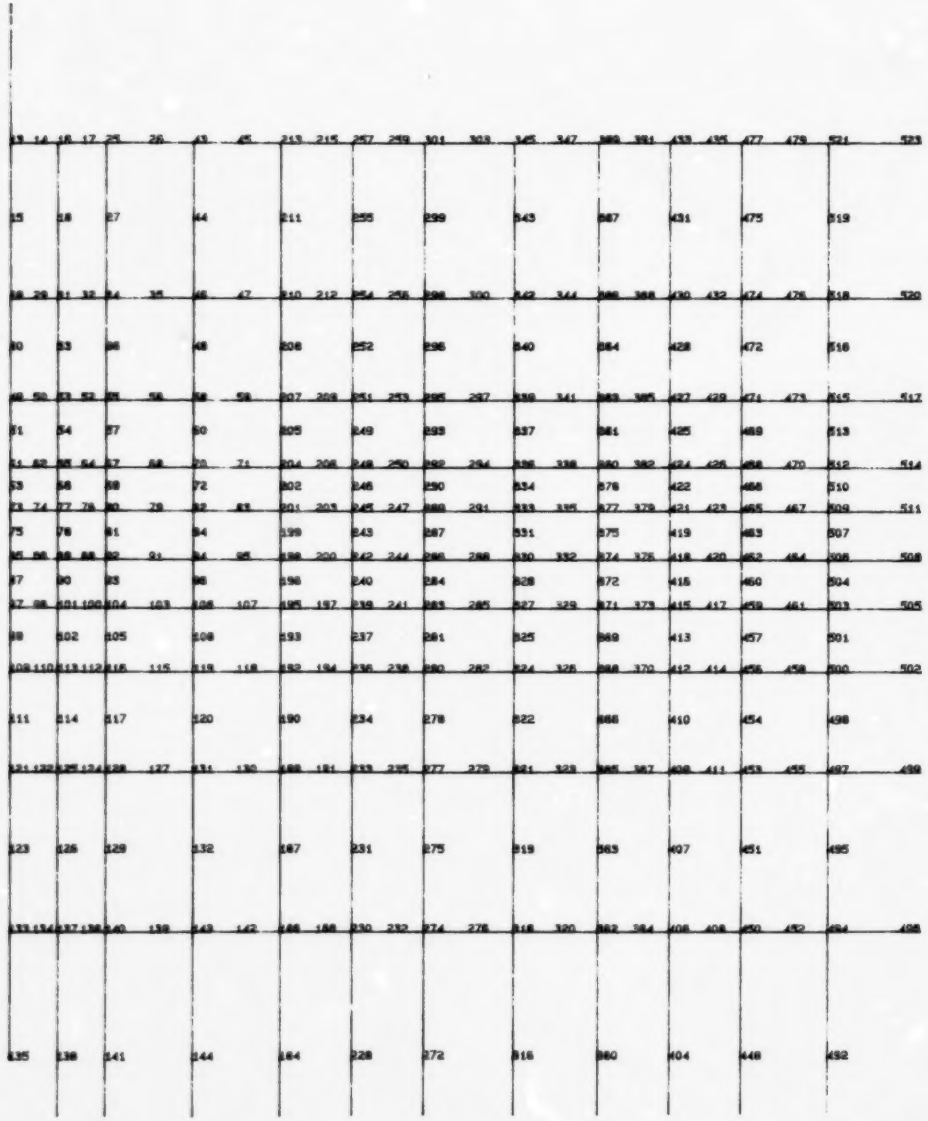

FIG. 10

Cominco 5-room entry (Dwg #3)

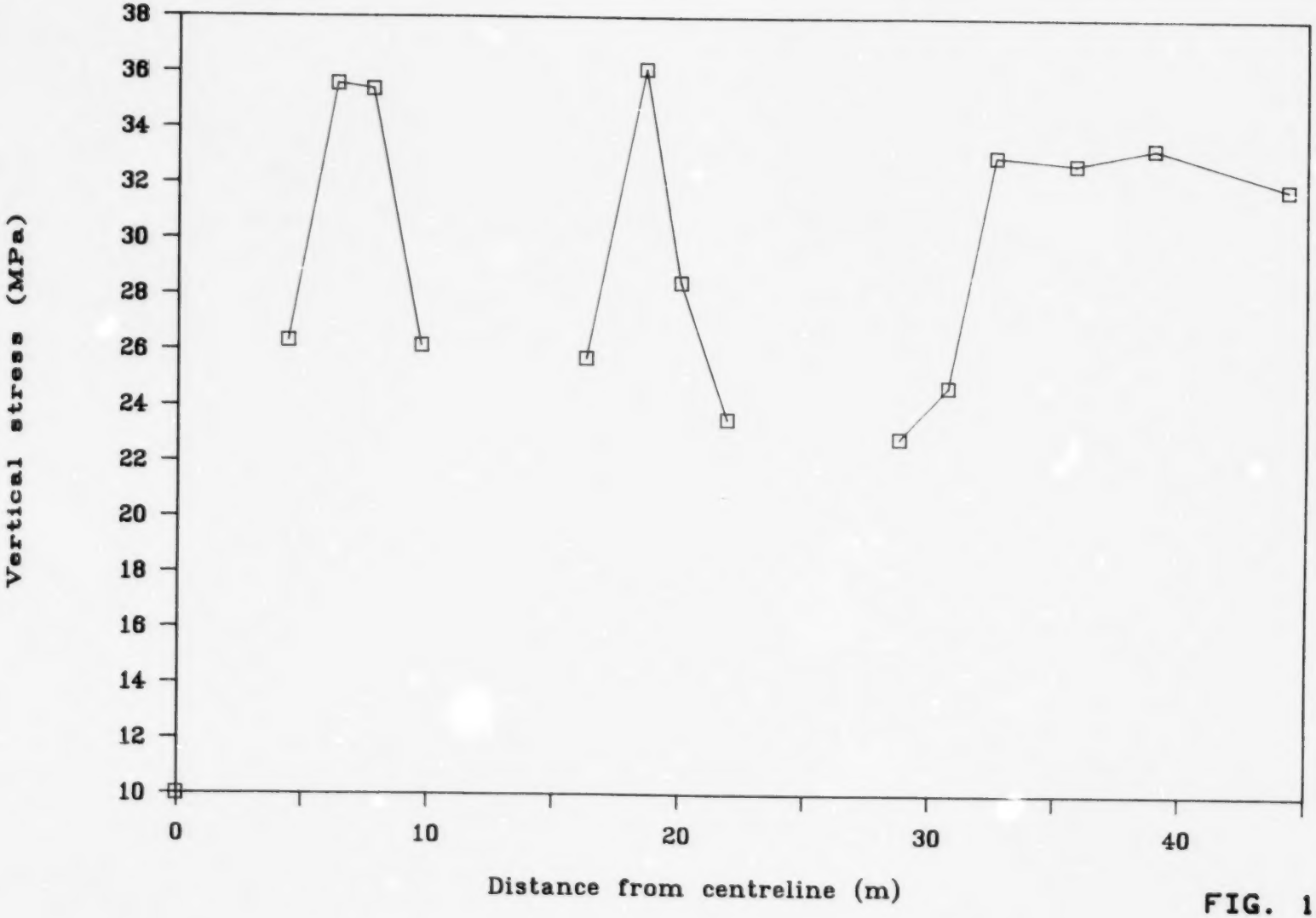
Vertical stress (MPa)
38
36
34
32
30
28
26
24
22
20
18
16
14
12
10
0
10
20
30
40
Distance from centreline (m)

FIG. 11

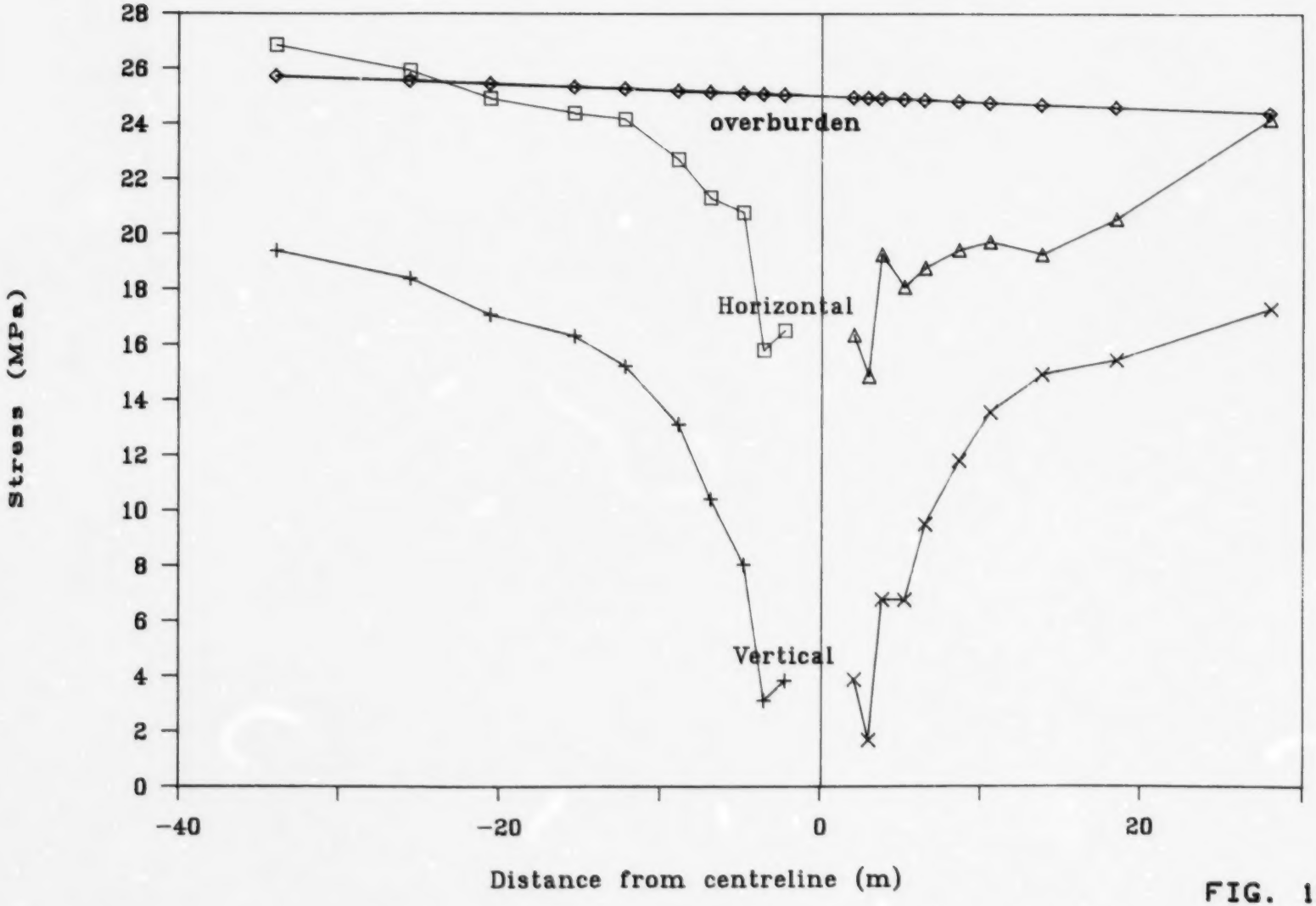
28
26
24
22
20
18
16
14
12
10
8
6
4
2
0
Stress (MPa)
overburden
Horizontal
Vertical
−40
−20
0
20
Distance from centreline (m)

FIG. 12

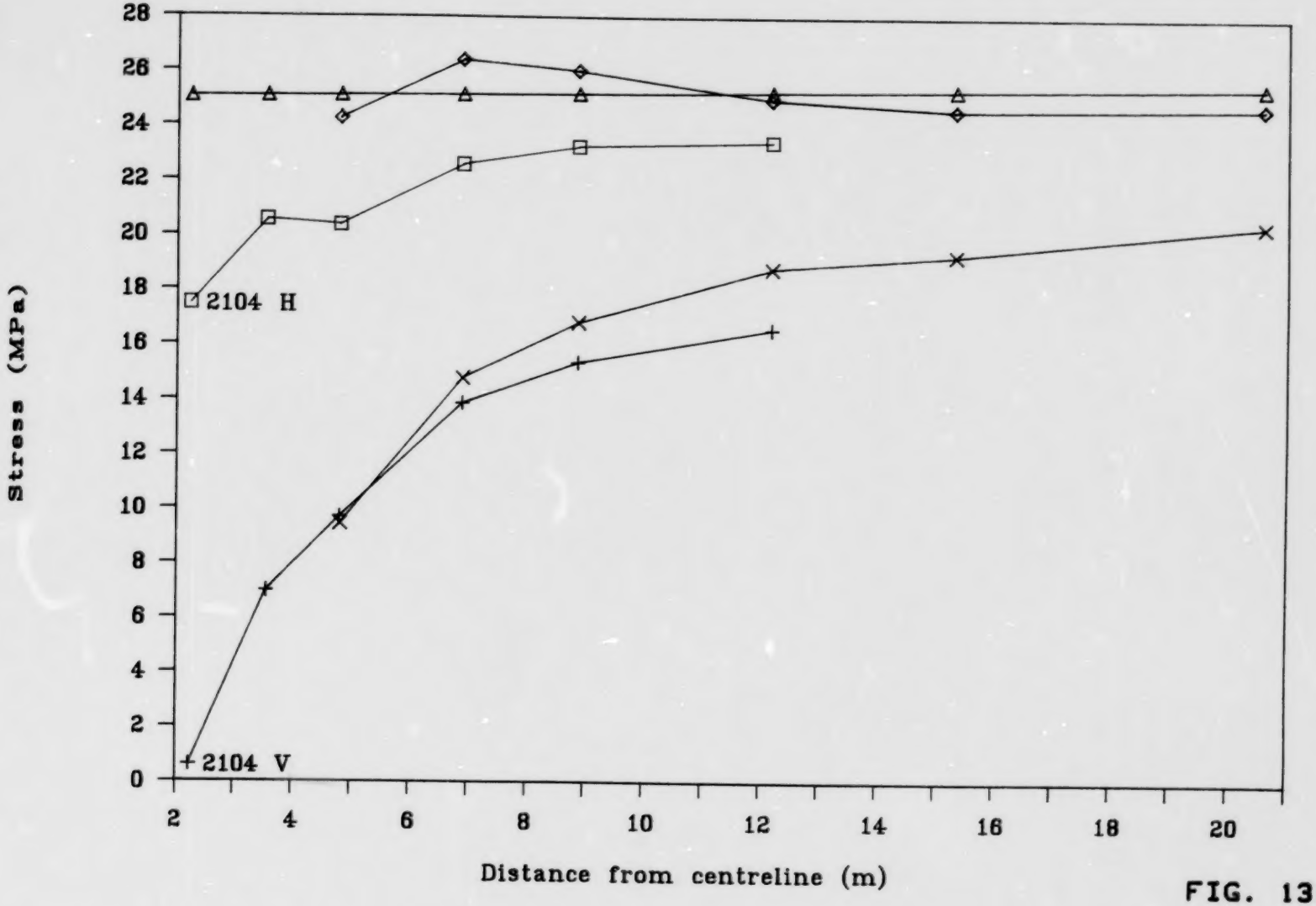
Stress (MPa)
28
26
24
22
20
18
16
14
12
10
8
6
4
2
0
2104 H
2104 V
2
4
6
8
10
12
14
16
18
20
Distance from centreline (m)

FIG. 13

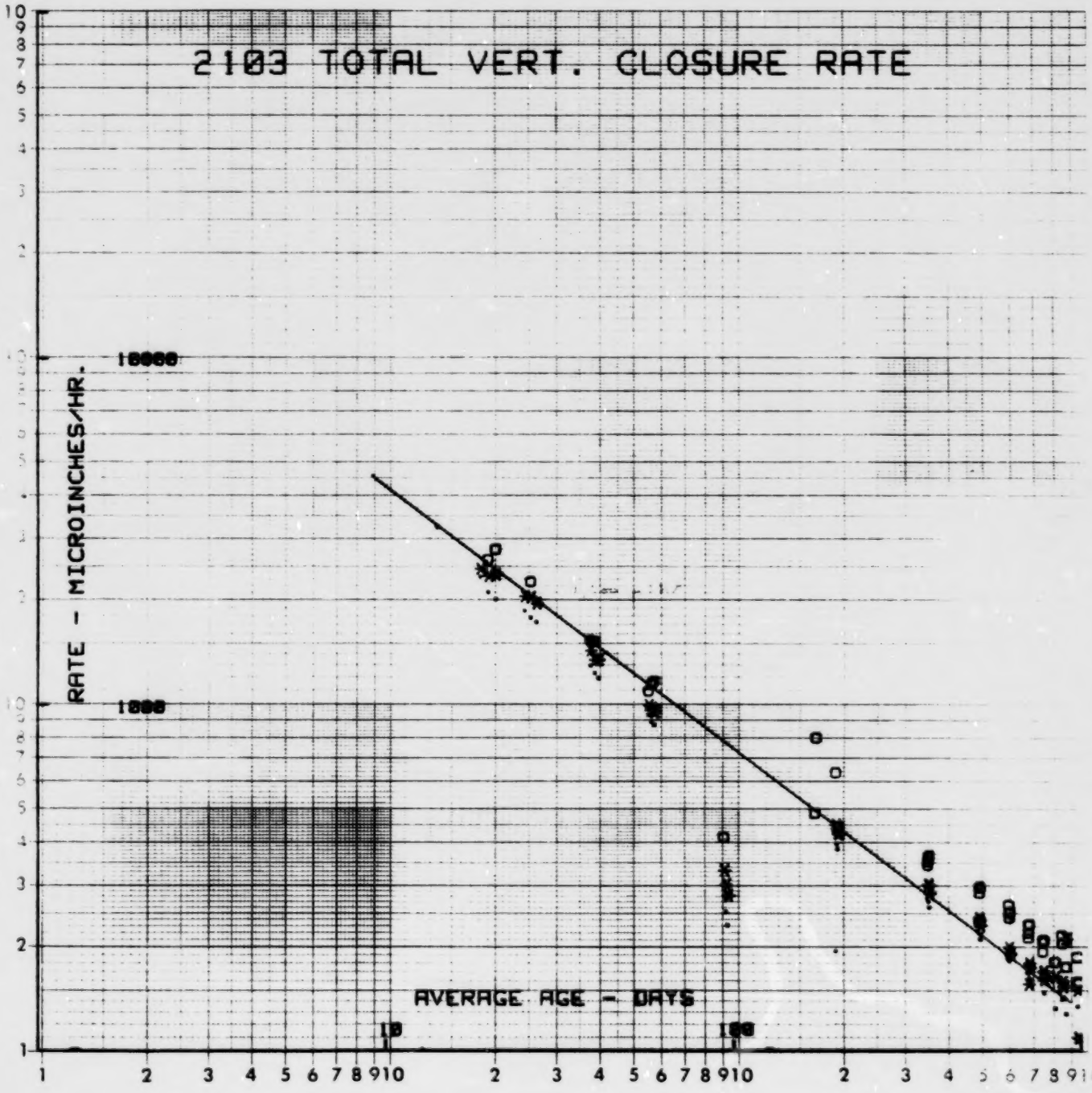
2103 TOTAL VERT. CLOSURE RATE
RATE - MICROINCHES/HR.
10000
1000
AVERAGE AGE - DAYS
10
100
1
2
3
4
5
6
7
8
9

FIG. 14

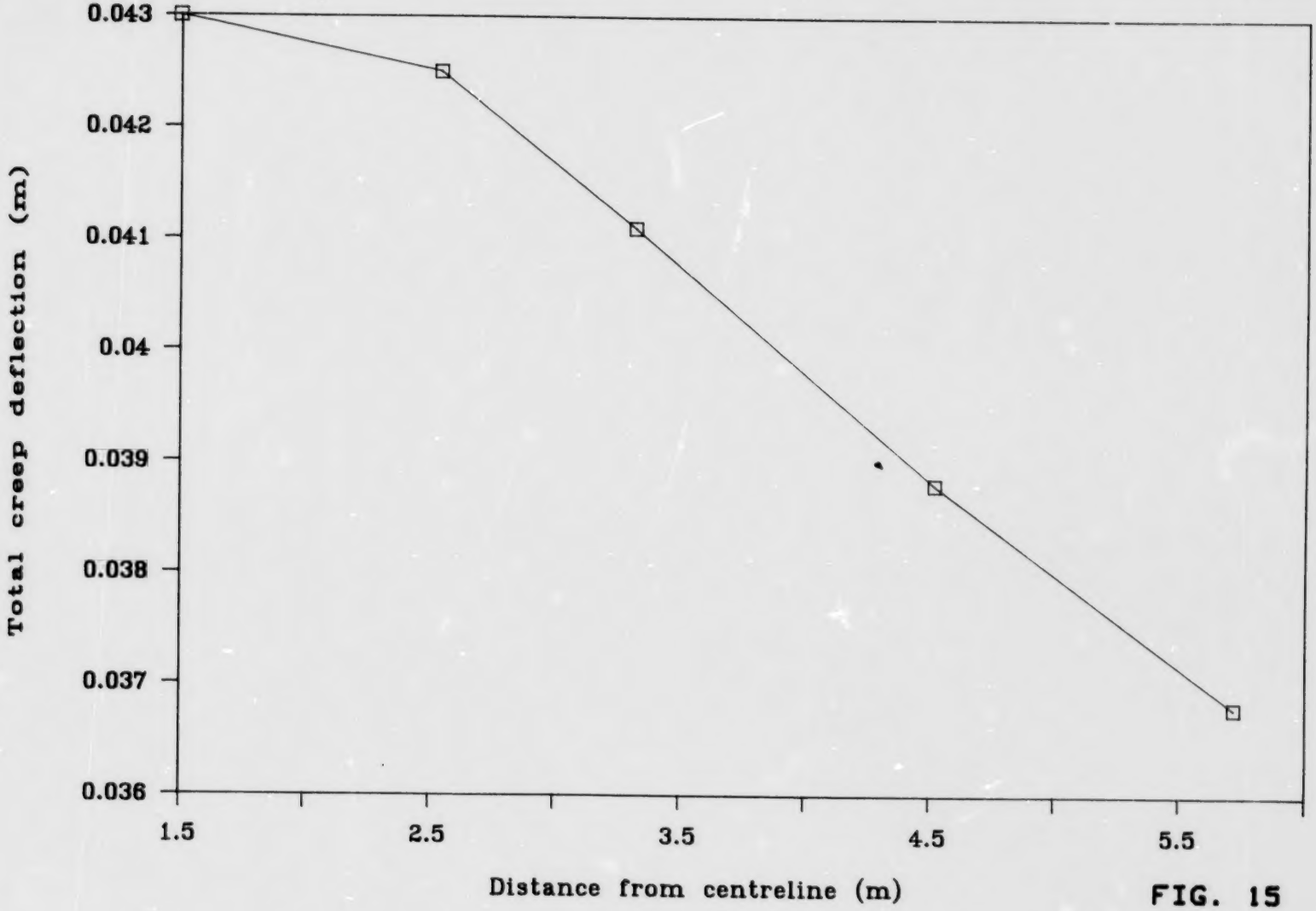
0.043
0.042
0.041
0.04
0.039
0.038
0.037
0.036
Total creep deflection (m)
1.5
2.5
3.5
4.5
5.5
Distance from centreline (m)

FIG. 15

APPENDIX A

1. USER'S GUIDE TO PC VERSION OF GEOROC
2. SUPPLEMENTARY NOTES TO USER'S GUIDE
3. USER NOTES ON GEOROC DATABASE SYSTEM
4. SUPPLEMENTARY NOTES TO THE GEOROC USERS MANUAL
5. PROCEDURE FOR USING GEOROC

USER'S GUIDE FOR PC VERSION OF GEOROC

A finite element package for mining simulations

The following guide describes the free format data file required for GEOROC. The file can be generated using the BASIC program GEOROCIN, contained on the GEOROC disc, which is run by simply typing the word GEOROCIN and hitting enter. Before running this program, however, it is necessary to generate a mesh for your problem using GEOMESH or the program microMESH, available from TECHWARE Ltd. Whichever mesh genarator is used, it should generate three files containing nodal connection arrays, nodal coordinates and boundary node fixity conditions.

Once the mesh and input data files have been created, GEOROC is run by typing:

GEOROC %1 %2 where the input file is %1.in and the three mesh files are %2.con, %2.nod and %2.ntp.

If GEOROC is being run under an operating system other than MS-DOS, the input file must be copied to a file named INPUT and the three mesh files must be concatenated into a file named MESHDATA before invoking GEOROC.

Data Format

All input is free formatted and data items may be separated by a comma or spaces. Lines must contain the required number of data items - blanks are not interpreted as zeros. Lines must not be more than 80 characters. A new line can be started at any point if there are too many data items to fit within 80 columns. Once all data items are entered on a line comments can be added to fill that line - this is sometimes helpful in documenting your data files. Floating point numbers can be entered in the form 1.01 .101E1 or 1.01E0 1.01D0 etc using upper or lower case letters.

Some types of analyses require different data from others. As a result, the input guide contains a number of decision points where the inclusion or omission of subsequent lines is dependent upon the values assigned previously to other variables or flags. If the instructions indicate lines of input are to be skipped, they must be completely omitted, not left blank.

Input Data File

LINE 1 NPOIN Number of nodal points (see GEOMESH output)

NELEM Number of elements (see GEOMESH output)

NVFIX Number of restrained nodes (see GEOMESH output)

NTYPE Type of geometric model used:
1 = plane stress
2 = plane strain
3 = axisymmetric

NMATS Number of different material types used

NPRBT Problem type:
1 = time dependent (creeping materials)
2 = static (elastic materials only)

NDATA Prepare a database (1 = yes, 0 = no)

NCHBC Number of boundary conditions changed after the initial elastic analysis (usually 0)

NELGP Number of elements whose material properties will change during the analysis. e.g. excavated elements which are subsequently backfilled

MFRON Maximum front width

LINE 2 TITLE Up to 80 characters describing the analysis

LINE 3 IAMDN Execution flag 0 = do a complete solution
1 = check the data file only

DECISION 4: for static problems skip to LINE 7

LINE 4 NINCS Number of time steps permitted before execution terminates. Determined by experience but try 100 for a first attempt

MXDTS Number of timestep maxima imposed. Usually 1 but more may be added to decrease the timestep below that automatically calculated following an excavation

LINE 5 FTIME Final time at which execution terminates

AMULT Multiplier on the critical time step. 0.3 is a typical value. Read supplementary notes for more details.

LINE 6 TTMXS Time at which this timestep maximum comes into effect (First one should be 0.0)

DTMXS Maximum size of timestep allowed

REPETITIONS: Repeat LINE 6 MXDTS times

LINE 7 NPRNT Print nodal coordinates and element connection arrays 0 = no, 1 = yes

NGPCD Print Gauss point coordinates 0 = no, 1 = yes. This flag is set internally to 1 if a database is has been requested.

IPRFO Print total external nodal forces 0 = no
1 = yes

IELAS Print elastic results 0 = no, 1 = yes

KOUTP Print option code:
1 = print displacements and residual forces
2 = print reactions at restrained nodes
3 = print Gauss point stresses
any combination in ascending order is allowed.

KPRNT Frequency of print for creep analyses:
0 = elastic run
1 = output every NOUTP timesteps
2 = output at NTIME specified times
3 = both 1 and 2 above control output

NOUTP Number of timesteps between outputs.
Must be 0 if KPRNT = 2

NTIME Number of times output will be printed.
Must be 0 if KPRNT is 0 or 1

NPRND Number of nodes at which output is required.

NPRNS Number of elements at which stresses are required

ISFOS Calculate Wawersik's strain related failure function. Note that SI units with stresses in MPa must be used for all data. 0 = no 1 = yes This option is currently disabled in the micro version of GEOROC

DECISION: If NTIME = 0 skip to DECISION 9

LINE 8 PTIME(1) Time at which first print is required
.
.

PTIME(NTIME) Time at which last print is required
Note: start new line after filling 80 columns

DECISION 9: If NPRND = 0 or NPRND => number of nodes skip to DECISION 10

LINE 9 NOUTD(1) First node at which output is required.
.
.

NOUTD(NPRND) Last node at which output is required.
Note: start new line after filling 80 columns

DECISION 10: If NPRNS = 0 or NPRNS +> number of elements skip to line 11

LINE 10 NOUTS(1) First element at which output is required.
.
.

NOUTS(NPRNS) Last element at which output is req'd.
Note: start a new line after filling 80 columns.

LINE 11 NUMAT Material type number. (use sequential numbers starting at 1)

NCRIT Material Type number:
0 = elastic
1 = time power law
2 = Rothenburg and Dusseault theory
3 = Norton law and/or rate theory

LINE 12 PROPS (1) Youngs Modulus
(2) Poisson' ratio
(3) Element thickness for plane stress problem

(4) Density - mass/vol units consistent with stress

Note:properties below only for visco-elastic materials

(5) Leading coefficient A
(6) Power on stress

For time power law:

(7) Power on time
(8) Rearrange law for strain hardening 0 = no
1 =yes

For Rothenburg and Dusseault theory

(7) Power on stress below 2XPrandtl limit
(8) Prandtl stress limit
(9) Uniaxial compressive strength
(10) Tensile strength

For Norton law and/or rate theory

(7) Q/R Activation energy/gas constant
(8) X Spectrum offset on energy axis
(9) B Spectrum height on Density axis
(10) V Activation volume

LINE 12a

PROPS(11) Flag indicating thermal stress calculations are required. 0 = no
1 =yes

(12) Coefficient of thermal expansion

NOTE: Nodal temperatures are read at each timestep from a file named NODTEMP

REPEAT LINES 11, 12 and 12a for each material type. There can be up to 10 materials and not all need be used in this analysis.

DECISION 13: If NCHBC = 0 skip to LINE 14

LINE 13 NOFIX Number of node fixed or released after elastic analysis

IFPRE Fixity code mn where:
m = x fixity: 1 = fixed 0 = free
n = y fixity: 1 = fixed 0 = free

PRESC(1) prescribed x displacement

PRESC(2) prescribed y displacement

LINE 14 NPLOD Number of nodal point loads

NEDGE Number of element edge loads

IGRAV Model loaded by gravity 0 = no 1 = yes

ISTRS Model load by initial stress field
0 = no 1 = yes
Note: see supplementary note for more information.

DECISION 15: If NPLOD = 0 skip to DECISION 16

LINE 15 LODPT Number of loaded node

POINT(1) Load applied in x (or R) direction

POINT(2) Load applied in y (or Z) direction

REPEAT line 15 NPLOD times

DECISION 16: If NEDGE = 0 skip to DECISION 18

LINE 16 NEASS Element number whose edge load is now given.

NOPRS(1) Node numbers on the loaded edge going round the element counter-clockwise
NOPRS(2)
NOPRS(3)

LINE 17 PRESS(1,1) Normal load applied to NOPRS(1)
PRESS(1,2) Normal load applied to NOPRS(1)
PRESS(2,1) Normal load applied to NOPRS(2)
PRESS(2,2) Normal load applied to NOPRS(2)
PRESS(3,1) Normal load applied to NOPRS(3)
PRESS(3,2) Normal load applied to NOPRS(3)

REPEAT LINES 16 and 17 NEDGE times

DECISION 18: If IGRAV and ISTRS = 0 skip to DECISION 19

LINE 18 THETA Angle between the direction of the gravitational vector and the y (or z) axis. If the y-axis is aligned with true vertical in the model this is 0.0

GRAVY Gravitational acceleration. Units are distance/second2. GRAVY is positive if the y-axis is positive upwards

DECISION 19: If IGRAV = 0 skip to LINE 21

LINE 19 NLAYS Number of layers for different initial stress specification. This must be at least 1

OBSTR Stress applied to top of model to simulate overburden pressure. (NEGATIVE stresses mean COMPRESSION)

LINE 20 YYTOP Top elevation of this layer

YYBOT Bottom elevation of this layer

AVDEN Average material density in this layer

XLESX In plane horizontal earth pressure coefficient

ZLESZ Out of plane horizontal earth pressure coefficient. Not required for plane stress.

REPEAT line 20 for each of NLAYS layers

LINE 21 NUMEX Number of excavations. Any number of elements removed or edge loads changed at one time is one excavation

DECISION 22: If NUMEX = 0 skip to DECISION 26

LINE 22 NEREM Number of elements removed on first excavation

NEPEX Number of elements with an edge exposed on the face of the first excavation.

TMEXC Time at which this excavation occurs.

DECISION 23: If NEREM = 0 skip to LINE 24

LINE 23 LEREM(1) Number of first element removed

.

.

LEREM(NEREM) Number of last element removed.

LINE 24 LEPEX Element number having an edge on the excavation face

NOEXS(1) Node numbers on the excavation face going around element LEPEX counter-clockwise

(2)

(3)

LINE 25 PNORM(1) Normal stress on excavated surface at node NOEXS(1)
PSHER(1) Shear stress on excavated surface at node NOEXS(1)
PNORM(2) etc
PSHER(2)
PNORM(3)
PSHER(3)

REPEAT lines 24 and 25 NEPEX times

REPEAT the group of lines 22-25 NUMEX times

DECISION 26: END here if NELGP = 0

LINE 26 RTOLG If material property change (backfilling) is to occur at a certain value of excavation closure, RTOLG is the ratio of (volume at backfill time)/(initial volume) If backfill is at a prescribed time, put 0.0

LINE 27 MELGP Element number whose material properties are to change

MATGP Material property number of new material type

BKTIM Time at which this element property is changed. Leave blank if backfilling is triggered by element volume ratio.

REPEAT line 27 NELGP times

Supplementary Notes to User's Guide.

Line 1....

NDATA - The program can write a binary database in addition to, or instead of, the printed output. This contains information for all nodes and elements at each requested print time regardless of the number of nodes or elements at which printed output is requested. It can be interrogated using DB_READ to yield tabulated data files for printing or plotting.

NCHBC - Nodes may be fixed or released after the elastic solution and before the start of creep to isolate some aspects of elastic and creep response if desired.

MFRON - GEOROC uses a matrix inversion and solution technique known as the Frontal solution. This makes efficient use of memory by eliminating the variables at a node as soon as every element containing that node has been assembled into the global stiffness matrix. Element numbering is optimized to minimize the number of new variables which must be assembled between the first and last occurrence of a particular node. The maximum number of active variables is called the Maximum FRONt width. MFRON is twice the front nodal width printed by the mesh generator, GEOMESH.

Lines 4 to 6.....

Appropriate choice of a timestep is critical to an accurate and stable solution. The following figure illustrates the error which may occur if the time step is to large.

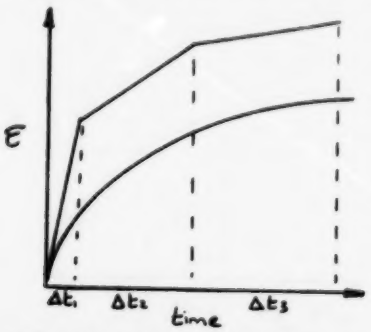

Each creep subroutines include an algorithm to calculate the critical timestep which depends upon the material properties, the strain rate and the effective or deviatoric stress. The calculated value should be small enough to ensure a stable solution i.e. one which will not diverge and crash due to excessive equivalent nodal forces. The accuracy

of the solution is not assured by this and thus an arbitrary multiplier is used to reduce the timestep:

$$critt = \frac{2(1+v).\sigma_e}{3E}\ \frac{}{e'} \qquad \text{where } e' = \text{effective strain rate}$$

timestep = AMULTX2XCRITT

A value for AMULT of 0.3 gives accurate solutions to many problems; however under some circumstances the solution may still begin to diverge and this will result in termination and an error message indicating that an effective stress value exceeded 1000. (If you are working in psi this value in the subroutine POWER should be increased to 100000.) If this happens it is likely that some value in the creep law parameters is unrealistically high. However, it can be overcome by reducing AMULT - say to 0.2. Try a second, smaller, value to ensure that the same solution is obtained; this is a good indication of a numerically accurate solution.

Line 14....

IGRAV - use this option for structures which are loaded by self-weight and external applied loads. Horizontal stresses due to self-weight will be related to the vertical stress by Poison's ratio.

ISTRS - use this option for structures which are initially loaded by a field stress (e.g. insitu stresses). This option allows arbitrary vertical and horizontal stresses to be specified at the start of the analysis.

Line 16,17.....

All loads are considered to be normal to, or parallel to, the edges of the elements on which they act. The orientation of the element with respect to the axes need not be considered. A positive load causes compression on the element edge and a negative load causes tension. Positive shear causes counterclockwise rotation of the element.

Line 19.....

NLAYS - The insitu or field stresses are specified for one or more layers of the mesh. In the most simple case, the entire mesh can be considered to be one layer and the vertical insitu stress at each element is calculated by adding the overburden stress on the top of the mesh to D X g X H where D is the rock density, g is gravitational acceleration and H is the distance of the element from the top of the mesh. As many layers can be used as desired and this gives the flexibity to use different rock densities and different earth pressure coefficients for each layer.

Line 20.....

XLESX, ZLESZ - these are earth pressure coefficients more traditionally denoted as K_o. The horizontal insitu stress in the plane of the mesh is calculated as :

XLESX X [OVERBURDEN STRESS + W]

where W is the self weight of the rock between the top of the mesh and the point being considered

Note that the two coefficients can only be identical if there are some unrestrained nodes (e.g. an excavation) at the beginning of the analysis. If there are no unrestrained nodes there will be zero deviator stress and the program will crash with a 'divide by zero' error.

Lines 21,22,23...

The term excavation is used loosely to mean any event which causes a change in stress on the edge of an element. This, of course, includes simulation of the mining process in which elements are "removed" (actually their material properties are changed to those of air) and the stresses on the edges of the surrounding elements are reduced to zero

In mining simulations, excavations may be used in the following situations:

a) If an element edge at the start of an analysis is to have an applied stress other than the insitu stress. For instance, if a mesh is formed of a completed tunnel profile, the exposed rock surface must be free of normal and shear stresses. An excavation is specified with 0 elements removed and with a prescribed zero stress on all the free edges of the surrounding elements.

b) If a tunnel is to be created in a mesh at some time after the start of the analysis. In this case some number of elements are specified as being removed and a zero stress is prescribed for the free edges of all elements on the resulting tunnel wall.

Note that excavated elements do not "disappear" and that the backfill process can reassign material properties to them at any time.

c) If a change of stress on a surface is required. This might be to simulate rock bolting, backfill or fluid pressure. No elements are removed, but again a new set of stresses must be prescribed for all element edges on the loaded surface.

Note that rock bolt pressures must be equilibrated by a set of forces at the anchor points.

Lines 26, 27.....

The material properties of any element can be changed at any time, the event being triggered by one of two criteria. To simulate backfilling of an open excavation, the elements within the excavation can change to a stiffer material following a given amount of closure. For instance, by specifying RTOLG = .6, the material property would change when the volume of the excavation is 60% of its original volume.

Alternatively, material properties can change at a given time which is more suitable for simulating staged construction of a structure, such as artificial roof support.

USER NOTES ON GEOROC DATABASE SYSTEM

1. Introduction

The FEMDAT database interpreter system is a language which can be used to define output from the GEOROC finite element program. Output can be in the form of printed files with column headers, similar to those printed by GEOROC, or they can be formatted tables of results suitable for transferring to a graphics program such as Symphony or Lotus 1-2-3. The advantage of the system is that results for every node and element are available in the database and the choice of what to view or print is completely arbitrary and need only be made at the end of the analysis. Results for any node, element or time steps can bejuxtaposed in a way that is not possible with conventional printed ouptut. Mathematical operations can be performed on any data - for instance, summing two displacements - permitting significant manipulation of results.

The language contains a number of keywords to define the variables, printing, mathematical operations, file output and simple loops. These keywords can be combined to define new words which are macros or mini-programs.

Like several other scientific software packages for dealing with large quantities of data, the system is written in the language FORTH and operates within the FORTH command interpreter. Reverse Polish Notation is used for all operations; that is, variables appear on the command line before the operation which affects them.

The program is started by typing FEMDAT <Enter>

2. Basic Keywords.

The following variables are available in the database:

DX - deflection in the x-direction at each node
DY - " " " y-direction " " "
VX - strain rate " " x-direction " " "
VY - " " " y-direction " " "
X - x-coordinates of each node
Y - y-coordinates of each node

SX - stress in the x-direction at each Gauss point
SY - " " " y-direction " " " "
SZ - " " " z-direction " " " "
S1 - major principal stress at each Gauss point
S2 - minor principal stress at each Gauss point
AN - angle between S1 and SX at each Gauss point
TXY - shear stress in the x-y plane at each Gauss point

SE - effective or deviator stress at each Gauss point
GPX - x-coordinate of each Gauss point
GPY - y-coordinate of each Gauss point

TIME - the time at a given print-time

The following words control print operations:

. - print an integer
F. - print a floating point number
E. - print floating point number in expontial format
PR - print in E. format with 4 significant figures in a 13 column field
PF - same as PR but format can be controlled with these commands:
n IS SIG-DIG sets n significant figures
m IS FLDWID sets field width to m columns
." string" - print an alpha numeric string. The space after ." is vital
CR - carriage return

The following mathematical operations can be used:

+ - * / operations on integers
F+ F- F* F/ operations on floating point numbers

for instance:
2 3 + . adds and prints the sum of the two integers
10. 2. F/ F. divides floating point 10 by 2 and prints the result.
10 2. / . is not valid. Integers and floating point cannot be mixed.

The following intrinsic functions are available:
FSQRT, F**2, FLOG10, FLOG2, FLN, F10**, F2**, FE**,
FSIN, FCOS, FTAN, FASIN, FACOS, FATAN, F->S, S->F

The following words establish defaults for subsequent operations:

NOW can be set to any print-time using n IS NOW
USE-NOW uses the value of NOW for all subsequent operations which need a print-time number
INPUT-TIME disables USE-NOW and allows the user to supply print-times
without changing the value of NOW
NODELIST name i , j , k , l , m , END-NODES establishes a list of node numbers with the given 'name'. This is a mechanism for indexing non-consequtive nodes in DO loops.
GPLIST name ei , gi , ej , gj , END-GPS establishes a list of element numbers and corresponding Gauss point numbers with the given 'name'.

The following words are for program control:

GNPREAD [d:][path]filename loads a database from the given drive and path. Filename is the name of a database file without the .GNP extension.
KEY?QUIT causes the program to break from a loop and return control to the command interpreter when ? is pressed.
BYE ends a session without closing a database file.
GBYE closes an open database file and ends the session.

Other words controlling file format:

DEFORM generates a file of nodal coordinates at a given print-time and with a given exaggeration of the deformations. This is for plotting with the mesh generator.

.TIMES prints all print times

.BASICS prints all file header information, coordinates, connection arrays

.TITLE prints title

.NCORDS prints nodal coordinates

.ELCON prints element connection arrays

.GPCS prints Gauss point coordinates

.DISPL-NOW prints displacements for all nodes at current time step

.DISPLS prints all displacements for all time steps

.ELEM-NOW prints element stresses at current time step

.ELEMS prints element stresses for all time steps

TRAJECT generates a file which allows plotting of stress trajectories.

Words controlling file i/o

TO: [filename] [file] TO-CRT sends [file] to the disk under the name filename
ADD-TO: [filename][file] TO-CRT adds [file] to the existing disk file filename

Loop Control

Loops can be created using the followinf format. Loops can only occur within newly defined words.

```
[upper limit+1][lower limit] DO
   [operations in loop]
 LOOP ;
```

If a list of nodes or Gauss points has been created the loop can use this list
in this way:
THRU [listname] DO [operations in loop] LOOP

3. Word Usage

a) Node based variables.

[print-time][node number] VARIABLE [operation]

e.g. 1 23 DY F. print y deflection of node 23 at second print time

2 23 DX 1 23 DX F- F. prints the difference between the x deflection at the second and third print times

Note: If USE-NOW is in operation the print-time is omitted.
The print-time is not required for the coordinates.

b) Element based variables.

[print-time][element number][Gauss point] VARIABLE [operation]

e.g. 0 12 3 TXY F. prints the shear stress at el. 12 gp. 3 for the first print-time.

Note: If USE-NOW is in operation the print-time is omitted.
The print-time is not required for printing Gauss point coords.

c) TIME

n TIME - the time at the (n+1)th print-time

e.g. 10 TIME F. prints the time at the eleventh print-time.

d) DEFORM

[print-time][exaggeration factor]DEFORM filename

e.g. 10 100. DEFORM MESH.OUT exaggerates all deflections by a factor of 100 and writes the nodal coordinates for the eleventh print-time to the disk file MESH.OUT

Note: Exaggeration factor must be floating point. Print-time is omitted if USE-NOW is in operation.

e) TRAJECT

FLOAD TRAJECT

TO: [filename][print-time] TRAJECT TO-CRT

Prints principal stresses and rotation angles to a file for plotting

4. Defining new words.

New words can be defined temporarily as combinations of the keywords. This allows tables of output values to be created. The format for a word definition is:

: WORD [series of operations on keywords] ;

The interpreter is insensitive to carriage returns so these can occur anywhere in the definition. The colon, semicolon and spaces, however, are critical.

Example:

```
: REPORT
CR ." NODAL DISPLACEMENTS" CR
NODELIST JIM 1 , 8 , 9 , 23 , 26 , END-NODES
10 0 DO
  I TIME F.
  I 2 JIM DY F. CR
LOOP ;
```

Typing REPORT now executes this word. It will produce a table headed NODAL DISPLACEMENTS with 10 lines each containing the time and y-displacement of node 8 at that time.The nodelist JIM is defined until the session is terminated so it could be used again in the following nested DO loop:

```
: REPORT2
 10 0 DO
  J TIME F.
  6 1 DO
   J I JIM DX PR
  LOOP CR
 LOOP ;
```

Typing REPORT2 will produce a neatly formatted table containing the time and the x displacement of each node of JIM on each line. Note that the inner loop has a counter I and the output loop a counter J.

Either of these words could have sent output to a file by using:

```
TO: DATA.FIL REPORT2 TO-CRT
```

Words can also appear within other words. The following is an example:

```
GPLIST BOB 4 , 1 , 3 , 1 , 5 , 1 , 6 , 1 , END-GPS

: REPORT3
5 1 DO
 NOW I BOB SX PR NOW I BOB SY PR
LOOP ;

: REPORT4
10 0 DO
 I IS NOW
 REPORT3 CR
LOOP ;
```

REPORT4 will now give SX and SY for each Gauss point in BOB for the 10 print-times in the second loop. A carriage return occurs between each print-time.

If a word is to used repeatedly it is worth writing it in a separate file and loading it into the system by typing FLOAD [filename]. This can be done in multi-tasking utility like DOSamatic by leaving the executing interpreter, starting the editor, writing the file, saving it then returning to the interpreter to do the FLOAD.

Supplementary notes to the GEOROC Users Manual.

1. Description of the Solution Procedure in GEOROC

In order to use many complex programs successfully it is necessary to have some understanding of the algorithms upon which they are based. As with any other system, an elementary knowledge of internal workings of a program gives one some ability to predict its behaviour under various operating conditions and to diagnose the reasons for any failures.

i)Finite Element Background

The essence of the finite element method upon which GEOROC is based is an equation relating the forces applied to a body to its deformation. As with a spring we can write:

$$K \times d = F \qquad (1)$$

where K is a stiffness parameter which depends upon the geometry and deformation modulus (length and spring constant) of the body.

This concept can be extended to a simple finite element. Suppose that we have a triangular element which is deformable only in one direction - say parallel to the x-axis.

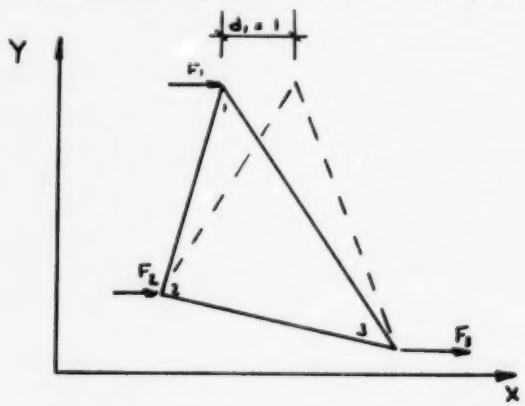

First we make the assumption that the displacement field, and hence the strains, throughout the element can be defined if we know the displacements at the corners, or nodes. We write an equation equivalent to (1) but in this case there are 3 forces and 3 displacements to consider:

$$\begin{vmatrix} k_{11} & k_{12} & k_{13} \\ k_{21} & k_{22} & k_{23} \\ k_{31} & k_{32} & k_{33} \end{vmatrix} \begin{vmatrix} d_1 \\ d_2 \\ d_3 \end{vmatrix} = \begin{vmatrix} F_1 \\ F_2 \\ F_3 \end{vmatrix} \qquad (2)$$

or

$$[K]\{d\} = \{F\} \qquad (3)$$

expanding this gives

$$\begin{aligned} k_{11}d_1 + k_{12}d_2 + k_{13}d_3 &= F_1 \\ k_{21}d_1 + k_{22}d_2 + k_{23}d_3 &= F_2 \\ k_{31}d_1 + k_{32}d_2 + k_{33}d_3 &= F_3 \end{aligned} \qquad (4)$$

[K] is called the stiffness matrix and its components in stress-strain problems can be expressed in physical terms. e.g.:

k_{11} is the force that must be applied at node 1 to cause a unit displacement with all other nodes held stationary.

k_{12} is the force that must be applied at node 1 to hold it stationary when a unit displacement is applied to node 2.

k_{21} is the force that must be applied at node 2 to hold it stationary when a unit displacement is applied to node 1.

etc.

all will have dimensions of force/unit displacement

In order to solve the equations for the unknown displacements caused by a known force field (typically applied loads, psuedo-loads caused by relieving the insitu stresses by excavation, and self weight) equation (3) must be rearranged to give:

$$\{d\} = [K]^{-1}\{F\} \qquad (5)$$

Once the displacements of the nodes are known it is possible to find the displacement at any point within the element using an approximation function known as a shape function. This is usually a low order polynomial - quadratic in the case of GEOROC. A shape function exists for each node of an element and it represents the assumed shape of the deformed element when that node has a unit displacement while all other nodes are held stationary. The displacements at any point within the element is predicted by superposition of the shape functions. Substitution of the known displacements into the shape functions and subsequent differentiation yields the strain at any desired point within the element. Finally, strains are related to stresses by a constitutive equation - in the simplest case this is Hooke's law :

$$\sigma = E\ e \qquad (6)$$

where E is Young's Modulus and e is strain.

The solution is now complete: even the most complex problems are solved by following these steps. It will be obvious, however, that while the stiffness matrix can be derived and inverted by inspection for very simple problems, most often this will require some more complicated procedures which can be generalised to cope with a variety of situations.

The Stiffness Matrix Components....

The stiffness matrix components are derived using the concept of minimization of potential energy. While it is not necessary to have a thorough grasp of the procedures it is useful to know that the required numerical integrations over the element volume involve the shape functions. As a result, the accuracy of the stiffness components depend upon the accuracy with which the assumed shape functions match the real shape of the deformed element. This is the primary reason that the 'true' solution to a problem is approached as the finite elements become smaller. Numerical integration by Gaussian Quadrature requires values on a curve to be calculated at only a small number of sampling points. This becomes important at the end of the solution process because stresses and strains are derived with most accuracy at these sampling or Gauss points.

Another point to bear in mind is that the stiffness components depend upon geometry so are strictly only accurate before load is applied to the element. If the element distorts significantly, as may happen near an excavation after a long period of creep, the stiffness components may become very inaccurate and yield useless solutions for the unknown displacements.

Stiffness Matrix Assembly.....

Since many problems are geometrically complex it is necessary to use a number of elements to model them. The requirements of accuracy also usually dictate that highly stressed portions of a structure are subdivided into a number of small elements. As a result it is necessary to create a stiffnes matrix for the entire structure by combining the individual stiffness matrices of the elements which comprise it. This process is called matrix assembly.

Using our example element with one degree of freedom for every node, the global stiffness matrix would contain one row and one column for every node in the structure. The

global stiffness component for any node is the sum of n terms from the element matrices where n is the number of elements that share that particular node.

Once the global stiffness matrix is assembled it is used in exactly the same way as the element stiffness matrix in the example above.

Stiffness Matrix Inversion.....

Inversion of the stiffness matrix is performed using Gaussian elimination. Several problems can cause the program to crash during equation solution - usually a 'zero or negative pivot' error is given. Data errors may be responsible (not fixing enough nodes for instance) or the matrix may be badly conditioned (very small mixed with very large numbers resulting in large round-off errors after divisions). Poissons's ratios close to 0.5 can cause extremely high stiffnesses giving rise to the latter type of error.

ii) Additional Features of GEOROC.

a) The element....

GEOROC uses an 8-noded quadrilateral element. It has 4 corner and 4 midside nodes and the sides can be parabolic in shape. The shape functions are also parabolic (2^{nd} order polynomials) and for this reason the elements are called isoparametric. It is the commonest of the higher-order elements, gives reasonable performance in non-linear problems and is able to model irregular boundaries with ease. The derivation of the stiffness matrix is accelerated by the use of a local coordinate system for each element which allows a common procedure whatever the element shape.

Each node has two degrees of freedom - orthogonal directions within the plane of the element.

b) Applied Loads.....

Any applied load, be it self weight, an edge or point load must be translated into a load acting on a node in order to be inserted into the load vector {F}. Thus point loads can only act at nodes and edge loads must be divided into equivalent nodal point loads. Body forces - loads spread over the area of an element - are converted to equivalent nodal loads by making use of the shape functions. Insitu

stresses are fictitious in that they do not contribute to the load vector and cause no deflections when applied. Their purpose is to provide a datum against which to measure stress changes. For instance, excavations are simulated by applying loads to a rock face which are sufficient to exactly balance the insitu stress. Creep solutions also require the absolute magnitude of stress rather than the stress change and thse can only be obtained by adding the stresses due to the applied loads to the initial insitu stress.

c) The Solution Procedure for Creep Problems....

Above, with the essential steps of an elastic analysis have been reviewed. The strategy for a creep solution is now described.

a) Form global stiffness matrix

b) Assemble the load vector and introduce boundary conditions e.g. nodes with prescribed or zero displacement.

c) Invert the stiffness matrix and store it in reduced form.

d) Solve the equation $\{d\} = [K]^{-1}\{F\}$

e) Solve for strains then stress

f) Calculate the effective, equivalent or deviatoric stress at each Gauss point. This is

$$[0.5(\sigma_x-\sigma_y)^2+(\sigma_x-\sigma_z)^2+(\sigma_y-\sigma_z)^2-6T_{xy}^2]^{1/2}$$

It is a measure of the deviation of the current stress from the hydrostat in principal stress space.

g) Calculate the strain rate at each Gauss point, at this value of stress, from one of the constitutive creep laws e.g. the power law $e=A\sigma^n t^a$

h) Using a suitably small increment of time calculate the incremental strain at each Gauss point at the end of the increment. Time increments are discussed further below.

i) Using Hooke's law find the stress which would cause the same value of strain. Notice the use of Hooke's law - although the overall material behaviour is non-linear we are making the assumption that within a small time-increment the response is approximated by linear elasticity.

j) Once the stress has been found it is translated to an equivalent set of nodal forces, much the same as any other body force.

k) These new nodal forces are added to the force vector where they act like a new set of applied loads. The deformations caused by these incremental loads will be the creep.

l) The solution cycle is now complete and the algorithm returns to d) to begin again for another time increment. The stiffnes matrix is not recalculated - the assumption is made that the deformations caused by creep are insufficient to make a significant difference to the stiffness components. In some cases this will be a poor assumption and it will be necessary to update the stiffness matrix. At present this is not possible without reprogramming but it is a minor task and some control over stiffness matrix reformation will be introduced in the future.

Procedure for Analysis using GEOROC

1. Create a mesh

A finite element analysis requires the formation of a mesh of elements with nodes along their edges. In the case of GEOROC these must be rectangular elements with a node at each corner and a node in the middle of each side. The description of the mesh is contained in three files which may be created either manually with an editor or by using a mesh generator. The mesh generator GEOMESH is provided with GEOROC and its data file format is described in the GEOMESH Users Manual. Once a data file has been prepared it can be run by typing the command:

MESH filename	where filname is the name to be used as the prefix for the output files

The three files needed to describe a mesh are:

a) filename.CON	filename is a user specified prefix

This file contains the element connection arrays which are lists of material types and node numbers associated with each element. The format is:

el. no. material no. node1 node2.....node8

.

.

.

nelem

The node numbers must be in counterclockwise order around the element. For instance, for the element illustrated below the line in the file would be:

7 1 1 4 2 3 5 7 8 10

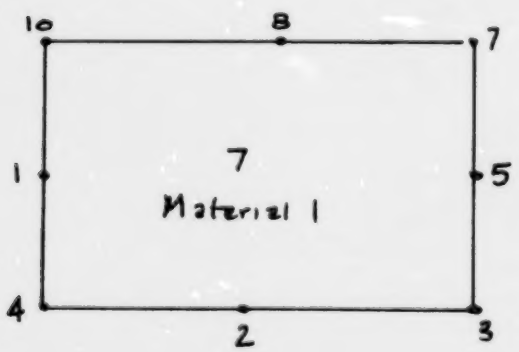

b) filename.NOD

This file contains the nodal coordinates and has the format:

```
node no.  x-coordinate  y-coordinate
   .
   .
   .
   .
npoin
```

c) filename.NTP

This file contains the boundary conditions or nodal fixities. It has the format:

```
fixed node no.  fixity code  x-displacement y-displacement
      .
      .
      .
   nvfix
```

The fixity code is a two digit number (01 10 or 11) in which the first digit indicates the x-direction fixity (0 is free, 1 is fixed) and the second digit indicates the y-direction fixity. The prescribed displacements are generally 0.0 but may be non-zero if a node is to be rigidly fixed in a deformed state as may be the case when simulating settlement of structural supports.

GEOMESH writes a fourth file called Messages which contains error messages if data file errors have been detected. If the mesh was generated successfully it contains a summary indicating the numbers of nodes, elements and fixed nodes in the mesh. The maximum nodal frontwidth is also given. GEOROC requires twice this value as an input parameter to permit dimensioning of arrays to hold equations for 2 degrees of freedom at each node.

2. Draw the mesh to confirm that it has been generated as desired and to view the node and element numbering. Display on an EGA graphics screen and plotting on Hewlett Packard and Houston Instrument plotters is supported by the plotting software provided. The utility is invoked by typing:

```
DRAW filename   where filename is the mesh
                file prefix
```

Take note of node and element numbers where loads are to be applied, excavations formed or printed results are required.

3. Prepare the GEOROC input file (filename.IN) by either following the GEOROC Users Guide or by invoking the program GEOROCIN which provides an interactive environment for file preparation.

4. Run GEOROC by typing the command:

GEOROC filename1 filename2

filename1 is the prefix of the input file (filename1.IN), filename2 is the prefix used for the mesh files.

Printed output will be written to the file filename1.OUT and a database will be written to the file filename1.GNP

5.Invoke the database interrogator by typing:

FEMDAT

Load in the database file by typing:

GNPLOAD filename1

The Users manual for FEMDAT describes the available commands.

APPENDIX B

COMINCO REFRACTION SEISMIC SURVEY

Conducted by:

PCS MINING, EARTH SCIENCES
June 1986

G. Phillips
Senior Geological Engineer
PCS Mining

ID-2491K

Introduction

A refraction seismic survey was conducted for Cominco Potash on June 25, 1986 by PCS Mining, Earth Sciences. The objective of the survey was to determine saltback thickness in a section of Room 2104 where a rock mechanics measuring station is installed.

A bison six channel engineering seismograph was used with a twelve geophone array. An attachment problem prevented use of one geophone and premature battery failure in the seismograph limited the number of readings taken, but it appears useful results were achieved.

Conclusions

Data quality was fair to good. A plot of results gives an acoustic velocity for salt of 12 689 fps. This is lower than the "generally accepted" value but may be due to fracturing and/or de-stressing near the mine opening. A Dawson Bay velocity of 20 314 fps is realistic, but is based on fewer data points than would have been preferred. Assuming a velocity of 11 000 fps for the Red Beds, based on well log information, and a thickness of 15 feet, the computed saltback thickness is 57.4 feet.

Discussion

Geophones were installed in hilti pins in the roof of 2104 entry at ten foot intervals between the 585 and 615 metre marks. A sledge hammer provided the energy source. Recordings were made from source locations at the 500, 550, 584 and 675 metre locations. P and S wave arrivals were recorded for each source geophone combination. After rejecting uninterpretable readings, 29 P wave arrivals were recorded and plotted. The analysis is based on these points. S wave arrivals were also recorded but showed no refractions, hence are not used.

Figure 1 is a plot of source to receiver distance vs time for the P wave arrivals. Two straight line segments are indicated, the slopes of which represent salt and Dawson Bay acoustic velocities (12 869 and 20 314 fps respectively). The Red Beds are not detectable with refraction due to their lower velocity. The distance to the Dawson Bay can be calculated based on the observed velocities and assuming values for the Red Beds velocity and thickness but is not directly obtained using a simple two layer model. The formula below, obtained from "Geophysical Prospecting" (Dobrin, 1960) was used to arrive at the saltback thickness figure of 57.4 feet.

$$Zo = \frac{Ti2 \cdot Vz \cdot Vo}{2\sqrt{V2^2 - Vo^2}} - \frac{Z1 \cdot Vo \cdot \sqrt{V2^2\ V1^2}}{V1 \cdot \sqrt{V2^2 - Vo^2}}$$

Where T12 is the intercept time of the Dawson Bay velocity line at the Y axis.

Figure 2 is a listing of the parameters used in the equation plus a listing of expected arrival times for direct waves (T1) and refracted waves (2) at a range of distances. Of course there will be NO T2 arrival if T2 is greater than T1 as this is within the critical distance, where refractions cannot be detected. In this case, the critical distance is between 300 and 350 feet.

It is unfortunate it was not possible to obtain more data at greater source-receiver separations in order to get a better "fix" on the limestone velocity. The few points which were plotted are at least reasonably consistent. The salt velocity shows more variability, but the length of the surveyed section is sufficient to derive a useable figure.

The lack of data beyond the 675 metre marker did not allow a check for changes in saltback thickness with distance along the entry.

Fugure surveys could usefully employ longer source-recevier spacing and perhaps could benefit from a dynamite energy source, particularly at the longer spacings, to enhance signal strength without the need for repeated sledge hammer blows.

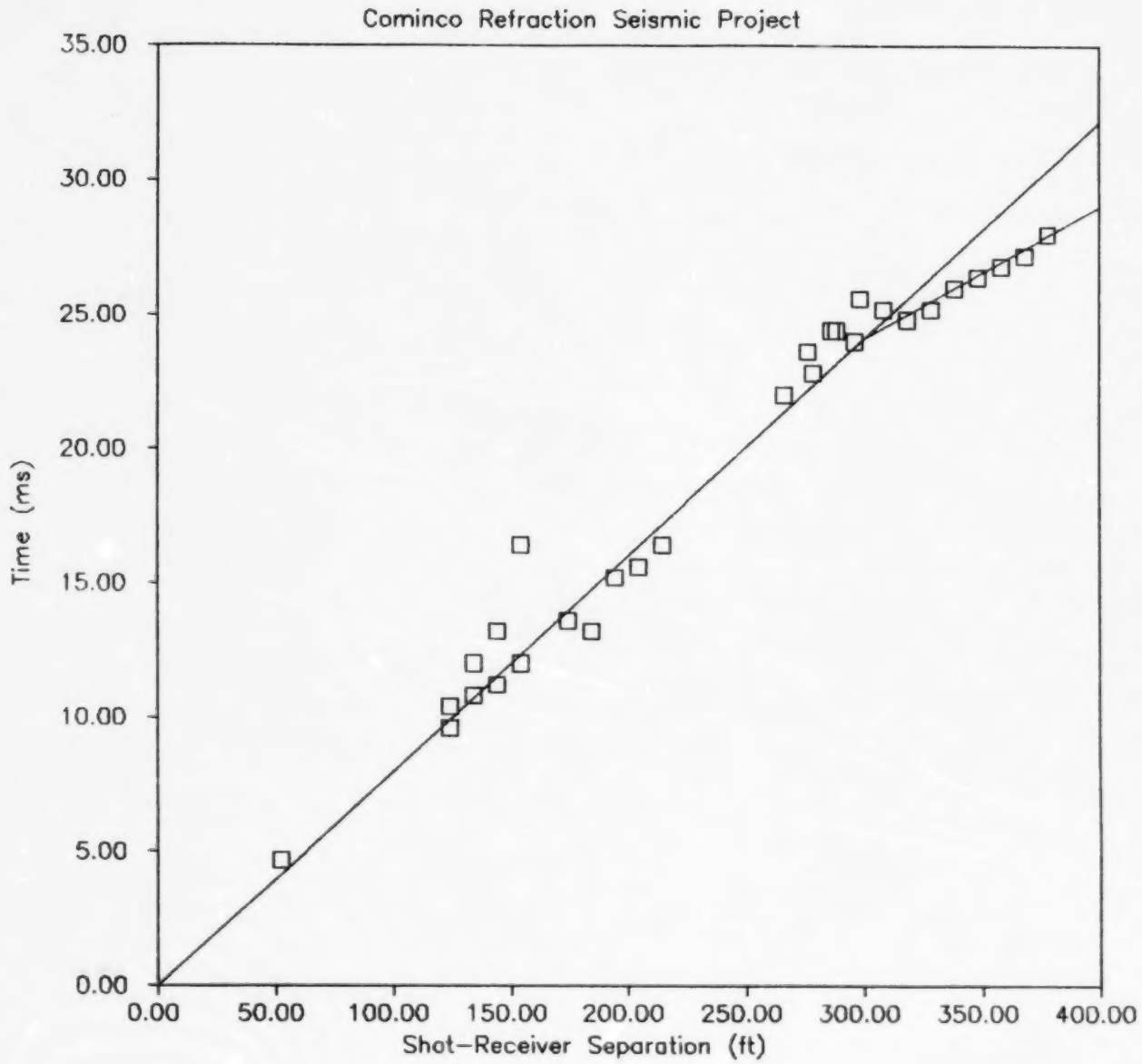
Cominco Refraction Seismic Project
35.00
30.00
25.00
20.00
15.00
10.00
5.00
0.00
Time (ms)
0.00
50.00
100.00
150.00
200.00
250.00
300.00
350.00
400.00
Shot-Receiver Separation (ft)

Figure 1

salt (v0)	12869	fps	Intercept time (Ti2)
r.b. (v1)	11000	fps	0.0092 seconds
DB (v2)	20314	fps	
RB (z1)	15	feet	
Saltback	57.440825	feet	

dist (ft)	t1 (ms)	t2 (ms)	FIRST (ms)
0	0.00	9.20	0.00
50	3.89	11.66	3.89
100	7.77	14.12	7.77
150	11.66	16.58	11.66
200	15.54	19.05	15.54
250	19.43	21.51	19.43
300	23.31	23.97	23.31
350	27.20	26.43	26.43
400	31.08	28.89	28.89
450	34.97	31.35	31.35
500	38.85	33.81	33.81
550	42.74	36.27	36.27
600	46.62	38.74	38.74
650	50.51	41.20	41.20
700	54.39	43.66	43.66
750	58.28	46.12	46.12
800	62.16	48.58	48.58
850	66.05	51.04	51.04
900	69.94	53.50	53.50
950	73.82	55.97	55.97
1000	77.71	58.43	58.43
1050	81.59	60.89	60.89
1100	85.48	63.35	63.35

Figure 2

APPENDIX C

Revised February 5, 1988

GENERAL SPECIFICATIONS AND HISTORY OF SRC'S TRIAXIAL TEST LABORATORY

The Triaxial Test Laboratory was designed and constructed by the Saskatchewan Research Council. The laboratory is located in the Saskatchewan Research Council Annex Building at 30 Campus Drive, Saskatoon.

The purpose of the laboratory is to test the creep behaviour of potash specimens under controlled conditions, but other "soft" materials may also be tested.

The general design specifications are as follows:

1. Civil Engineering

   i) Laboratory is of wood frame construction, fire retardant covering and concrete floors which meet standard laboratory specifications.

   ii) The total plant consists of four areas:

      a) Office and security area.

         A windowed office area acts as both a planning-analysis area and as a security area providing a limited entry to the control room in terms of rapid environmental changes and unwanted personnel.

      b) Control Room.

         A windowless temperature controlled room with a floor area of approximately 20 square metres is used to house the computer control and monitoring system. Some storage area is available for specimens and related test equipment.

c) Testing Area.

The main test laboratory utilizes a 33 square metre temperature and air infiltration controlled room in which the ten triaxial cells are located. The wood frame walls are insulated and sealed to reduce heat loss (gain) and humidity changes. Independent heater controls are located within the room. Individual lighting circuits are included with explosion proof light shields.

d) Bay Area.

A 37 square metre area with a 4.9 metre ceiling accompanies the laboratory. This area is used to facilitate the loading, unloading and preparation of equipment and test specimens. General construction is of wood frame with fiberglass insulation and fire resistant walls. All floors are of reinforced concrete to withstand the approximately 23,000 kg cell load. The bay room has an overhead door and loading ramp.

2. Triaxial Test Cells.

i) Ten triaxial test cells (Figures 1 and 2) of identical design are located in the test laboratory. These cells can be individually controlled, and are capable of testing specimens up to 200 mm in diameter by 400 mm long. Based on a specimen size of 200 mm diameter by 400 mm long, we believe that the triaxial cells can achieve any mean stress (p) and shear stress (q) path within the shaded area shown in Figure 3. The piston diameter is 432 mm, the maximum piston travel is 152 mm and stresses can be maintained to better than 0.1 MPa. The 610 mm

OD by 1370 mm long by 76 mm thick wall pressure jacket was manufactured in Chicago to meet ASME SA217 Grade C5 steel pressure vessel standards. The centrifugally cast steel jackets were x-rayed, certified and rough finished prior to shipment. The end seals, piston etc., are made of 4140 steel specially forged. All other machining was done in Saskatoon. The piston applies the axial pressure to the specimen and is sealed by Molythane "PolyPak" seals. A unique "shear load" hold down system is used to transmit the force to the outer jacket eliminating the need for a special external framework.

ii) Pressure Controls.

The radial pressure system and the axial pressure system are isolated to enable independent control of required loads. Air actuated hydraulic valves in conjunction with solenoid air valves operated by computer control maintain the required radial and axial stresses on each sample.

An air operated hydraulic pressure pump in conjunction with a bank of accumulators is used for pressure maintenance.

The independent control systems were designed to maintain a test over a number of months on one or more of the triaxial cells.

iii) Sensors.

Strain gauges and linear potentiometers attached directly to the specimen are used to measure strains. Pressure transducers and pressure gauges are used to monitor applied hydraulic pressures. Temperature sensors can be installed for both

monitoring and control of temperatures at or above ambient room temperature.

iv) Computer System.

The original design consisted of a Hewlett Packard 9825A desk top computer with 6K RAM storage for the monitoring of pressures, temperature, displacement, etc., and also for the control of the applied rates of pressure. The computer was to be interfaced to a NEFF 64 channel multiplexor, signal conditioner and output controller and the computer system was to be interfaced to plotter, printers, modems etc., for report writing and data analysis output. This computer system was never assembled.

Initial Testing of Triaxial Test Cells

A 12-month program of testing of one triaxial test cell for DSS on behalf of CANMET was begun in November 1983. The purpose of this program was to evaluate the performance of a triaxial cell. Tests were performed using an aluminum test piece for calibration purposes and a number of 200 mm diameter by 400 mm long potash cores obtained from Saskatchewan potash mines. The results of this program have shown that the triaxial cell tested, and we assume the other cells, are capable of obtaining useful test data from large potash cores. One objective not realized from this program was the testing of potash cores using computer control. This objective was not realized due to leaky solenoid control valve seal failure which could not be repaired in time to be used in this program.

Since 1984 a number of potash specimens have been successfully tested under fully automatic computer control using five of the triaxial cells.

The control and logging capabilities have evolved to the following status:

1. Data is logged by two data loggers interfaced to IBM PC desk top computers.
2. Signal conditioning of strain gauge inputs is provided by a NEFF signal conditioner.
3. Pressure control is accomplished with air actuated control valves, in conjunction with solenoid air valves operated by computer control.
4. Axial strains in the specimens can be detected with linear potentiometers attached to a specimen, to approximately 10 microstrains. Circumferencial strains are measured with foil strain gauges attached to the specimen.
5. Pressure transducers used are capable of detecting pressure differences of 0.07 MPa or better.
6. Data acquisition and control software has been developed, debugged and utilized in long term tests which provides fully automatic operation of up to four triaxial test cells simultaneously with one data logger/computer combination.
7. Six triaxial cells are now operational and equipped to test specimens under computer control.

Triaxial Test Cell Specifications

Maximum confining stress	50 MPa
Maximum uniaxial stress	225 MPa
Maximum axial stress at 10 MPa confining	190 MPa
Maximum axial stress at 20 MPa confining	155 MPa
Maximum axial stress at 30 MPa confining	120 MPa
Maximum axial stress at 40 MPa confining	95 MPa
Maximum axial stress at 50 MPa confining	50 MPa
Pressure transducer precision	±.07 MPa
Pressure transducer accuracy	±.40 MPa
Maximum axial strain	15 %
Maximum radial strain	15 %
Linear potentiometer precision	± 9 microstrains
Linear potentiometer accuracy	±20 microstrains
Strain gauge precision	± 1 microstrains
Strain gauge accuracy	± 5 microstrains
Maximum relaxation rate	> .2 MPa/sec
Maximum creep rate	125 millistrains/sec
Minimum stress increment	± .1 MPa
Pore pressure control	Not Available
Laboratory temperature control	± 1 Celsius
Minimum cell temperature	Ambient
Maximum cell temperature	> 30 Celsius
Cell temperature control	Not Available

Fig.1: LSTTF hydraulic, logging and control systems 10/84

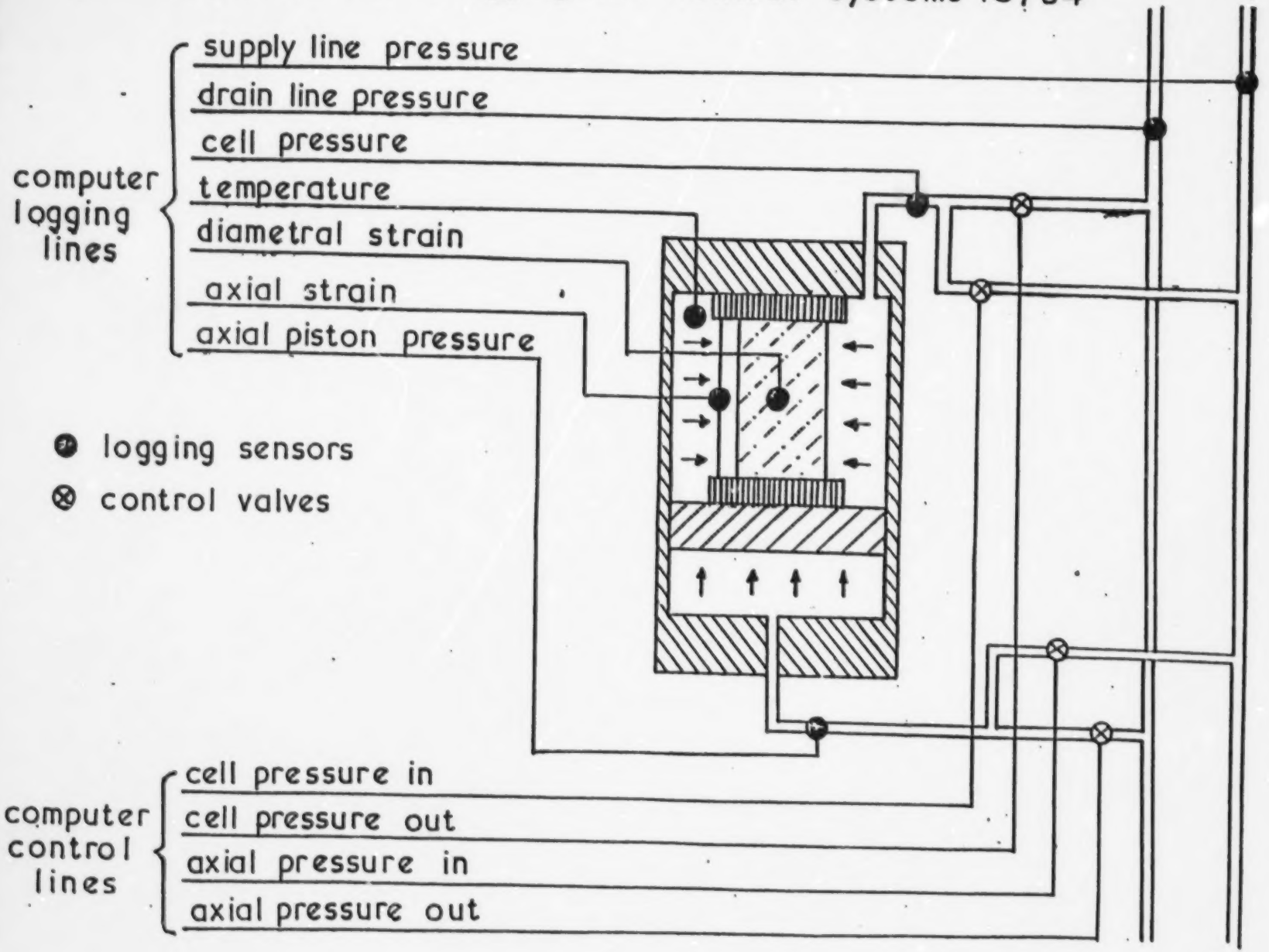

FG 2

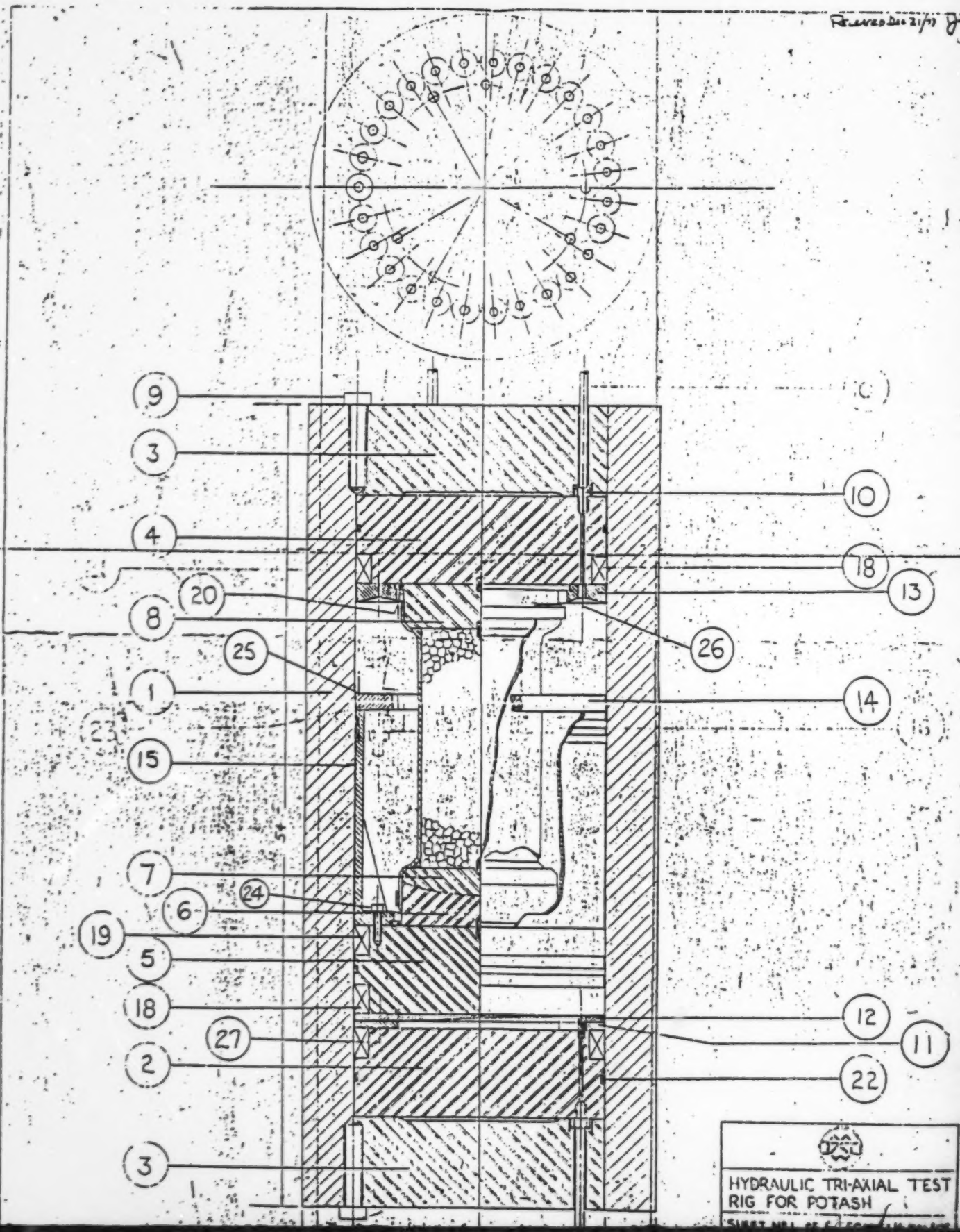

HYDRAULIC TRI-AXIAL TEST RIG FOR POTASH

FIG. 3 OBTAINABLE p-q STRESS PATHS ARE INDICATED BY SHADED AREA

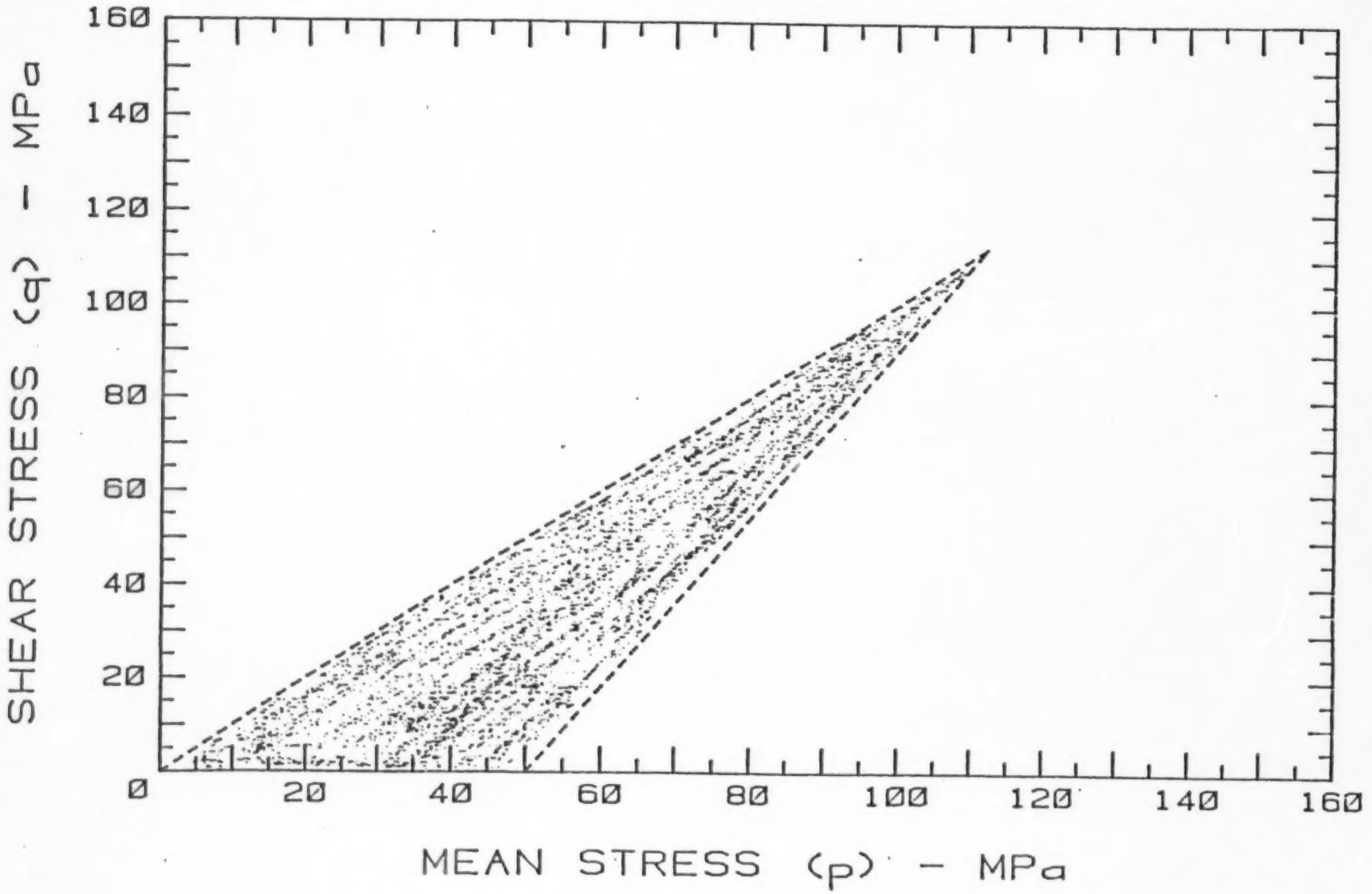

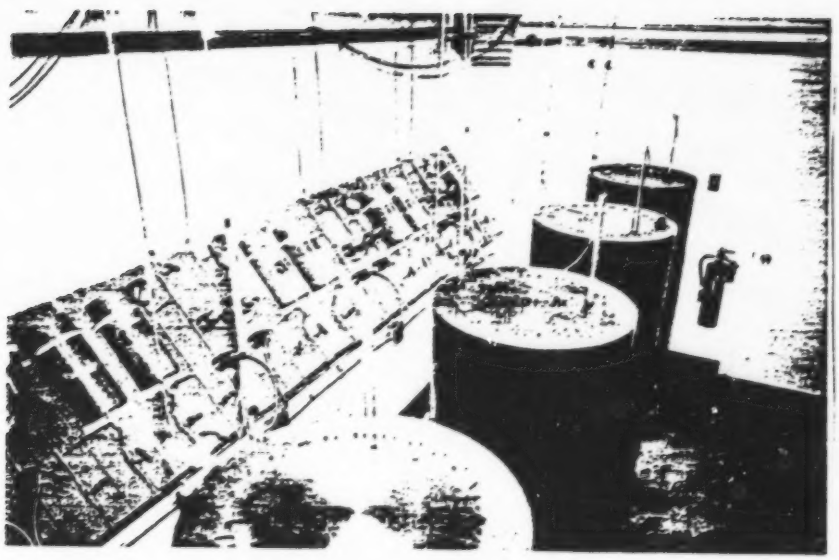

TRIAXIAL TEST CELL FACILITY